Islamic University of Gaza
Deanery of higher studies
Faculty of Science
Department of Physics

THEORITICAL CHARACTERIZATION OF DIFFERENT SAMPLES USING ROTATING POLARIZER AND ANALYZER ELLIPSOMETER WITH A FIXED COMPENSATOR

By

Anass A. Al-kanoo

Supervisors

Dr. Taher El-Agez

Dr. Sofyan Taya

Submitted to the Faculty of Science as a Partial Fulfillment of the Master of Science (M. Sc.) in Physics

1433 - 2012

To my dear parents. To my wife. To my sisters and brothers

To my homeland Palestine the only place in which I feel alive.

Anass A. Al-kanoo

ACKNOWLEDGMENTS

In the name of Allah to whom I am overwhelmed with gratitude for His continuous help and guidance throughout the path of knowledge. I would like to express my gratitude to all those who gave me the possibility to complete this thesis.

I am extremely indebted to supervisors Dr. Taher El-Agez and Dr. Sofyan Taya for their constant support and whose help, stimulating suggestions and encouragement helped me in all time of research for, arranging and writing of this thesis. Also, I would like to express my thank to Dr. Ahmed Altayan my advisor for his support and guidance.

ABSTRACT

Ellipsometry is an extremely powerful tool for the study the optical properties of materials with high optical data precision in measurement. Being accurate, fast and non-destructive in data acquisition and characterization of the samples, ellipsometry has been widely applied especially in the scientific research labs and microelectronic industry with continuous efforts and progress made by developing different theoretical models and experimental techniques.

In this work, an ellipsometer using a fixed phase retarder and a rotating polarizer and analyzer at any speed ratio is presented. Muller formalism is employed to extract Stokes parameters from which the intensity received by the detector is obtained. A comparison between different configurations is held regarding the effect of the noise on the results extracted from each one and the uncertainties in the ellipsometric parameters as functions of the uncertainties of the Fourier coefficients.

Moreover, a set of ellipsometric configurations using a rotating polarizer, compensator, and analyzer at any speed ratio is studied. All configurations are applied to bulk c-Si and GaAs to calculate the real and imaginary parts of the refractive index of the samples. The comparison among different configurations reveals that rotating compensator-analyzer configuration corresponds to the minimum error in the calculated optical parameters.

List of Figure Captions

CHAPTER ONE

CHAPTER TWO

CHAPTER THREE

CHAPTER FIVE

CONTENTS

CHAPTER ONE :INTRODUCTION

CHAPTER TWO :A Spectroscopic Ellipsometer Using Rotating Polarizer And Analyzer At A Speed Ratio 1:1 And A Fixed Compensator

CHAPTER ONE

INTRODUCTION

Ellipsometers have been widely used in thin film characterization. They have shown a high degree of accuracy. An ellipsometer measures the change in the polarization state of incident light. If linearly polarized light of known orientation is reflected from a surface, then the reflected light will be elliptically polarized. The shape and orientation of the ellipse depends on the angle of incidence, the direction of the polarized incident light, and the reflection properties of the surface. In this chapter, an introduction to electromagnetic theory and principles of ellipsometry are presented.

1.1 Historical Review:

The history of ellipsometry began in 1887 when Drude derived the equations of ellipsometry. Since then, ellipsometry has attracted researchers and scientists. Until the early 1970s, ellipsometry measurements were time consuming. In 1975, the automation of spectroscopic ellipsometry measurement was achieved by Aspenes et al. [14]. This breakthrough in the field improved the measurement time as well as the measurement precision. In 1984, real time monitoring ellipsometry was constructed [15]. Since then, different ellipsometric configurations have been studied in the literature. The speed ratio with which the optical elements rotate was the main difference among these structures. The most common configuration was the rotating analyzer ellipsometer (RAE) [16]. In such a model, the polarizer angle P is fixed while the analyzer angle A rotates at an angular speed ω. In terms of $A = \omega t$, the intensity of light emerging from the analyzer can be written as one dc and two ac components from which the ellipsometric parameters ψ and Δ are extracted. The RAE has the advantage of simple system design but it involves the dc component which causes a serious problem. The reduction of the dc background requires particular techniques and the calibration of such system is also time consuming.

Rotating polarizer and analyzer ellipsometer (RPAE) has also been proposed in different forms. The speed ratio, with which the optical elements rotate, was the main difference among these structures.

Azzam [17] suggested synchronously rotating both the polarizer and the analyzer with the ratio 1:3. In his work, the intensity of light reaching the detector includes four cosine and four sine terms. His system suffers a lack of clear explanation of each coefficient and it's relation to the ellipsometric parameters ψ and Δ [18].

In 1987, a rotating polarizer and analyzer RPA spectroscopic ellipsometer was proposed and constructed [18]. In the design, the polarizer and the analyzer rotate with a speed ratio 1:2. The final light intensity then contains three cosine terms from which ψ and Δ are calculated. In this design, the errors arising from the phase shift and dc background are eliminated.

An improved RPA spectroscopic ellipsometer was proposed [19,20] with the speed ratio still being 1:2 but with the incident angle being fully variable. Moreover, a fixed polarizer was placed in the optical path to eliminate the source polarization effect. The final light intensity thus contains four AC components. The optical constants and the ellipsometric parameters were obtained by calculating any one of the two sets of AC signals.

Rotating compensator ellipsometers have been also proposed [21-23]. Systematic error sources for the rotating-compensator ellipsometer are discussed [22]. Starting from a general formalism, they derived explicit first-order expressions for the errors $\delta\psi$ and $\delta\Delta$ caused by azimuthal errors and residual ellipticity introduced by imperfect polarizers or compensators and windows.

A spectroscopic ellipsometer in which the polarizer and the analyzer are rotating synchronously in opposite directions at the same speed was proposed [24]. The light intensity involves four components, one dc and three cosine terms, with frequencies of 2ω, 4ω, and 6ω. The main advantage of the proposed ellipsometer is that: it is feasible to extract the ellipsometric parameters ψ and Δ from the even Fourier coefficients without relying on the dc component which is considered to be a serious problem in a rotating-analyzer or -polarizer ellipsometer. This allows measurements in semi-dark room without

worrying about stray light problems, dark currents in detectors, and long term fluctuations in light sources. The calculations of the optical parameters of c-Si, Au, and GaAs are in excellent agreement with the published data.

Moreover, a spectroscopic ellipsometer in which the polarizer and the analyzer are rotating synchronously in the same direction with the same angular speed was also investigated [25]. The results from the simulated spectra of the complex refractive index of c-Si, and Au were presented. The noise effect on the proposed ellipsometer was simulated and plotted for the two samples.

The full description of a scanning ellipsometer that incorporates the rotation of two polarizing elements simultaneously with a speed ratio 1:2 was presented theoretically in details [26] and constructed experimentally [27]. The ideal Fourier spectrum of this signal includes nine coefficients from which five are even and the rest are odd. All of these coefficients contain valuable information about the physical properties of the studied sample. Therefore, it is feasible to extract the ellipsometric parameters ψ and Δ as well as the optical parameters of the sample using any set containing three different coefficients.

Recently, a spectroscopic ellipsometer was presented in whcih the polarizer and the analyzer are rotating synchronously in the same direction at a speed ratio 1:3 [28]. The light intensity received by the detector contains six components, one dc and five AC, with frequencies of 2ω, 4ω, 6ω, 8ω, and 10ω, respectively. One can independently extract the ellipsometric parameters ψ and Δ as well as the optical constants using any of six different sets of the Fourier coefficients. A comparison among these sets shows that the sets containing the coefficients (a_1, a_2, a_3) and (a_1, a_2, a_4) correspond to the minimum percent error in the calculation of the real and imaginary parts of the dielectric function. The results from the calculated spectra of the complex refractive index of c-Si, ZnSe, and GaP show a remarkable consistency with published data.

The proposed structures in Refs [24], [25], and [28] were tested only for bulk samples. The theoretical characterization of 100 nm SiO_2 thin film using spectroscopic rotating polarizer analyzer ellipsometer (RPAE) with speed ratios 1:-1 [29], 1:1 [30], and 1:3 [31]

was investigated. The proposed sample consists of air (ambient)/SiO2 (thin film)/Si (substrate). The ellipsometric parameters ψ and Δ are calculated when a clean signal is received by the detector and when a hypothetical noise is imposed on this signal. The film thickness and the optical constants of the film are calculated from the noisy signal in the spectrum range 200–800 nm. The results are compared with the proposed thickness and with the published values for SiO2 optical constants.

Different types of spectroscopic ellipsometric structures concerning the effect of the noise on the optical parameters extracted from these systems were studied [32]. The comparison involves the rotating analyzer spectroscopic ellipsometer and the rotating polarizer and analyzer spectroscopic ellipsometer in which the polarizer and the analyzer rotate with different speed ratios. All systems under comparison are investigated for c-Si and GaAs samples for a noisy signal. The percent error in the real and imaginary parts of the refractive index of the samples is calculated and plotted with energy in the range 1.5-3 eV photon energy. The results reveal that the rotating polarizer and analyzer spectroscopic ellipsometer in which the polarizer and the analyzer rotate with a ratio 1:1 corresponds to the minimum error.

1.2. Theoretical Background

A brief review of the interaction of the electric and magnetic fields with any linear isotropic homogeneous medium will be presented. Moreover, the boundary conditions, Maxwell equations, and the wave equation will be reviewed. The propagation of monochromatic plane waves will be reviewed. Reflection of p- and s-polarizations from a bulk material as well as reflection from different structures will be discussed. Jones calculus and many different polarizing elements are presented at the end of this chapter.

1.3. Electric Field And Electric Displacement

For a polarized dielectric material of electric polarization **P** (permanent or induced), the macroscopic field vector **D** is given by [13]

$$\mathbf{D} = \varepsilon_0 \mathbf{E} + \mathbf{P} \tag{1.1}$$

where **D** is called the electric displacement and ε_0 is the electric permittivity of vacuum. In many dielectric media the polarization occurs in response to the applied field. For a linear and isotropic dielectric medium, the polarization is given by

$$\mathbf{P} = \varepsilon_0 \chi_e \mathbf{E} \tag{1.2}$$

The constant χ_e is a scalar quantity called the electric susceptibility. The electric field and the electric displacement are related by [13]

$$\mathbf{D} = \varepsilon \mathbf{E} = \varepsilon_0 (1 + \chi_e) \mathbf{E} \tag{1.3}$$

where ε is the electric permittivity of the medium. The ratio $\varepsilon / \varepsilon_0$ is known as the relative complex dielectric constant (permittivity) of the medium and is given by [13]

$$\varepsilon_r = \frac{\varepsilon}{\varepsilon_0} = 1 + \chi_e = \varepsilon_1 - i\varepsilon_2 \tag{1.4}$$

where ε_1 and ε_2 are the real and imaginary parts of the relative complex dielectric function of the medium, respectively. The dielectric loss in an absorbing medium is due to the imaginary part ε_2.

1.4 Boundary Conditions

The boundary conditions on both **E** and **D** can be found by applying the integral form of Gauss's law, namely [13]

$$\oint_s \mathbf{D}.d\mathbf{s} = \int_v \rho\, dv\,. \tag{1.5}$$

The integration is carried out onto a small pillbox constructed at the interface between 1 and 2 media yielding to

$$D_{2n} - D_{1n} = \sigma\,, \tag{1.6}$$

where σ is the surface density of the external charge at the interface while D_{n1} and D_{2n} are the normal electric field density in 1 and 2 media, respectively.

Therefore, the normal components of **D** is discontinuous and this discontinuity is given by the surface density of the external charge on the interface.

The boundary conditions on **E** can be found by applying Stoke's theorem on the equation $\nabla \times \mathbf{E} = \mathbf{0}$ (static case) to give

$$E_{2t} = E_{1t}\,. \tag{1.7}$$

Thus, the tangential components of the electric filed is continuous at the interface.

1.4.1 Boundary Conditions For B and H

By using a similar argument as before, the normal components of the magnetic field **B** is continuous at the interface that is

$$B_{2n} = B_{1n}, \tag{1.8}$$

and the tangential component of **H** is discontinuous namely

$$H_{2t} - H_{1t} = j_s, \tag{1.9}$$

where j_s is the surface current density at the interface.

1.4 Maxwell's Equations

The electric field vectors **E** and **D** together with the magnetic field vectors **B** and **H** classically describe an electromagnetic wave. These vectors are related by Maxwell's equations, which are fully describe the propagation of the electromagnetic radiation in any medium. The differential form of the time varying of Maxwell's equations is [13]

$$\nabla \times \mathbf{E} = -\frac{\partial \mathbf{B}}{\partial t}. \tag{1.10}$$

$$\nabla \times \mathbf{H} = \mathbf{J} + \frac{\partial \mathbf{D}}{\partial t}, \tag{1.11}$$

$$\nabla \cdot \mathbf{D} = \rho, \tag{1.12}$$

$$\nabla \cdot \mathbf{B} = \mathbf{0}. \tag{1.13}$$

For linear and isotropic medium the following relations are valid [13]

$$\mathbf{J} = \sigma(\omega)\mathbf{E}, \tag{1.14}$$

$$\mathbf{D} = \varepsilon(\omega)\mathbf{E}, \tag{1.15}$$

and

$$\mathbf{B} = \mu(\omega)\mathbf{H}. \tag{1.16}$$

1.5 The Wave Equation

The wave equation is one of the most important consequences of Maxwell's equations. A closer look at the first two Maxwell's equations reveals that they are a set of coupled partial differential equations. Taking the curl of equations (1.10) and (1.11), then assuming that the medium is linear, homogenous and isotropic and the gradient of the scalars ε, μ and σ vanish, again substituting equations (1.10) and (1.11) into the obtained two equations and using $\nabla \cdot \mathbf{B} = 0$ and $\nabla \cdot \mathbf{E} = 0$ for a source free medium gives the final form of the wave equations for both **E** and **B** namely

$$\nabla^2 \mathbf{E} - \varepsilon\mu \frac{\partial^2 \mathbf{E}}{\partial t^2} = \mathbf{0}, \tag{1.17}$$

$$\nabla^2 \mathbf{B} - \varepsilon\mu \frac{\partial^2 \mathbf{B}}{\partial t^2} = \mathbf{0}. \tag{1.18}$$

The phase velocity in a non-conducting medium is given by

$$V_{ph}(\omega) = \frac{1}{\sqrt{\mu(\omega)\varepsilon(\omega)}}, \tag{1.19}$$

and for free space

$$V_{ph} = c = \frac{1}{\sqrt{\mu_0 \varepsilon_0}}. \tag{1.20}$$

The x-component of the electric field the y-component of the magnetic field are given by

$$E_x(z,t) = E_0 e^{i(\omega t - kz)}, \tag{1.21}$$

$$H_y(z,t) = \sqrt{\frac{\varepsilon}{\mu}} E_0 e^{i(\omega t - kz)}. \tag{1.22}$$

Eqns. (1.21) and (1.22) are necessary when talking about the reflection of monochromatic waves from dielectric interfaces.

1.6. Refractive Index And Dispersion Relations For A Dielectric Medium

The refractive index of any medium is the ratio of the speed of light in vacuum *c* to the phase velocity of light in that medium. The complex refractive index is described by [13]

$$N = n - ik \tag{1.23}$$

where *n* is the index of refraction and *k* is the extinction coefficient. From the definition of the refractive index are obtains

$$N(\omega) = \frac{c}{V_{ph}(\omega)}. \tag{1.24}$$

Substituting eqn. (1.19) and eqn. (1.20) into the last equation gives,

$$N(\omega) = \frac{c}{V_{ph}(\omega)} = \sqrt{\frac{\mu(\omega)\varepsilon(\omega)}{\mu_0 \varepsilon_0}}, \tag{1.25}$$

or

$$N(\omega) = \sqrt{\mu_r(\omega)\varepsilon_r(\omega)}. \tag{1.26}$$

Assuming a non-magnetic medium i.e., $\mu_r = 1$, eqn. (1.26) becomes

$$N(\omega) = n(\omega) - ik(\omega) = \sqrt{\varepsilon_r(\omega)} = \sqrt{\varepsilon_1(\omega) - i\varepsilon_1(\omega)} \tag{1.27}$$

The index of refraction and the extinction coefficients can be written in terms of the real and complex parts of the dielectric function as

$$n(\omega) = \sqrt{\frac{\left[\varepsilon_1^{\,2}(\omega) + \varepsilon_2^{\,2}(\omega)\right]^{\frac{1}{2}} + \varepsilon_1(\omega)}{2}} \tag{1.28}$$

$$k(\omega) = \sqrt{\frac{\left[\varepsilon_1^{\,2}(\omega) + \varepsilon_2^{\,2}(\omega)\right]^{\frac{1}{2}} - \varepsilon_1(\omega)}{2}} \tag{1.29}$$

1.7 Cauchy Relation

The refractive index can be written in terms of the wavelength as [13]

$$n(\lambda) = N_0 + \frac{N_2}{\lambda^2} + \frac{N_4}{\lambda^4} + \ldots \tag{1.30}$$

This relation is called Cauchy relation. The parameters N_0, N_2, and N_4 are the Cauchy parameters. The Cauchy relation is used to describe the normal dispersion of dielectric materials in the visible spectrum.

1.8 Oblique Reflection Of Plane Polarized Monochromatic Wave At A Dielectric, Metallic and Semiconductor Interfaces

1.8.1 Terms And Definitions

Plane Of Incidence

The plane of incidence is defined as the plane normal to the surface and contains both the incident and the reflected beams as shown in figure 1.

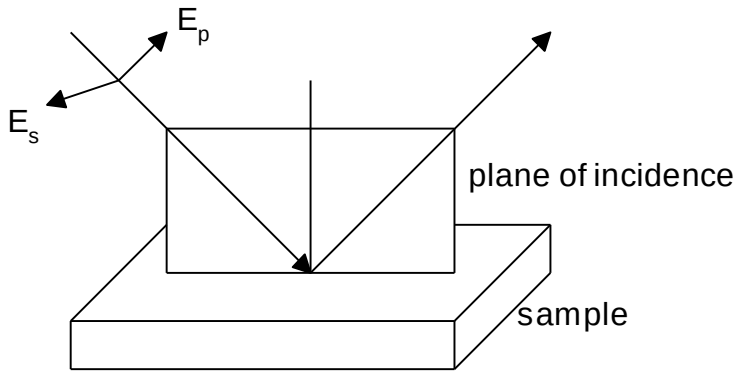

Figure 1.1. Plane of incidence.

p-polarization

If the direction of vibration of the electric field vector is parallel to the plane of incidence, the polarized light is called p-polarized.

s-polarization

If the direction of vibration of the electric field vector is normal to the plane of incidence, the polarized light is called s-polarized (s stands for the German word ”senkrecht”, meaning “perpendicular”).

1.8.2 Reflection of p-linearly Polarized Light

Consider a p-polarized plane wave is incident on the interface between two semi-infinite dielectric media 0 and 1 with parameters ε_0, μ_0, and ε_1, μ_1, respectively, at an angle of incidence ϕ_0 as shown in figure 1.2 below.

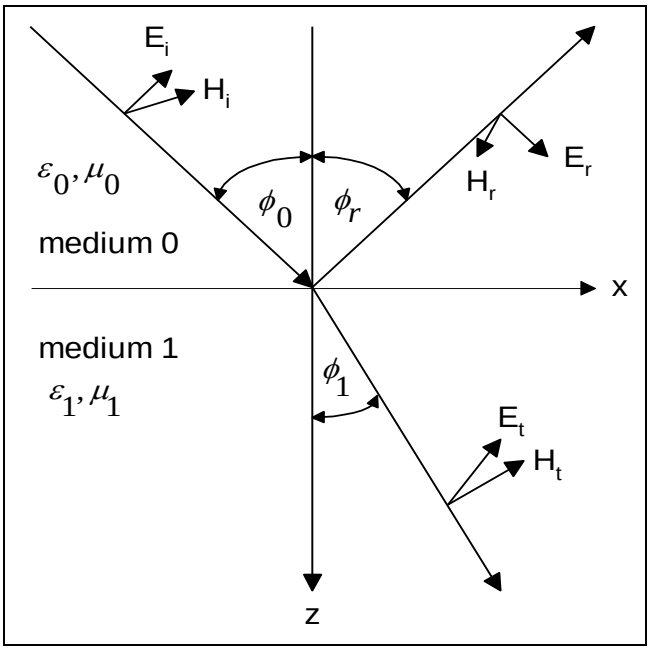

Figure 1.2. Oblique reflection of P-polarized light.

The incident electric and magnetic fields are given by

$$\mathbf{E}_i = E_0[(\cos(\phi_0)\hat{\mathbf{i}} - \sin(\phi_0)\hat{\mathbf{k}})e^{-ik_0[x\sin(\phi_0) + z\cos(\phi_0)]}, \tag{1.31}$$

$$\mathbf{H}_i = \frac{E_0 e^{-ik_0[x\sin(\phi_0) + z\cos(\phi_0)]}}{\eta_0}\hat{\mathbf{j}}, \tag{1.32}$$

where $\eta_0 = \sqrt{\frac{\mu_0}{\varepsilon_0}}$ is the wave impedance of medium 0 and $k_0 = \omega\sqrt{\mu_0\varepsilon_0}$.

The reflected electric and magnetic fields are given by [13]

$$\mathbf{E}_r = E_0 r_p[\cos(\phi_r)\hat{i} + \sin(\phi_r)\hat{k}]e^{-ik_0[x\sin(\phi_r) - z\cos(\phi_r)]}, \tag{1.33}$$

$$\mathbf{H}_r = \frac{E_0 r_p e^{-ik_0[x\sin(\phi_r) - z\cos(\phi_r)]}}{\eta_0}\hat{\mathbf{j}}. \tag{1.34}$$

The transmitted fields are

$$\mathbf{E}_t = E_0 t_p[(\cos(\phi_1)\hat{\mathbf{i}} - \sin(\phi_1)\hat{\mathbf{k}})e^{-ik_1[x\sin(\phi_1) + z\cos(\phi_1)]}, \tag{1.35}$$

$$\mathbf{H}_t = \frac{E_0 t_p e^{-ik_1[x\sin(\phi_1) + z\cos(\phi_1)]}}{\eta_1}\hat{\mathbf{j}}, \tag{1.36}$$

where $\eta_1 = \sqrt{\frac{\mu_1}{\varepsilon_1}}$ and $k_1 = \omega\sqrt{\mu_1\varepsilon_1}$.

The boundary conditions assumed no charges or currents at the interface lead to [13]

$$\cos(\phi_0)e^{-ik_0 x\sin(\phi_0)} + r_p\cos(\phi_r)e^{-ik_0 x\sin(\phi_r)} = t_p\cos(\phi_1)e^{-ik_1 x\sin(\phi_r)}, \tag{1.37}$$

and

$$\frac{1}{\eta_0}e^{-ik_0 x\sin(\phi_0)} - \frac{1}{\eta_0}r_p e^{-ik_0 x\sin(\phi_r)} = \frac{t_p}{\eta_1}e^{-ik_1 x\sin(\phi_r)}. \tag{1.38}$$

If the solution is to be valid for any value of *x* then the exponents on both sides of eqn. (1.37) and eqn. (1.38) should be equal. The following results are obtained [13]

$$\phi_0 = \phi_r \tag{1.39}$$

and

$$k_0\sin(\phi_0) = k_1\sin(\phi_1) \tag{1.40}$$

Relation (1.40) is known as Snell's law.

Snell's law in terms of the refractive indices can be obtained using the relations $k = \omega\sqrt{\mu\varepsilon}$ and $n = \sqrt{\varepsilon_r}$ which gives

$$\sqrt{\mu_0\varepsilon_0}\sin(\phi_0) = \sqrt{\mu_1\varepsilon_1}\sin(\phi_1) \tag{1.41}$$

If the media are non-magnetic that is $\mu_1 = \mu_0$, then

$$n_0\sin(\phi_0) = n_1\sin(\phi_1) \tag{1.42}$$

The p-polarization reflection coefficient is given by [13]

$$\begin{aligned} r_p &= \frac{\eta_0\cos(\phi_0) - \eta_1\cos(\phi_1)}{\eta_0\cos(\phi_0) + \eta_1\cos(\phi_1)} \\ &= \frac{\sqrt{\frac{\mu_0}{\varepsilon_0}}\cos(\phi_0) - \sqrt{\frac{\mu_1}{\varepsilon_1}}\cos(\phi_1)}{\sqrt{\frac{\mu_0}{\varepsilon_0}}\cos(\phi_0) + \sqrt{\frac{\mu_1}{\varepsilon_1}}\cos(\phi_1)} \end{aligned} . \tag{1.43}$$

This is the most general form of the p-reflection coefficient for the reflection at the interface of two dielectric media in terms of the electric permittivity and the magnetic permeability. It can be written in terms of the refractive indices for non-magnetic media as [13]

$$r_p = \frac{N_1\cos(\phi_0) - N_0\cos(\phi_1)}{N_1\cos(\phi_0) + N_0\cos(\phi_1)}. \tag{1.44}$$

On the other hand, the p-polarization transmission coefficient is [13]

$$t_p = \frac{2N_0 \cos(\phi_0)}{N_1 \cos(\phi_0) + N_0 \cos(\phi_1)}. \tag{1.45}$$

1.8.3 Reflection Of s–linearly Polarized Light

Using a similar discussion for the s-polarization, the reflection and transmission coefficients are given by [13]

$$\begin{aligned} r_s &= \frac{\eta_1 \cos(\phi_0) - \eta_0 \cos(\phi_1)}{\eta_1 \cos(\phi_0) + \eta_0 \cos(\phi_1)} \\ &= \frac{\sqrt{\frac{\mu_1}{\varepsilon_1}} \cos(\phi_0) - \sqrt{\frac{\mu_0}{\varepsilon_0}} \cos(\phi_1)}{\sqrt{\frac{\mu_1}{\varepsilon_1}} \cos(\phi_0) + \sqrt{\frac{\mu_0}{\varepsilon_0}} \cos(\phi_1)} \end{aligned} . \tag{1.46}$$

In terms of the refractive indices for non-magnetic media eqn. (1.46) becomes

$$r_s = \frac{N_0 \cos(\phi_0) - N_1 \cos(\phi_1)}{N_0 \cos(\phi_0) + N_1 \cos(\phi_1)}. \tag{1.47}$$

The s- polarization transmission coefficient

$$t_s = \frac{2N_0 \cos(\phi_0)}{N_0 \cos(\phi_0) + N_1 \cos(\phi_1)} \tag{1.48}$$

The p as well as the s reflection coefficients can be written in polar form as [13]

$$r_p = \rho_p \exp(i\delta r_p), \tag{1.49}$$

$$r_s = \rho_s \exp(i\delta r_s). \tag{1.50}$$

where ρ_p and ρ_s are the amplitudes of the p and s reflection coefficients respectively and δr_p is the phase shift of the electric field parallel to the plane of incidence upon reflection from the sample and δr_s is the same but for s polarized light.

1.8.4 Reflection From A Dielectric Interface

It is known that the reflection coefficients (magnitudes and phases) are functions of the angle of incidence [13]. The magnitude of the p-reflection coefficient r_p at a dielectric interface between two media with indices of refraction n_1 and n_0 goes to zero at a certain angle of incidence called the Brewster's angle ϕ_B as shown in figure 1.3. The value of this angle in terms of the refractive indices is given by [13]

$$\tan(\phi_B) = \frac{n_1}{n_0} \tag{1.51}$$

At this angle ϕ_B the p-component is totally refracted into the second medium while the reflected wave is purely s-polarized. On the other hand, the magnitude of the s-polarization reflection coefficient is greater than zero for all angles of incidence. The phases of the reflection coefficients are affected by changing the angle of incidence.

For a dielectric interface the value of δr_s remains constant at π for all angles of incidence but δr_p jumps from 2π to π at the Brewster's angle.

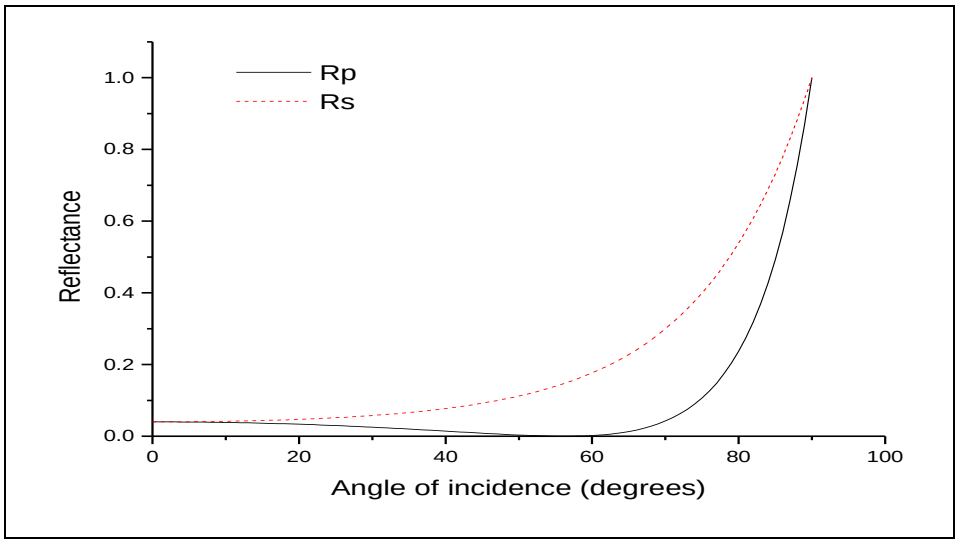

Figure 1.3. The intensity reflectance R_p and R_s of air/glass interface at λ =5461 Å, N=1.5 and ϕ_B =56.31 degrees.

1.8.5 Reflection From An Absorbing Material

The expressions for the p and s reflection coefficients from an absorbing material are the same as above. The p-reflection coefficient does not go to zero as the angle of incidence is changed. Instead, the reflectance r_p goes to minimum at a certain angle called the pseudo-Brewster angle ϕ_p as shown in figure 1.4. The value of this minimum depends on the extinction coefficient *k*. The following diagram shows this behavior for the air/gold interface.

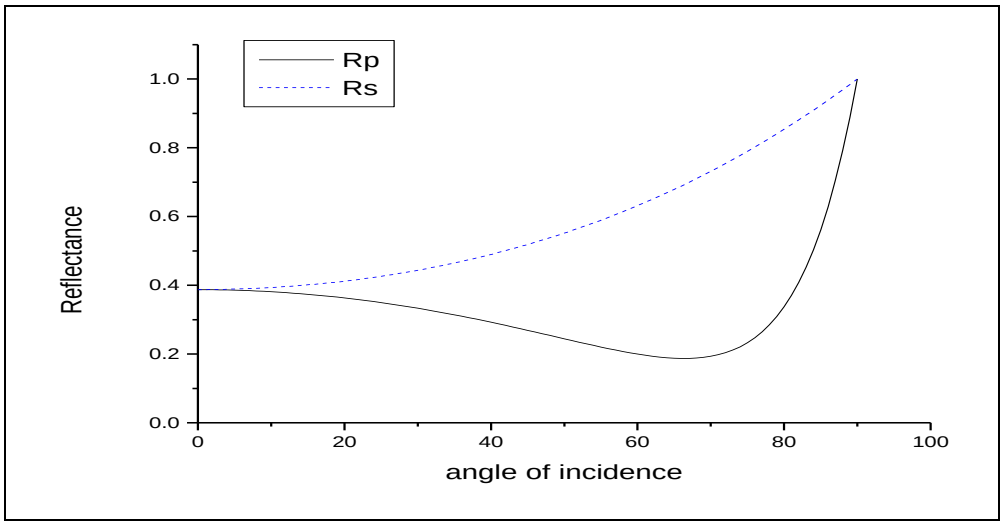

Figure 1.4. The intensity reflectance R_p and R_s of air/gold interface at λ =4400 Å, n=1.577-1.912i and the pseudo-Brewster's angle ϕ_p = 66 degrees.

1.9 Reflection And Transmission Of Polarized Light By A Single Film

Consider a film with parallel–plane boundaries and with thickness d on top of a substrate. Assume that the ambient, the film and the substrate are isotropic and homogeneous with indices of refraction N_0, N_1 and N_2 respectively as shown in figure 1.5. If a plane wave is incident at the 0-1 interface at an angle ϕ_0, then part will be reflected and the other part will be refracted into the film. This part will suffer multiple internal reflection between the 1-2 and 1-0 interfaces. A phase change of [13]

$$\beta = 2\pi \frac{d}{\lambda} N_1 \cos(\phi_1) . \qquad (1.52)$$

is added when light travels between the interfaces [13].

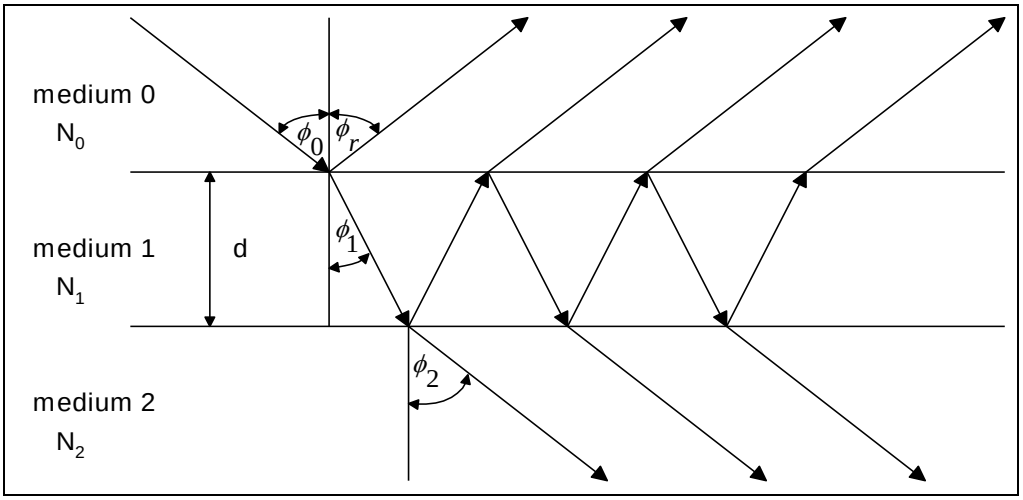

Figure 1.5. Multiple reflection and transmission in a parallel plate.

The total reflection coefficient of this system is given by [13]

$$r = \frac{r_{01} + r_{12}\exp(-2i\beta)}{1 + r_{01}r_{12}\exp(-2i\beta)}. \tag{1.53}$$

Similarly, the transmission coefficient is [13]

$$t = \frac{t_{01}t_{12}\exp(-2i\beta)}{1 + r_{01}r_{12}\exp(-2i\beta)}. \tag{1.54}$$

For p and s polarization, we have

$$r_p = \frac{r_{01p} + r_{12p}\exp(-2i\beta)}{1 + r_{01p}r_{12p}\exp(-2i\beta)}, \tag{1.55}$$

$$t_p = \frac{t_{01p}t_{12p}\exp(-2i\beta)}{1 + r_{01p}r_{12p}\exp(-2i\beta)}, \tag{1.56}$$

$$r_s = \frac{r_{01s} + r_{12s}\exp(-2i\beta)}{1 + r_{01s}r_{12s}\exp(-2i\beta)}, \tag{1.57}$$

$$t_s = \frac{t_{01s}t_{12s}\exp(-2i\beta)}{1 + r_{01s}r_{12s}\exp(-2i\beta)}, \tag{1.58}$$

where

$$r_{01p} = \frac{N_1\cos(\phi_0) - N_0\cos(\phi_1)}{N_1\cos(\phi_0) + N_0\cos(\phi_1)} \qquad r_{12p} = \frac{N_2\cos(\phi_1) - N_1\cos(\phi_2)}{N_2\cos(\phi_1) + N_1\cos(\phi_2)} \tag{1.59}$$

$$r_{01s} = \frac{N_0\cos(\phi_0) - N_1\cos(\phi_1)}{N_0\cos(\phi_0) + N_1\cos(\phi_1)} \qquad r_{12s} = \frac{N_1\cos(\phi_1) - N_2\cos(\phi_2)}{N_1\cos(\phi_1) + N_2\cos(\phi_2)} \tag{1.60}$$

$$t_{01p} = \frac{2N_0\cos(\phi_0)}{N_1\cos(\phi_0) + N_0\cos(\phi_1)} \qquad t_{12p} = \frac{2N_1\cos(\phi_1)}{N_2\cos(\phi_1) + N_1\cos(\phi_2)} \tag{1.61}$$

$$t_{01s} = \frac{2N_0\cos(\phi_0)}{N_0\cos(\phi_0) + N_1\cos(\phi_1)} \qquad t_{12s} = \frac{2N_1\cos(\phi_1)}{N_1\cos(\phi_1) + N_2\cos(\phi_2)} \tag{1.62}$$

The angles ϕ_0, ϕ_1 and ϕ_2 are related by Snell's law

$$N_0 \sin(\phi_0) = N_1 \sin(\phi_1) = N_2 \sin(\phi_2). \tag{1.63}$$

1.10. Introduction To Ellipsometry

The basic principles of ellipsometry have been established more than 100 years ago, but it has not become of high importance in science and technology until the 1990s because of its versatile applications in material characterization and thin film technology [1-12].

At the beginning, ellipsometers were single wavelength instruments. With the emergence of spectroscopic ellipsometry, the ellipsometry technique became of high importance to wide research areas from semiconductors to organic materials. Ellipsometers may, in general, contain light sources, polarizers, analyzers, depolarizers, compensators, samples to be studied, detectors, etc. When a sample is to be studied, it is located in the light path and the beam reflected or transmitted from the sample is collected and analyzed.

An ellipsometer measures the change in the polarization state of incident light. If linearly polarized light of known orientation is reflected from a surface, then the reflected light will be elliptically polarized. The shape and orientation of the ellipse depends on the angle of incidence, the direction of the polarized incident light, and the reflection properties of the surface. The two parameters ψ (the ratio of reflection coefficients) and Δ (phase change between p- and s-polarized lights) are determined in one single ellipsometric measurement. This makes it possible to obtain both the real and imaginary parts of the complex dielectric function of a homogeneous material. For a reflecting surface, the forms of Δ and ψ are given by [13].

$$\Delta = \delta_p - \delta_s \quad \text{and} \quad \tan\psi = \frac{|r_p|}{|r_s|}, \tag{1.64}$$

where δ_p and δ_s are the phase changes for the *p* and the *s* components of polarized light and r_p and r_s are the complex Fresnel reflection coefficients for the *p* and *s* components which may be written as [13]

$$\left.\begin{aligned} r_p &= \rho_p e^{i\delta_p} \\ r_s &= \rho_s e^{i\delta_s} \end{aligned}\right\}. \tag{1.65}$$

Ellipsometry allows for the determination of the complex reflectance ratio ρ of a surface. This quantity is defined as the ratio of p and s reflection coefficients, r_p and r_s respectively. Commonly, the reflectance ratio is expressed in terms of ψ and Δ as [13]

$$\rho = \frac{r_p}{r_s} = \tan(\psi) e^{i\Delta}. \tag{1.66}$$

The expressions for r_p and r_s for a single interface between medium 0 (ambient), with a complex refractive index N_0, and medium 1 (substrate), with a complex refractive index N_1 are given by Eq. (1.44) and Eq. (1.47).

1.11 Jones Formalism

A matrix representation called the Jones matrix allows the mathematical description of optical components. If we apply the Jones formalism, we can express variations in polarized light from matrix calculation, even when there are many optical elements in the structure. The Jones matrix is also utilized when we describe ellipsometry measurement mathematically. On the other hand, the Jones vector is used when we express states of polarization including linear and elliptical polarizations [13].

1.11.1 Jones Vector

Consider an electromagnetic wave propagates in the z-direction and the two components of **E** are given by [13]

$$E_x = E_{ox} \exp(i\delta_x), \tag{1.67}$$

$$E_y = E_{oy} \exp(i\delta_y). \tag{1.68}$$

Where E_{ox} and E_{oy} are the *x* and *y* components of electric field amplitude and the vector $E(z,t)$ may be written in terms of E_x and E_y in a column matrix as follows

$$E(z,t) = \begin{bmatrix} E_x \\ E_y \end{bmatrix}. \tag{1.69}$$

From Eq. (1.69) we can find the intensity as follow

$$I = \overline{E(z,t)}\,E(z,t) = E_x E_x^* + E_y E_y^* \tag{1.70}$$

Where $\overline{E(z,t)}$ is the transposed matrix of $E(z,t)$.

For example, linearly polarized light parallel to the x- and y-directions are expressed by

$$E_x = \begin{bmatrix} 1 \\ 0 \end{bmatrix}, \quad E_y = \begin{bmatrix} 0 \\ 1 \end{bmatrix} \tag{1.71}$$

The Jones vector that describes linearly polarized light oriented at +45 is written as,

$$E_{+45} = \frac{1}{\sqrt{2}} \begin{bmatrix} 1 \\ 1 \end{bmatrix} \tag{1.72}$$

On the other hand, right circular polarization E_R , and left circular polarization E_L is written as

$$E_R = \frac{1}{\sqrt{2}} \begin{bmatrix} 1 \\ i \end{bmatrix}, \quad E_L = \frac{1}{\sqrt{2}} \begin{bmatrix} 1 \\ -i \end{bmatrix} \tag{1.73}$$

The matrix that describes the elliptic polarized light can be written as

$$E_{elliptic} = \begin{bmatrix} \sin(\psi)e^{i\Delta} \\ \cos(\psi) \end{bmatrix} \tag{1.74}$$

1.11.2 Jones Matrices Of Optical Elements

The Jones matrix consists of a 2×2 square matrix. The optical elements to be considered as polarizer (analyzer) P(A), compensator (retarder) (C) and sample (B) are discussed in details as follows:

The Polarizer (Analyzer)

A polarizer is generally placed in front of the light source and is utilized to extract linearly polarized light from unpolarized light. On the other hand, an analyzer is placed in front of a light detector and the state of polarization is determined from the intensity of light transmitted through the analyzer. [13]

$$A = P = \begin{bmatrix} 1 & 0 \\ 0 & 0 \end{bmatrix} \tag{1.75}$$

The Compensator (Retarder)

A compensator (or retarder) is generally placed behind a polarizer or in front of an analyzer and is often employed to convert linear polarization to circular polarization and vice versa. The compensator generates a phase difference between the electric field vectors E_x and E_y. which is given by [13]

$$\delta = \frac{2\pi d}{\lambda}(n_e - n_o), \tag{1.76}$$

where d is the thickness of the compensator and n_e and n_o are respectively its extraordinary and ordinary refractive indices. The matrix of compensator (or retarder) is given by [13],

$$C = \begin{bmatrix} 1 & 0 \\ 0 & e^{-i\delta} \end{bmatrix} \tag{1.77}$$

An Isotropic Sample

The matrix of an isotropic sample can be written as [13]

$$B = \begin{bmatrix} \sin(\psi)e^{i\Delta} & 0 \\ 0 & \cos(\psi) \end{bmatrix} \tag{1.78}$$

The samples that are used in the next chapters are considered to be isotropic.

The Rotation Matrix

The rotation matrix $R(\vartheta)$ is given by [13],

$$R(\vartheta) = \begin{bmatrix} \cos(\vartheta) & \sin(\vartheta) \\ -\sin(\vartheta) & \cos(\vartheta) \end{bmatrix} \tag{1.79}$$

Where ϑ is the rotation angle.

1.12 Stokes Vector And Mueller Formalism

1.12.1 Stokes Vector

Jones vector is the most common method for describing polarized light. Unpolarized or partially polarized light can not be expressed by using Jones vector. In order to describe unpolarized or partially polarized light, Stokes parameters are usually used. These parameters are able to describe all types of polarizations. For an isotropic sample, a significant roughness of the surface induces depolarization and cross-polarization phenomena which affect the ellipsometric measurements. In these cases, the Jones formalism and the Jones matrix associated can not describe correctly the sample [13]. It is necessary to use the Mueller-stokes formalism. In actual ellipsometry measurement, Stokes parameters can be measured. In the Stokes vector representation, the optical elements are described by the so called Mueller matrix [13]. The Stokes-vector consists of four elements, S_0, S_1, S_2, and S_3, which can be expressed in terms of the intensities as,

$$S_0 = I_x + I_y, \tag{1.80}$$

$$S_1 = I_x - I_y, \tag{1.81}$$

$$S_2 = I_{+45} - I_{-45}, \tag{1.82}$$

$$S_3 = I_R - I_L, \tag{1.83}$$

$$S_0^2 = S_1^2 + S_2^2 + S_3^2, \tag{1.84}$$

where S_0 is the total intensity of the light beam. Eq. (1.84) represents a sphere of three dimension S_1, S_2 and S_3 with radius S_0 this sphere called a Pioncare sphere . The parameters I_x, I_y, and $I_{\pm 45}$ describe the intensities transmitted by a linear polarizer with its transmission axis in the x-, y-, $\pm\pi/4$-directions, respectively. On the other hand, I_R and I_L

are the intensities transmitted by a polarizer which transmits right handed and left handed circular polarized light, respectively.

The stokes vector is given by [13]

$$S = \begin{bmatrix} S_0 \\ S_1 \\ S_2 \\ S_3 \end{bmatrix} \tag{1.85}$$

The normalized Stokes vector assigns S_0 to be 1 for various polarizations. For example, the linear polarization in the x direction is represented by $S_0 = S_1 = 1$, while the linear polarization in the y direction is denoted by $S_0 = 1$ and $S_1 = -1$. The Stokes vector for elliptical polarization is expressed by using the (ψ, Δ) coordinate system given by Eq. (1.86) can be expressed as [13]

$$S = \begin{bmatrix} 1 \\ -\cos(2\psi) \\ \sin(2\psi)\cos(\Delta) \\ -\sin(2\psi)\sin(\Delta) \end{bmatrix}. \tag{1.86}$$

The unpolarized light using Stokes vector is given by

$$S = \begin{bmatrix} 1 \\ 0 \\ 0 \\ 0 \end{bmatrix} \tag{1.87}$$

1.12.2 Mueller Formalism

The effect of an optical element on the polarization state of light is usually described by a 4 × 4 Muller matrix. In the following, we express these matrices associated with the optical elements employed in the proposed ellipsometric structure [13].

The rotation matrix with an angle α, $R(\alpha)$ is given by

$$R(\alpha)=\begin{bmatrix}1 & 0 & 0 & 0\\ 0 & \cos(2\alpha) & \sin(2\alpha) & 0\\ 0 & -\sin(2\alpha) & \cos(2\alpha) & 0\\ 0 & 0 & 0 & 1\end{bmatrix}. \tag{1.88}$$

The matrix of an ideal fixed polarizer or analyzer P or A is

$$P=A=\frac{1}{2}\begin{bmatrix}1 & 1 & 0 & 0\\ 1 & 1 & 0 & 0\\ 0 & 0 & 0 & 0\\ 0 & 0 & 0 & 0\end{bmatrix}. \tag{1.89}$$

The matrix of an ideal fixed compensator C is

$$C=\begin{bmatrix}1 & 0 & 0 & 0\\ 0 & 1 & 0 & 0\\ 0 & 0 & \cos(\delta) & \sin(\delta)\\ 0 & 0 & -\sin(\delta) & \cos(\delta)\end{bmatrix}. \tag{1.90}$$

The matrix of an ideal sample B is

$$B=\begin{bmatrix}1 & -\cos(2\psi) & 0 & 0\\ -\cos(2\psi) & 1 & 0 & 0\\ 0 & 0 & \sin(2\psi)\cos(\Delta) & \sin(2\psi)\sin(\Delta)\\ 0 & 0 & -\sin(2\psi)\sin(\Delta) & \sin(2\psi)\cos(\Delta)\end{bmatrix}. \tag{1.91}$$

An Example

a) Using Mueller Formalism

If the unpolarized light incident on a polarizer with angle α then we get a linear polarization with angle α by the multiplication of matrices as follows: we begin from right, the matrix of unpolarized light S_{in} multiplied by the polarizer matrix (P) multiplied by the rotation matrix R(α) and multiplied by P to get by detector the output Stokes vector S_{out}

$$S_{out} = P\,R(\alpha)\,P\,S_{in} \tag{1.92}$$

$$S_{out} = \frac{1}{2}\begin{bmatrix} 1 & 1 & 0 & 0 \\ 1 & 1 & 0 & 0 \\ 0 & 0 & 0 & 0 \\ 0 & 0 & 0 & 0 \end{bmatrix}\begin{bmatrix} 1 & 0 & 0 & 0 \\ 0 & \cos(2\alpha) & \sin(2\alpha) & 0 \\ 0 & -\sin(2\alpha) & \cos(2\alpha) & 0 \\ 0 & 0 & 0 & 1 \end{bmatrix}\frac{1}{2}\begin{bmatrix} 1 & 1 & 0 & 0 \\ 1 & 1 & 0 & 0 \\ 0 & 0 & 0 & 0 \\ 0 & 0 & 0 & 0 \end{bmatrix}\begin{bmatrix} 1 \\ 0 \\ 0 \\ 0 \end{bmatrix} \tag{1.93}$$

$$S_{out} = \frac{1}{2}\begin{bmatrix} \cos^2(\alpha) \\ \cos^2(\alpha) \\ 0 \\ 0 \end{bmatrix} \tag{1.94}$$

The detected intensity is obtained from the first element of the Stokes vector S_{out}, namely S_0 then

$$I = S_0 = \frac{1}{2}\cos^2(\alpha) \tag{1.95}$$

Relation (1.95) is known as Malus's law, which is illustrated in Figure (1.6) shows the intensity as a function of rotation angle of the polarizer.

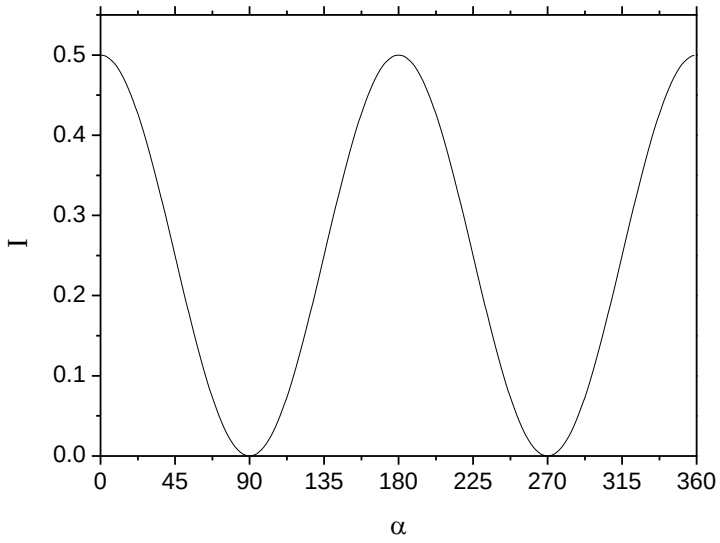

Figure. 1.6. The calculated intensity as a function of rotation angle of the polarizer.

b) Using Jones Formalism

We can find the same result using Jones formalism by the same way as follows,

$$L_{out} = \begin{bmatrix} E_x \\ E_y \end{bmatrix} = \begin{bmatrix} 1 & 0 \\ 0 & 0 \end{bmatrix} \begin{bmatrix} \cos(\alpha) & \sin(\alpha) \\ -\sin(\alpha) & \cos(\alpha) \end{bmatrix} \begin{bmatrix} 1 & 0 \\ 0 & 0 \end{bmatrix} \begin{bmatrix} 1 \\ 0 \end{bmatrix} \tag{1.96}$$

The intensity given by multiplying the output transposed matrix $\overline{L_{out}}$ by L_{out} is

$$I = \overline{L_{out}} L_{out} \tag{1.97}$$

$$I = \frac{1}{2}\cos^2(\alpha) \tag{1.98}$$

CHAPTER TWO

A Spectroscopic Ellipsometer Using Rotating Polarizer And Analyzer At A Speed Ratio 1:1 And A Fixed Compensator

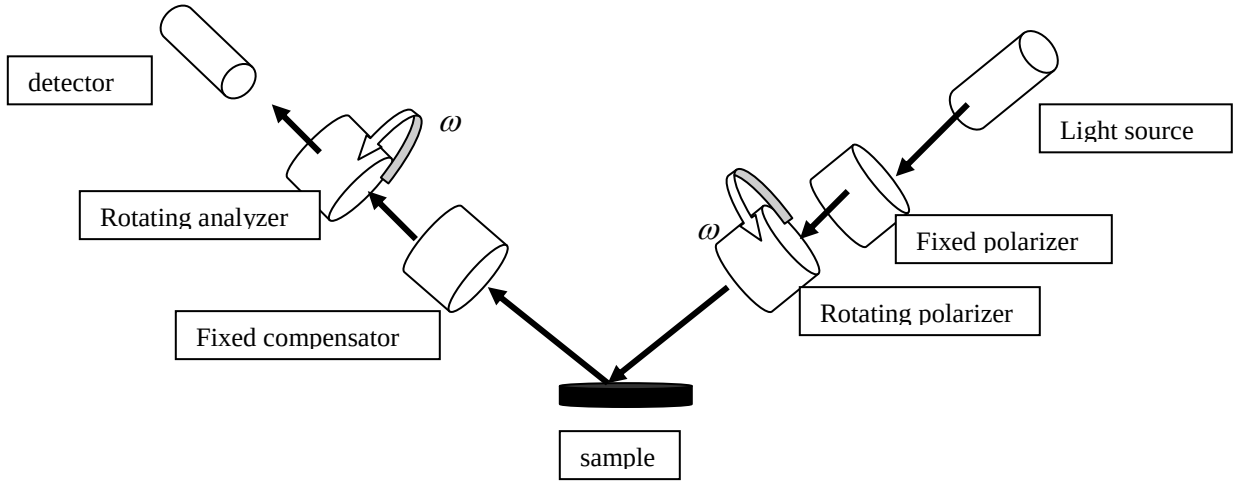

Figure 2.1 Optical configuration of ellipsometry, rotating polarizer and analyzer with speed ratio 1:1

In this chapter a rotating polarizer and analyzer ellipsometer at a speed ratio 1:1 with a fixed compensator placed just after the rotating polarizer is proposed. The calculations of the optical properties of c-Si, SiO_2, and GaAs reveal a substantial decrease in the absolute error due to the fixed compensator. The uncertainties in the ellipsometric parameters as functions of the uncertainties of the Fourier coefficients are presented in details.

2.1. Rotating Polarizer And Analyzer Ellipsometer With A Fixed Compensator

The azimuth angle of the rotating polarizer is assumed to be $\beta_P = \omega t$ and that of the rotating analyzer is assumed to have the form $\beta_A = \omega t$. The fast axis of the compensator is assumed to have an angle β_c with the *p*-polarization. In the rotating polarizer-analyzer configuration, and using the matrices in Eqs. (1.88-1.91), the Stokes vector of the detected light is given by

$$S = R(-\beta_A)\, A\, R(\beta_A)\, B R(-\beta_c)\, C R(\beta_c)\, R(-\beta_P)\, P\, R(\beta_P)\, P\, S_i \qquad (2.1)$$

where $S_i = [1,0,0,0]^T$. The product of all matrices in the right hand side of Eq. (2.1) yields a four-element column vector which is denoted by S. The vector S represents the total effect the incident light undergoes as a result of crossing the elements of the proposed structure. The elements of the vector *S* are called Stokes parameters S_0, S_1, S_2, and S_3.

Two special cases of the orientation of the fixed compensator will be considered.

2.1.1 Case I: $\beta_c = 0^\circ$

After performing the product of matrices given by Eq. (2.1) and rearranging the result, the elements S_0, S_1, S_2, and S_3 are found to have the forms

$$\begin{aligned} S_0 &= [1-\frac{1}{2}\cos(2\psi)] + [1-\cos(2\psi)]\cos(2\omega t) - \frac{1}{2}\cos(2\psi)\cos(4\omega t) \\ &+ [\frac{1}{2} - \cos(2\psi)]\cos(2\omega t) \\ &+ \frac{1}{2}[1-\cos(2\psi) - \sin(2\psi)\cos(\Delta-\delta)]\cos 4\omega t \\ &+ \frac{1}{2}[1-\cos(2\psi) + \sin(2\psi)\cos(\Delta-\delta)] \\ &+ \frac{1}{4}[1-\sin(2\psi)\cos(\Delta-\delta)]\cos 6\omega t \\ &+ \frac{1}{4}[1+\sin(2\psi)\cos(\Delta-\delta)]\cos 2\omega t, \end{aligned} \tag{2.2}$$

$$S_1 = S_0 \cos(2\omega t), \tag{2.3}$$

$$S_2 = S_0 \sin(2\omega t), \tag{2.4}$$

$$S_3 = 0\,. \tag{2.5}$$

The detected light intensity is given as

$$I = S_0 \tag{2.6}$$

The Fourier transform of the detected intensity generates a DC term and three AC terms which may be written as

$$I(t) = a_0 + \sum_{n=1}^{3} a_n \cos(2n\omega t)\,. \tag{2.7}$$

The coefficients a_0, a_1, a_2, and a_3 are given by

$$a_0 = [\frac{3}{2} - \cos(2\psi) + \frac{1}{2}\sin(2\psi)\cos(\Delta - \delta)], \tag{2.8}$$

$$a_1 = [\frac{7}{4} - 2\cos(2\psi) + \frac{1}{4}\sin(2\psi)\cos(\Delta - \delta)], \tag{2.9}$$

$$a_2 = [\frac{1}{2} - \cos(2\psi) - \frac{1}{2}\sin(2\psi)\cos(\Delta - \delta)], \tag{2.10}$$

$$a_3 = \frac{1}{4}[1 - \sin(2\psi)\cos(\Delta - \delta)]\,. \tag{2.11}$$

Solving the last three equations for ψ and $\Delta - \delta$ in terms of a_1, a_2 and a_3, we get,

$$\tan(\psi) = \sqrt{\frac{2a_1 + 2a_3}{2a_1 - 8a_2 + 18a_3}}, \tag{2.12}$$

$$\cos(\Delta - \delta) = \frac{a_1 - 2a_2 - 3a_3}{\sqrt{a_1 + a_3}\sqrt{a_1 - 4a_2 + 9a_3}}. \tag{2.13}$$

As expected, the comparison between Eqs. (2.12) and (2.13) with the corresponding ones in [25] reveals that the fixed compensator has no impact on ψ but it shifts the phase change Δ by an angle δ.

With the above expressions, it is now possible to investigate the uncertainties δψ and δΔ in ψ and Δ, respectively, as functions of system parameters and the uncertainties of the Fourier coefficients. The uncertainties δψ and δΔ represent the fluctuations of ψ and Δ about their ideal values. In practical applications δψ and δΔ are not of highly interest but the uncertainties of sample parameters, such as the layer thicknesses and the index of refraction that are calculated from ψ and Δ. However, investigation at the sample-parameter level is unrealistic due to the huge number of possible sample configurations [21]. Thus, the uncertainty is usually addressed as δψ and δΔ or in some cases as $\delta\rho = [\delta(\tan\psi) + i\,\delta\Delta\,\tan\psi]e^{i\Delta}$. The use of δΔ overestimates the importance of Δ, which becomes particularly apparent as either r_p or r_s approaches zero. At r_p or r_s = 0, Δ is completely indeterminate [21]. However, this indeterminate in Δ does not map over into a total uncertainty in the parameters of the sample parameters. Concerning δρ, it has two disadvantages. First, it does not reveal the individual contribution of δψ and δΔ. Second, it diverges as ψ = 0^o. To calculate δψ and δΔ, Eqs. (2.12) and (2.13) are differentiated with respect a_j (j = 1, 2, 3) while keeping the other coefficients as constants, which gives that

$$\frac{\delta\psi}{\delta a_1} = \frac{a_2 - 2a_3}{\sqrt{a_1 + a_3}\sqrt{a_1 - 4a_2 + 9a_3}(-a_1 + 2a_2 - 5a_3)}, \tag{2.14}$$

$$\frac{\partial \psi}{\partial a_2} = \frac{-(a_1 + a_3)}{\sqrt{a_1 + a_3}\sqrt{a_1 - 4a_2 + 9a_3}(-a_1 + 2a_2 - 5a_3)}, \tag{1.15}$$

$$\frac{\partial \psi}{\partial a_3} = \frac{2a_1 + a_2}{\sqrt{a_1 + a_3}\sqrt{a_1 - 4a_2 + 9a_3}(-a_1 + 2a_2 - 5a_3)}, \tag{2.16}$$

$$\frac{\partial \Delta}{\partial a_1} = \frac{4a_1a_3 + 12(a_3)^2 - 2(a_2)^2}{(a_1 + a_3)\,(-a_1 + 4a_2 - 9a_3)(4a_1a_3 - 4a_3a_2 - (a_2)^2)}, \tag{2.17}$$

$$\frac{\partial \Delta}{\partial a_2} = \frac{2a_2 - 12a_3}{(-a_1 + 4a_2 - 9a_3)(4a_1a_3 - 4a_3a_2 - (a_2)^2)}, \tag{2.18}$$

$$\frac{\partial \Delta}{\partial a_3} = \frac{-4(a_1)^2 + 12a_1a_2 - 12a_1a_3 + 12a_3a_2 - 2(a_2)^2}{(a_1 + a_3)\,(-a_1 + 4a_2 - 9a_3)(4a_1a_3 - 4a_3a_2 - (a_2)^2)}. \tag{2.19}$$

2.1.2 Case II: $\beta_c = 45^\circ$

The light intensity given by Eq. (2.2) is derived based on considering the offset angle of the compensator is set to zero. On the other hand, if we assume β_c =45 then another set of three AC terms emerge in addition to a_1, a_2 and a_3 and Eq. (2.1) reads

$$I = a_0 + \sum_{n=1}^{3} a_n \cos(2n\omega t) + \sum_{n=1}^{3} b_n \sin(2n\omega t), \tag{2.20}$$

where

$$a_1 = 1 - \cos(2\psi)\cos(\delta) - \cos(2\psi) + \frac{6}{8}\cos(\delta) + \frac{1}{4}\sin(2\psi)\cos(\Delta), \tag{2.21}$$

$$a_2 = -\frac{1}{2}\cos(2\psi)\cos(\delta) - \frac{1}{2}\cos(2\psi) + \frac{1}{2}\cos(\delta) - \frac{1}{2}\sin(2\psi)\cos(\Delta), \tag{2.22}$$

$$a_3 = \frac{1}{4}\cos(\delta) - \frac{1}{4}\sin(2\psi)\cos(\Delta), \tag{2.23}$$

$$b_1 = \frac{1}{4}\sin(2\psi)\sin(\Delta)\sin(\delta), \tag{2.24}$$

$$b_2 = \frac{1}{2}\sin(2\psi)\sin(\Delta)\sin(\delta), \tag{2.25}$$

$$b_3 = \frac{1}{4}\sin(2\psi)\sin(\Delta)\sin(\delta). \tag{2.26}$$

Only three coefficients are required to calculate the ellipsometric parameters. Considering again a_1, a_2 and a_3 and solving Eqs. (2.21), (2.22), and (2.23), ψ and Δ will be given by

$$\tan(\psi) = \sqrt{\frac{2a_1 + 2a_3}{2a_1 - 8a_2 + 18a_3}}, \tag{2.27}$$

$$\cos(\Delta) = \frac{2\left(a_1 - 2a_2 + a_3 - \frac{4}{\cos(\delta)}a_3\right)\cos(\delta)}{\sqrt{2a_1 + 2a_3}\sqrt{2a_1 - 8a_2 + 18a_3}}. \tag{2.28}$$

Comparing Eqs. (2.12) and (2.13) with Eqs. (2.27) and (2.28) shows that ψ does not depend on β_c but Δ does.

Differentiating Eqs. (2.27) and (2.28) with respect a_j (j = 1, 2, 3) while keeping the other coefficients as constants yields the uncertainties $\delta\psi$ and $\delta\Delta$. The same results for $\delta\psi$, as

those appearing in Eqs. (2.14)-(2.16), are obtained. but for δΔ the following results are obtained.

$$\frac{\partial \Delta}{\partial a_1} = -\frac{2\,Q - \dfrac{F\,Q}{2a_1 + 2a_3} - \dfrac{F\,Q}{2a_1 - 8a_2 + 18a_3}}{\sqrt{1 - Q^2 F^2}}, \tag{2.29}$$

$$\frac{\partial \Delta}{\partial a_2} = \frac{4Q - \dfrac{4F\,Q}{2a_1 - 8a_2 + 18a_3}}{\sqrt{1 - Q^2 F^2}}, \tag{2.30}$$

$$\frac{\partial \Delta}{\partial a_3} = -\frac{\left(2 - \dfrac{8}{\cos(\delta)}\right) Q - \dfrac{F\,Q}{2a_1 + 2a_3} - \dfrac{9F\,Q}{2a_1 - 8a_2 + 18a_3}}{\sqrt{1 - Q^2 F^2}}, \tag{2.31}$$

where

$$Q = \frac{\cos(\delta)}{\sqrt{2a_1 + 2a_3}\sqrt{2a_1 - 8a_2 + 18a_3}}, \tag{2.32}$$

$$F = 2a_1 - 4a_2 + 2a_3 - \frac{8a_3}{\cos(\delta)}. \tag{2.33}$$

2.2. Results And Discussions

A sample, consisting of one interface separating a semi-infinite air layer of refractive index N_0 as an ambient and a bulk c-Si material of refractive index N_1, is considered. The incidence angle is taken to be 70^o. Phase retarders mainly made from a $CaCO_3$ crystal (calcite) are rarely used as compensator. This is because the value of $|n_e - n_o|$ is quite large in calcite. Therefore, the thickness required for making a compensator becomes too thin. Thus, in spectroscopic ellipsometry measurement, compensators made

from MgF_2 and mica have been employed [13]. In particular, MgF_2 (transmission wavelength > 120 nm) shows superior light transmittance in the UV region, compared with mica (transmission wavelength > 290 nm). In recent years, therefore, MgF_2 compensators have been used widely. Consequently, A zero-order MgF_2 compensator centered at 4 eV is considered. The extraordinary and ordinary refractive indices of the compensator are taken from Palik [35].

Fourier transform of the generated signal was taken to extract the coefficients a_0 through a_3. Eqs. (2.12) and (2.13) are used to calculate the ellipsometric parameters ψ and Δ in the photon energy range 1.5 – 6 eV. These values of the ellipsometric parameters correspond to the clean signal without considering any noise. In practical situations, random fluctuations in the recorded signal appear due to the noise. In order to simulate real signals, noise was generated using MathCAD code and was superimposed on the clean signal according to the following equation

$$I_{noise} = (rnd(c) - c/2)I + (rnd(e) - e/2) + 0.0001 I_{\max}, \qquad (2.34)$$

where MathCAD's *rnd*(*c*) function produces uniform random noise in the range from 0 to *c* and *rnd*(*e*) function produces uniform random noise in the range from 0 to *e*. Figure 1 shows the noise superimposed on the clean signal. In the simulation, we take $c = e = 1$. Considering higher values for *c* and *e* will increase the noise level.

The first term in the right hand side of Eq. (2.34) represents the random noise recorded by the detector due to the thermal fluctuations of the light source after passing through the system, the second corresponds to Johnson noise and shot noise encountered in the detector and readout electronics, and the third term represents the dc offset due to long time drifts.

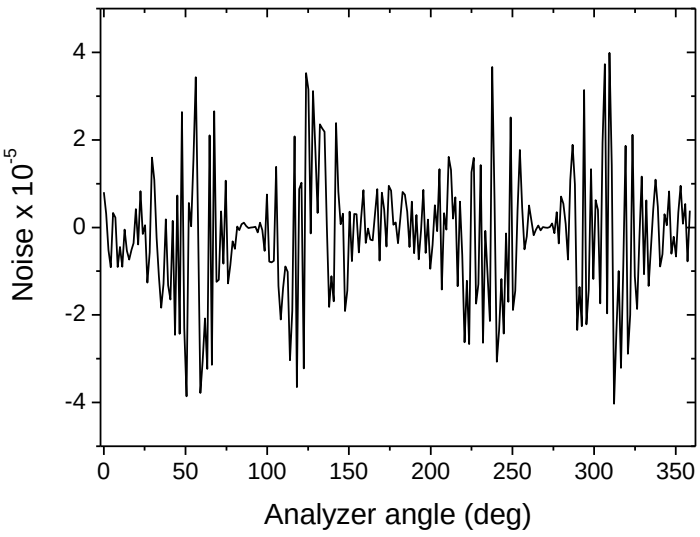

Figure 2.2. Noise superimposed on the clean signal.

This noise is added to the pure signal. Fourier transform of the noisy signal is taken to extract the new coefficients a_0 through a_3 in the presence of the noise. Eqs. (2.12) and (2.13) are used again to calculate the ellipsometric parameters ψ and Δ for the noisy signal in the same photon energy range.

To calculate the complex refractive index of the sample, the well known equation is used [13]

$$\varepsilon_r = \sin^2\theta_0 + \sin^2\theta_0 \tan^2\theta_0 \left(\frac{1-\rho}{1+\rho}\right)^2, \qquad (2.35)$$

where $\rho = \frac{r_p}{r_s} = \tan\psi\, e^{i\Delta}$, $\varepsilon_r = \varepsilon_1 + i\varepsilon_2$, $N = \sqrt{\varepsilon} = n + ik$, $\varepsilon_1 = n^2 - k^2$, and $\varepsilon_2 = 2nk$.

The calculated and the published [35] values of *n* and *k* for c-Si are plotted in Fig. 2.2. The points in Fig. 2.2 represent the calculated real and imaginary parts of the refractive

index of c-Si using the noisy signal for $\beta_c = 0^o$. To show the noise effect on the results obtained from the structure without a fixed compensator and those obtained from the present structure with a fixed compensator, the matrix of the compensator in the above mathematical argument is replaced with a unit matrix and *n* and *k* for c-Si are calculated again. The absolute error in *n* and *k* relative to the published values [35] are then calculated for both structures. Figure 2.3 shows the absolute error in *n* of c-Si as a function of energy in the photon energy range 1.5 to 6 eV for the proposed ellipsometric structure without and with a compensator for $\beta_c = 0^o$ and $\beta_c = 45^o$ whereas Fig. 2.4 shows the same for the extinction factor k. Generally, the absolute error in *n* is very small in the presence and absence of the compensator with a little preference to the structure comprising the compensator for $\beta_c = 0^o$. The most striking feature for the structure including the compensator can be obviously seen in Fig. 2.4. The absolute error in *k* is relatively high for the structure without the compensator. This error can be drastically reduced with the introduction of a compensator between the rotating polarizer and the sample.

Moreover, the proposed structure is tested for two additional samples; namely silicon dioxide (SiO_2) and gallium arsenide (GaAs). The calculated and published values of the refractive index of SiO_2 using the proposed ellipsometric structure are plotted in Fig. 2.5. In Fig. 2.6, the absolute error in *n* of SiO_2 as a function of energy is plotted for the proposed structure without and with a compensator for $\beta_c = 0^o$. In both ellipsometric configurations, the absolute error in *n* is very small with a clear preference to the structure including the compensator. On the other hand, the calculated and published values of *n* and *k* of GaAs are shown in Fig. 2.7. Figures 2.8 and 2.9 show, respectively, the absolute error in *n* and *k* of GaAs versus the energy. The reduction in the absolute error in the presence of the compensator is obvious for the three samples.

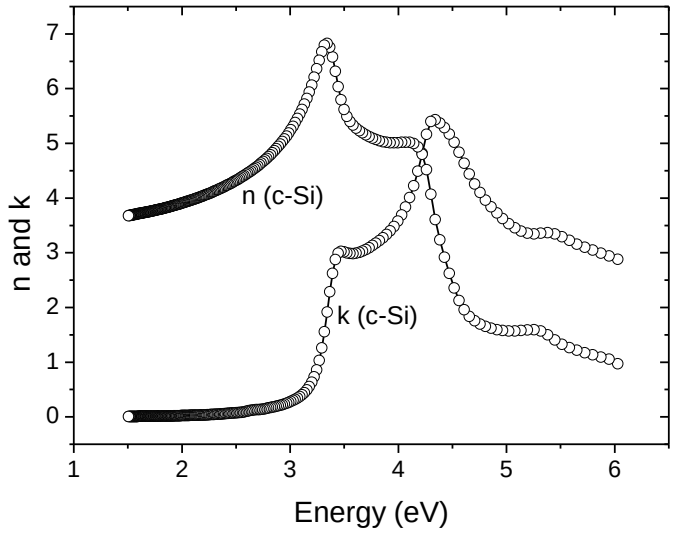

Figure. 2.3. The real and the imaginary parts of the refractive index of c-Si in the photon range 1.5 to 6 eV. Lines: accepted values, Points: calculated values.

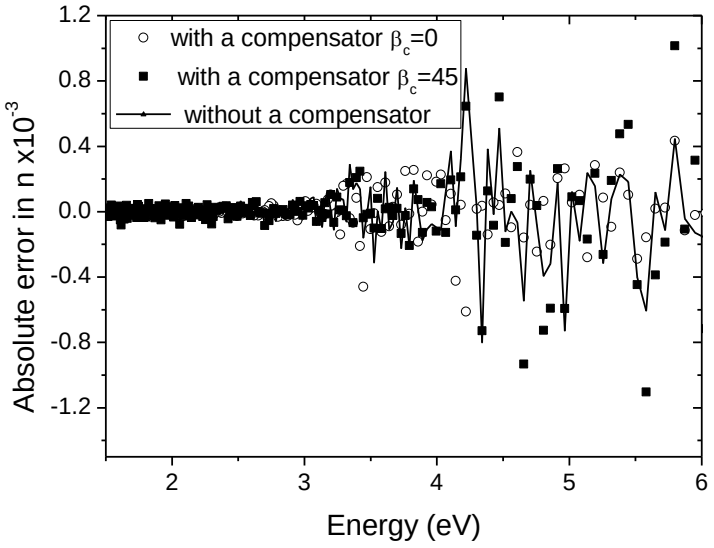

Figure. 2.4. Absolute error in the real part of the refractive index of c-Si in the photon range 1.5 to 6 eV.

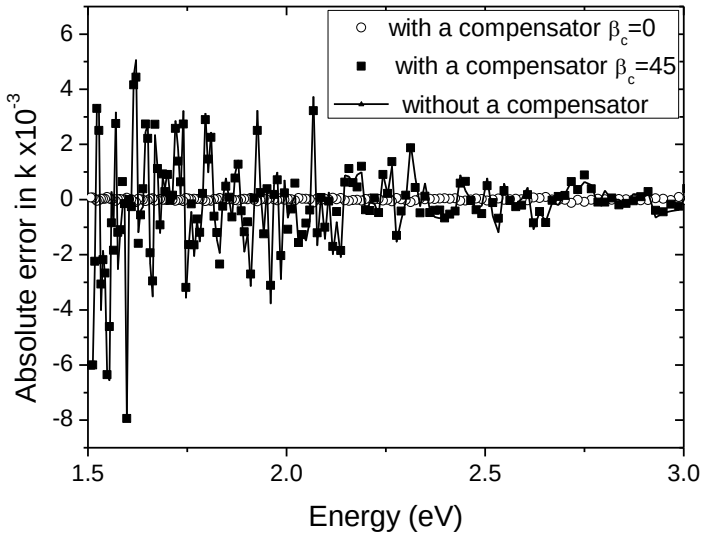

Figure. 2.5. Absolute error in the imaginary part of the refractive index of c-Si in the photon range 1.5 to 3 eV.

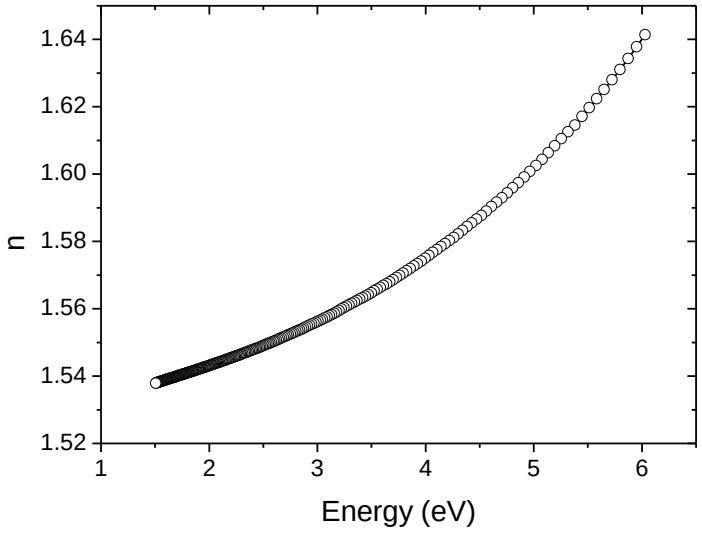

Figure. 2.6. The real part of the refractive index of SiO_2 in the photon range 1.5 to 6 eV. Lines: accepted values, Points: calculated values.

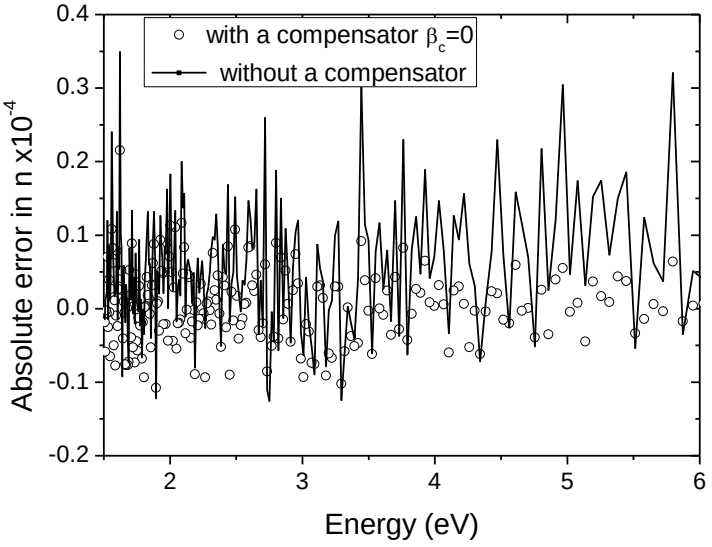

Figure. 2.7. Absolute error in the real part of the refractive index of SiO_2 in the photon range 1.5 to 6 eV.

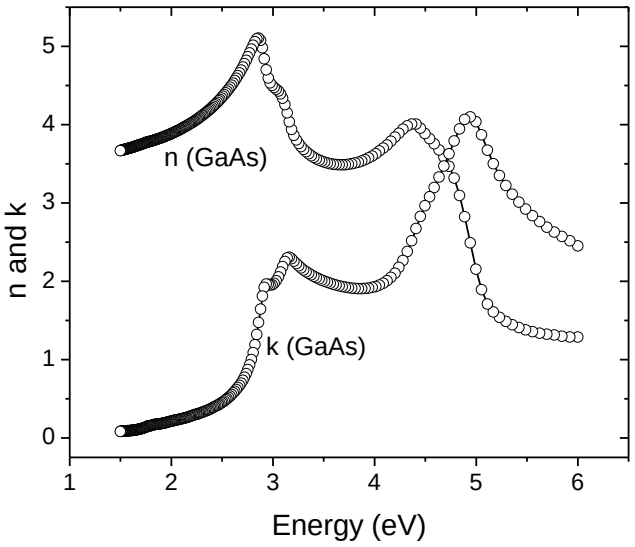

Figure 2.8. The real and imaginary parts of the refractive index of GaAs in the photon range 1.5 to 6 eV. Lines: accepted values, Points: calculated values.

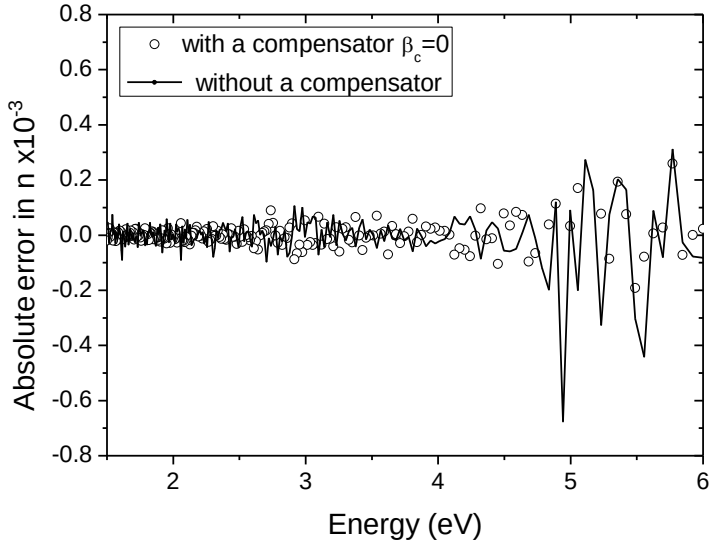

Figure 2.9. Absolute error in the real part of the refractive index of GaAs in the photon range 1.5 to 6 eV.

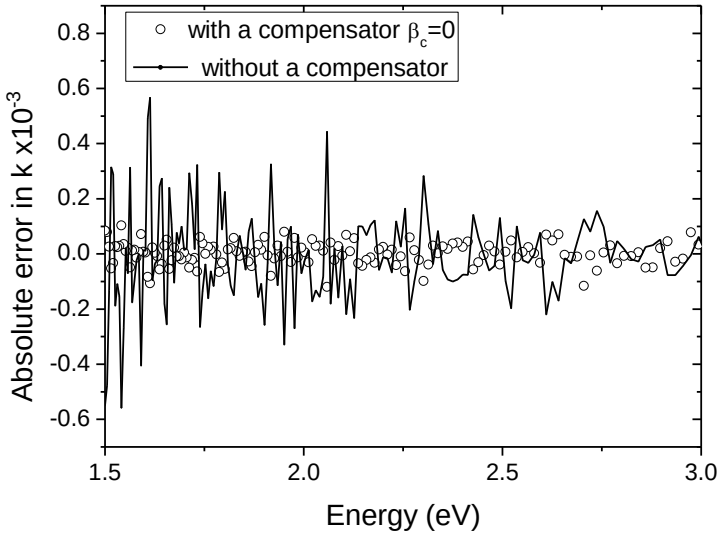

Figure 2.10. Absolute error in imaginary part of the refractive index of GaAs in the photon range 1.5 to 3 eV.

The uncertainty of ψ to the coefficients a_1, a_2, and a_3 is shown in Fig. 2.10 for c-Si in the photon energy range 1.5-6 eV for two values of β_c. The ellipsometric parameter ψ exhibits a little sensitivity to the uncertainties of the Fourier coefficients with a relatively high sensitivity of ψ at low energies compared to the high energy region. Moreover, ψ is less sensitive to a_2 compared to a_1 and a_3. On the other hand, this uncertainty is independent on the value of the compensator offset β_c. Moreover, if Fig. 2.10 shows that this sensitivity is also independent of the presence compensator. The uncertainty of ψ is the same regardless of the presence of the compensator. Figures 2.11 and 2.12 show the uncertainty of Δ to the coefficients a_1, a_2, and a_3 for $\beta_c = 0^o$ and $\beta_c = 45^o$, respectively. The ellipsometric parameter Δ exhibits a high sensitivity to the uncertainties of the Fourier coefficients compared to ψ. This sensitivity of Δ is much higher at low energies compared to the high energy region. Moreover, Δ is very sensitive to a_1 and a_2 with an important feature: the sensitivity to a_2 is positive whereas it is negative to a_1. This effect has the advantage of reducing the whole sensitivity of Δ. This can be attributed to the fact that the total change in Δ is given by the sum of all partial changes due to the change in a_j, that is, $d\Delta = \frac{\partial \Delta}{\partial a_1} da_1 + \frac{\partial \Delta}{\partial a_2} da_2 + \frac{\partial \Delta}{\partial a_3} da_3$. The effect of the value of the compensator offset is very crucial in the uncertainty of Δ. Fig. 2.12, Δ exhibits much higher uncertainty than that in Fig. 2.11.

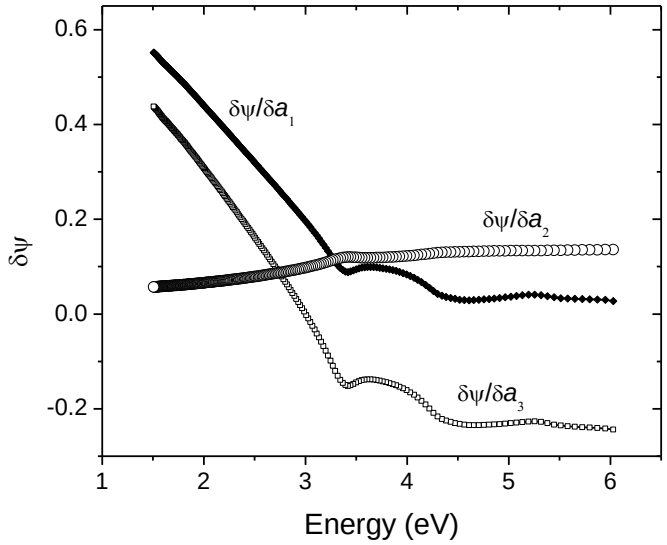

Figure 2.11. The uncertainty of ψ to a_1, a_2 and a_3 of c-Si in the photon range 1.5 to 6 eV. Lines represent the case when $\beta_c = 0^o$ while points represent the case when $\beta_c = 45^o$.

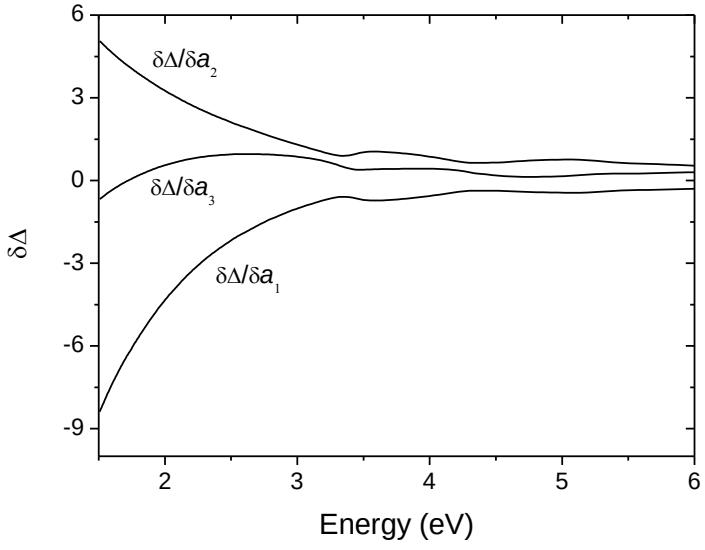

Figure 2.12. The uncertainty of Δ to a_1, a_2 and a_3 of c-Si in the photon range 1.5 to 6 eV for $\beta_c = 0^o$.

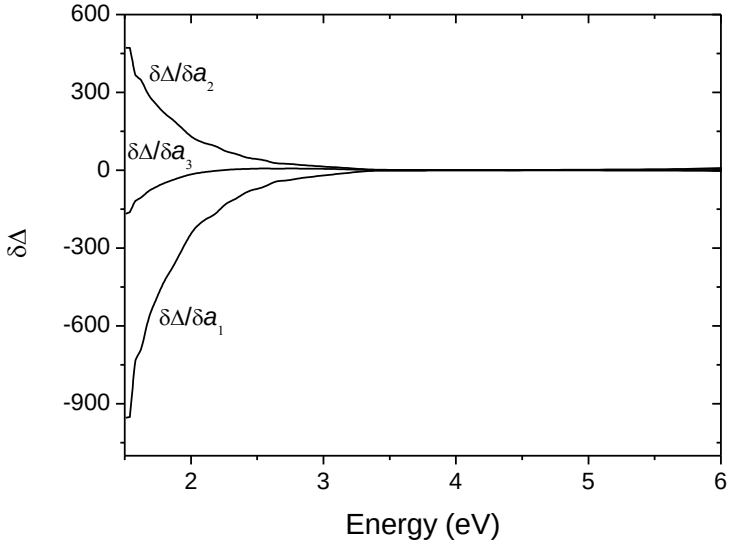

Figure 2.13. The uncertainty of Δ to a_1, a_2 and a_3 of c-Si in the photon range 1.5 to 6 eV for $\beta_c = 45^o$.

As mentioned in the section 2.1, extracting the ellipsometric parameters ψ and Δ from the AC Fourier coefficients without relying on the DC component is considered one of the significant advantages of the of proposed ellipsometer. It is worth to investigate the effect of the DC term by considering a set of three coefficients including a_0. Solving Eqs. (2.8), (2.10), and (2.11) for ψ and Δ in terms of a_0, a_2 and a_3, gives

$$\tan(\psi) = \sqrt{\frac{a_0 + a_2}{a_0 - 3a_2 + 8a_3}}, \tag{2.36}$$

$$\cos(\Delta) = \frac{a_0 - a_2 - 4a_3}{2\sin(\psi)\cos(\psi)}, \tag{2.37}$$

To calculate δψ and δΔ, Eqs. (2.36) and (2.37) are differentiated with respect a_j while keeping the other coefficients as constants.these uncertainties are given by

$$\frac{\partial \Delta}{\partial a_0} = \frac{-1}{2\sin(\Delta)\sin(\psi)\cos(\psi)}\left[1 - \frac{\cos(\Delta)}{2}\left(\tan(\psi) + \cot(\psi)\right)\right], \tag{2.38}$$

$$\frac{\partial \Delta}{\partial a_2} = \frac{1}{2\sin(\Delta)\sin(\psi)\cos(\psi)}\left[1 + \frac{\cos(\Delta)}{2}\left(-3\tan(\psi) + \cot(\psi)\right)\right], \tag{2.39}$$

$$\frac{\partial \Delta}{\partial a_3} = \frac{2}{\sin(\Delta)\sin(\psi)\cos(\psi)}\left[\cos(\Delta)\tan(\psi)\right], \tag{2.40}$$

$$\frac{\partial \psi}{\partial a_0} = \frac{1}{1+\tan^2(\psi)}\frac{\left(\cot(\psi) - \tan(\psi)\right)}{4\cos^2(\psi)}, \tag{2.41}$$

$$\frac{\partial \psi}{\partial a_2} = \frac{1}{1+\tan^2(\psi)}\frac{\left(\cot(\psi) + 3\tan(\psi)\right)}{4\cos^2(\psi)}, \tag{2.42}$$

$$\frac{\partial \psi}{\partial a_3} = \frac{2}{1+\tan^2(\psi)}\frac{1}{\cos(\psi)\sin(\psi)}. \tag{2.43}$$

The uncertainty of ψ to the coefficients a_0, a_2, and a_3 is shown in Fig. 2.13 for c-Si in the photon energy range 1.5-6 eV. In analogous to Fig. 2.10, the ellipsometric parameter ψ exhibits a little sensitivity to the uncertainties of the Fourier coefficients with a relatively high sensitivity of ψ at low energies compared to the high energy region. The advantage of excluding the DC term when calculating the ellipsometric parameters is obviously seen in the uncertainty of Δ. Figure 2.14 shows the uncertainty of Δ to the coefficients a_0, a_2, and a_3 for $\beta_c = 0^o$. Compared to Fig. 2.11, the ellipsometric parameter Δ exhibits a much

higher sensitivity to the uncertainties of the Fourier coefficients when the DC term is considered in the set from which ψ and Δ are calculated.

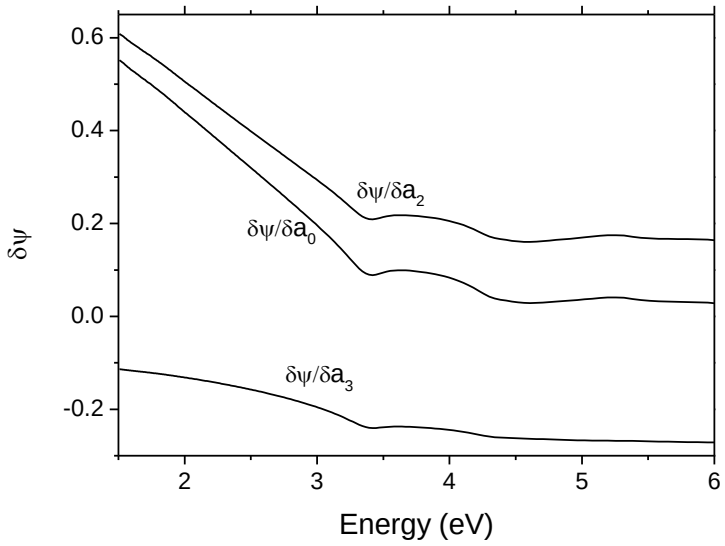

Figure 2.14. The uncertainty of ψ to a_0, a_2 and a_3 of c-Si in the photon range 1.5 to 6 eV for $\beta_c = 0^o$.

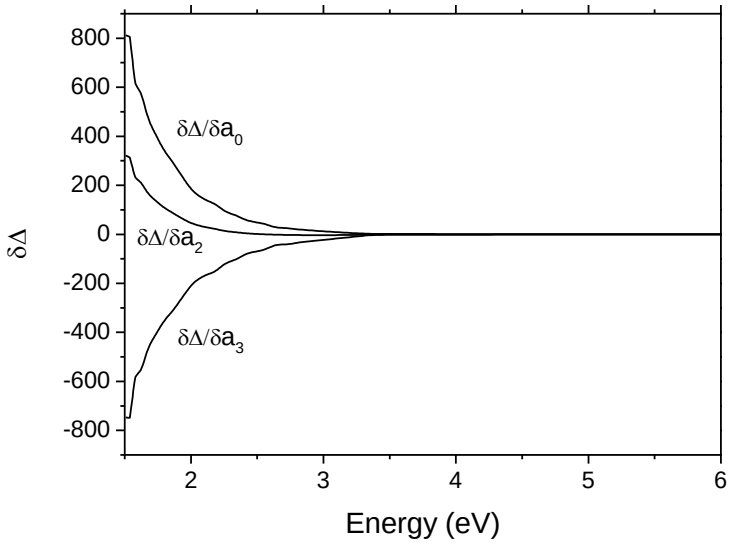

Figure 2.15. The uncertainty of Δ to a_0, a_2 and a_3 of c-Si in the photon range 1.5 to 6 eV for $\beta_c = 0^o$.

So far the proposed structure has been applied to bulk samples. It is instructive to check the feasibility of it for thin film characterization. The characterization of 10 nm SiO_2 thin film using the proposed structure with and without a compensator is presented theoretically. a structure consisting of air (ambient)/SiO_2 (thin film)/c-Si (substrate) is assumed. The SiO_2 film is assumed to have a refractive index N_1 and is sandwiched between an ambient (air) of refractive index N_0 and a Si substrate of refractive index N_2. The Fresnel reflection coefficients of the system are given by [13]

$$r_j = \frac{r_{01j} + r_{12j}\exp(-i2\beta)}{1 + r_{01j}r_{12j}\exp(-i2\beta)}, \qquad (2.44)$$

Where j stands for s in s-polarization and for p in p-polarization. The coefficients r_{01j} and r_{12j} are given by

$$r_{01s} = \frac{N_0 \cos(\theta_0) - N_1 \cos(\theta_1)}{N_0 \cos(\theta_0) + N_1 \cos(\theta_1)}, \tag{2.45}$$

$$r_{12s} = \frac{N_1 \cos(\theta_1) - N_2 \cos(\theta_2)}{N_1 \cos(\theta_1) + N_2 \cos(\theta_2)}, \tag{2.46}$$

$$r_{01p} = \frac{N_1 \cos(\theta_0) - N_0 \cos(\theta_1)}{N_1 \cos(\theta_0) + N_0 \cos(\theta_1)}, \tag{2.47}$$

$$r_{12p} = \frac{N_2 \cos(\theta_1) - N_1 \cos(\theta_2)}{N_2 \cos(\theta_1) + N_1 \cos(\theta_2)}. \tag{2.48}$$

The angle β is given by

$$\beta = \frac{2\pi d\, N_1 \cos(\theta_1)}{\lambda}, \tag{2.49}$$

Where θ_1 and θ_2 are the refraction angles in the sample and the substrate, respectively.

The ellipsometric parameters ψ and Δ are calculated in the presence and in the absence of a compensator. TFCompanion software (TFCompanion-optical metrology software obtained from Semiconsoft,Inc, USA) is then used to analyze the results and to extract the thickness and the refractive index of the sample. The film thickness and the optical constants of the film are calculated for the noisy signal in the spectrum range 200–900 nm. The results are compared with the proposed thickness and with the accepted values for SiO_2 optical constants. The calculated thickness obtained from TFCompanion software was 10 ± 0.8974 nm in the presence of a compensator and 10 ± 0.9195 in the absence of a compensator. Moreover, the spectroscopic calculations of the refractive index of the SiO_2 film in the spectral range 200 nm to 900 nm are shown in Fig. 2.15. The preference of the structure comprising the compensator over the other one is obvious.

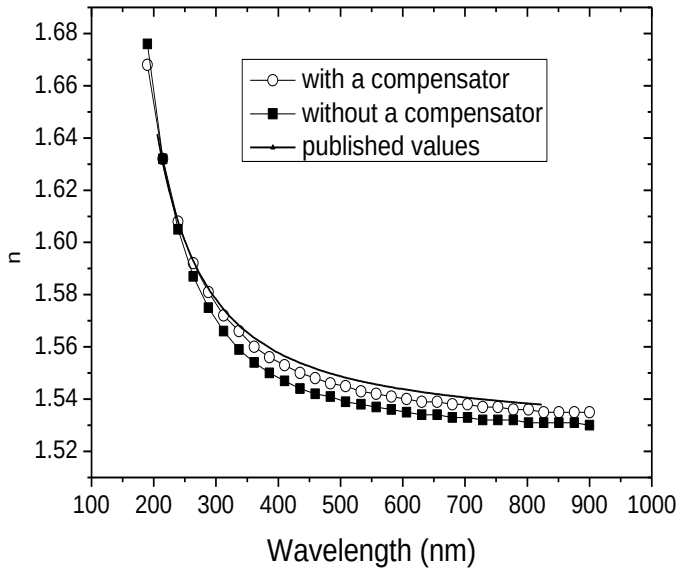

Figure 2.16. The refractive index of SiO_2 thin film in the range 200 to 900 nm. Lines

CHAPTER THREE

Ellipsometric Configurations Using A Fixed Compensator And A Rotating Polarizer And Analyzer At Any Speed Ratio

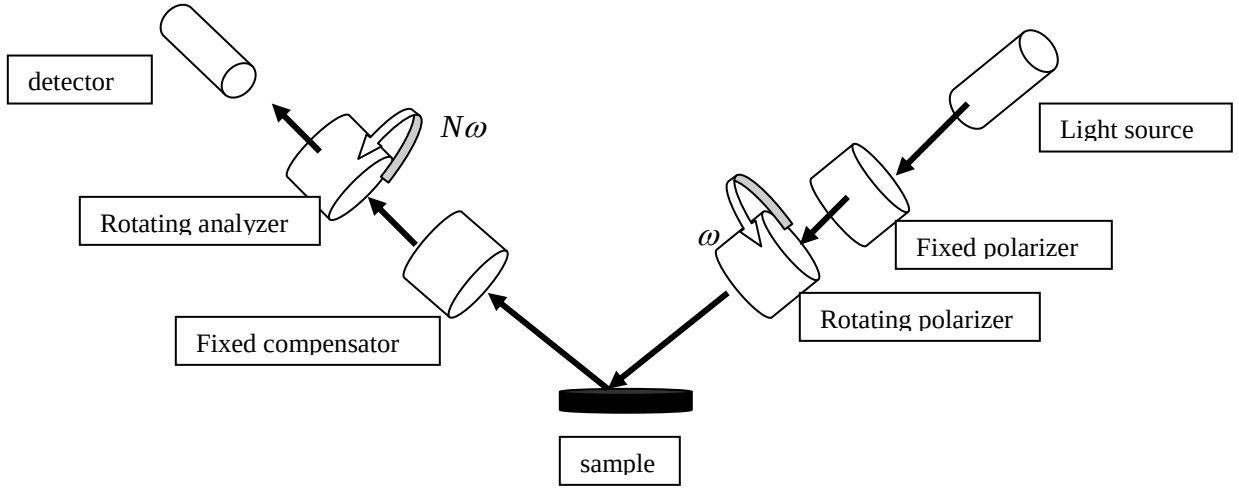

Figure 3.1 Optical configuration of ellipsometry, rotating polarizer analyzer with speed ratio 1:N

In this chapter an ellipsometer using a compensator and a rotating polarizer and analyzer at a speed ratio 1:N will be presented. Different ellipsometric configurations are presented by assuming N = 1, 2, and 3. Moreover, two values of the offset angle of the retarder are considered for each ellipsometric configuration. Muller formalism is employed to extract Stokes parameters from which the intensity received by the detector is obtained. The optical properties of c-Si are calculated using all configurations. A comparison between different configurations is held regarding the effect of the noise on the results extracted from each one and the uncertainties in the ellipsometric parameters as functions of the uncertainties of the Fourier coefficients. It is found that the alignment of the compensator has a crucial impact on the results and the ellipsometric configuration with a speed ratio 1:1 has a preference over other configurations.

3.1. Rotating Polarizer And Analyzer Elliupsometer With A Speed Ratio 1 : N And A Fixed Compensator With $\beta_c = 0^o$ And $\beta_c = 45^o$

In the ellipsometric configurations under study, the compensator is assumed to be fixed with its fast axis makes an angle β_c with the *p*-polarization. Two different orientations of the fixed phase retarder, namely $\beta_c = 0^o$ and $\beta_c = 45^o$, will be considered. For each orientation, many ellipsometric configurations by assuming different speed ratios for the rotating elements will be studied. The azimuth angle of the rotating polarizer is assumed to be $\beta_P = \omega t + \tau$ and that of the rotating analyzer is assumed to have the form $\beta_A = N\omega t + \alpha$, where *N* is an integer, τ and α are, respectively, the initial azimuth angles of the polarizer and analyzer. On the other hand, the azimuth angle of the fixed polarizer is assumed to be θ.

Using the matrices in Eqs (1.88-1.91) into Eq. 3.1, the Stokes vector of the detected light of the proposed structure is given by

$$S = R(-\beta_A)\, A\, R(\beta_A)\, L\, R(-\beta_c)\, C\, R(\beta_c)\, R(-\beta_P)\, P\, R(\beta_P)\, R(-\theta)\, P\, R(\theta)\, S_i \ . \quad (3.1)$$

where $S_i = [1,0,0,0]^T$ and S is a four-element column vector containing the Stokes parameters S_0, S_1, S_2, and S_3.

3.2. Rotating Polarizer And Analyzer Ellipsometer With A Speed Ratio 1 : N And A Fixed Compensator With $\beta_c = 0^o$

After performing the product of matrices given by Eq. (3.1) and assuming that $\beta_P = \omega t$ and $\beta_A = N\omega t$ ($\theta = 0, \alpha = 0$ and $\tau = 0$) and after rearranging the result, Stokes-vector elements, S_0, S_1, S_2, and S_3 are obtained. The intensity of the light received by the detector is given by S_0 and is found to be

$$
\begin{aligned}
I = S_0 &= [1-\frac{1}{2}\cos(2\psi)] + [1-\cos(2\psi)]\cos(2\omega t) - \frac{1}{2}\cos(2\psi)\cos(4\omega t) \\
&+ [\frac{1}{2} - \cos(2\psi)]\cos(2N\omega t) \\
&+ \frac{1}{2}[1-\cos(2\psi) - \sin(2\psi)\cos(\Delta-\delta)]\cos 2(N+1)\omega t \\
&+ \frac{1}{2}[1-\cos(2\psi) + \sin(2\psi)\cos(\Delta-\delta)]\cos 2(N-1)\omega t \\
&+ \frac{1}{4}[1-\sin(2\psi)\cos(\Delta-\delta)]\cos 2(N+2)\omega t \\
&+ \frac{1}{4}[1+\sin(2\psi)\cos(\Delta-\delta)]\cos 2(N-2)\omega t,
\end{aligned}
\tag{3.2}
$$

The Fourier transform of the detected intensity generates the DC term and N+2 AC terms which may be written

$$
I(t) = a_0 + \sum_{n=1}^{N+2} a_n \cos(2n\omega t)\,. \tag{3.3}
$$

Special cases can be obtained by letting N = 1, 2, … . In the following subsections, three special cases in which N = 1, 2, and 3 will be addressed. For each ellipsometric configuration, we find the Fourier coefficients, then calculate the ellipsometric parameters (ψ and Δ) in terms of these coefficients, and the uncertainty in the ellipsometric parameters as a function of the uncertainties in the Fourier coefficient.

3.2.1. Rotating Polarizer And Analyzer Ellipsometer With A Speed Ratio 1:1 ($\beta_c = 0^o$)

a RPAE with a speed ratio 1:1 is considered. Setting N = 1 into Eq. (3.2) and comparing it with Eq. (3.3), the coefficients a_0, a_1, a_2, and a_3 are given by

$$a_0=\frac{3}{2}-\cos(2\psi)+\frac{1}{2}\sin(2\psi)\cos(\Delta-\delta), \tag{3.4}$$

$$a_1=\frac{7}{4}-2\cos(2\psi)+\frac{1}{4}\sin(2\psi)\cos(\Delta-\delta), \tag{3.5}$$

$$a_2=\frac{1}{2}-\cos(2\psi)-\frac{1}{2}\sin(2\psi)\cos(\Delta-\delta), \tag{3.6}$$

$$a_3=\frac{1}{4}[1-\sin(2\psi)\cos(\Delta-\delta)]. \tag{3.7}$$

Solving the last three equations for ψ and $\Delta-\delta$ in terms of AC terms a_1, a_2 and a_3 yields

$$\sin(\psi)=\sqrt{\frac{a_1+a_3}{2}}, \tag{3.8}$$

$$\cos(\psi)=\sqrt{\frac{a_1-4a_2+9a_3}{2}}, \tag{3.9}$$

$$\tan(\psi)=\sqrt{\frac{a_1+a_3}{a_1-4a_2+9a_3}}, \tag{3.10}$$

$$\cos(\Delta-\delta)=\frac{a_1-2a_2-3a_3}{2\sin(\psi)\cos(\psi)}. \tag{3.11}$$

It is significant to study the fluctuations of ψ and Δ about their ideal values. Since the sample parameters, layer thicknesses and the index of refraction, are calculated from ψ

and Δ, these fluctuations lead to the uncertainties of the sample parameters. The uncertainties δψ and δΔ in ψ and Δ, respectively, as functions the uncertainties of the Fourier coefficients are obtained by differentiating Eqs. (3.10) and (3.11) with respect a_j (j = 1, 2, 3) while keeping the other coefficients as constants, we obtain.

$$\frac{\partial \psi}{\partial a_1} = \frac{a_2 - 2a_3}{\sqrt{a_1 + a_3}\sqrt{a_1 - 4a_2 + 9a_3}(-a_1 + 2a_2 - 5a_3)}, \tag{3.12}$$

$$\frac{\partial \psi}{\partial a_2} = \frac{-(a_1 + a_3)}{\sqrt{a_1 + a_3}\sqrt{a_1 - 4a_2 + 9a_3}(-a_1 + 2a_2 - 5a_3)}, \tag{3.13}$$

$$\frac{\partial \psi}{\partial a_3} = \frac{2a_1 + a_2}{\sqrt{a_1 + a_3}\sqrt{a_1 - 4a_2 + 9a_3}(-a_1 + 2a_2 - 5a_3)}, \tag{3.14}$$

$$\frac{\partial \Delta}{\partial a_1} = \frac{4a_1a_3 + 12(a_3)^2 - 2(a_2)^2}{(a_1 + a_3)\,(-a_1 + 4a_2 - 9a_3)(4a_1a_3 - 4a_3a_2 - (a_2)^2)}, \tag{3.15}$$

$$\frac{\partial \Delta}{\partial a_2} = \frac{2a_2 - 12a_3}{(-a_1 + 4a_2 - 9a_3)(4a_1a_3 - 4a_3a_2 - (a_2)^2)}, \tag{3.16}$$

and

$$\frac{\partial \Delta}{\partial a_3} = \frac{-4(a_1)^2 + 12a_1a_2 - 12a_1a_3 + 12a_3a_2 - 2(a_2)^2}{(a_1 + a_3)\,(-a_1 + 4a_2 - 9a_3)(4a_1a_3 - 4a_3a_2 - (a_2)^2)}. \tag{3.17}$$

3.2.2. Rotating Polarizer And Analyzer Ellipsometer With A Speed Ratio 1:2 ($\beta_c = 0^o$)

Another ellipsometric configuration can be obtained by letting N = 2 into Eq. (3.2). In this case, the DC term and four AC terms may be written as

$$a_0=\frac{5}{4}-\frac{1}{2}\cos(2\psi)+\frac{1}{4}\sin(2\psi)\cos(\Delta-\delta), \tag{3.18}$$

$$a_1=\frac{3}{2}-\frac{3}{2}\cos(2\psi)+\frac{1}{2}\sin(2\psi)\cos(\Delta-\delta), \tag{3.19}$$

$$a_2=\frac{1}{2}-\frac{3}{2}\cos(2\psi), \tag{3.20}$$

$$a_3=\frac{1}{2}-\frac{1}{2}\cos(2\psi)-\frac{1}{2}\sin(2\psi)\cos(\Delta-\delta), \tag{3.21}$$

and

$$a_4=\frac{1}{4}-\frac{1}{4}\sin(2\psi)\cos(\Delta-\delta). \tag{2.22}$$

ψ and $\Delta-\delta$ may be evaluated in terms of any set of coefficients set comprising three Fourier terms. Consequently, excluding the DC term, three sets: (a_1, a_2, a_3), (a_1, a_3, a_4), and (a_2, a_3, a_4) are available. These three sets are shown below

Case I: Extracting ψ and Δ using the set (a_1, a_2, a_3)

$$\sin(\psi)=\sqrt{\frac{a_1+a_3}{4}}, \tag{3.23}$$

$$\cos(\psi)=\sqrt{\frac{2a_1-2a_2+a_3}{2}}, \tag{3.24}$$

$$\tan(\psi)=\sqrt{\frac{a_1+a_3}{4a_1-4a_2+2a_3}}, \tag{3.25}$$

$$\cos(\Delta-\delta)=\frac{a_1-3a_3}{4\sin(\psi)\cos(\psi)}. \tag{3.26}$$

Case II: Extracting ψ and Δ using the set (a_1, a_2, a_4)

$$\sin(\psi)=\sqrt{\frac{2a_1+a_2+4a_4}{9}}\ , \tag{3.27}$$

$$\cos(\psi)=\sqrt{\frac{4a_1-7a_2+8a_4}{9}}\ , \tag{3.28}$$

$$\tan(\psi)=\sqrt{\frac{2a_1+a_2+4a_4}{4a_1-7a_2+8a_4}}\ , \tag{3.29}$$

$$\cos(\Delta-\delta)=\frac{a_1-a_2-4a_4}{3\sin(\psi)\cos(\psi)}, \tag{3.30}$$

Case III: Extracting ψ and Δ using the set (a_2, a_3, a_4)

$$\sin(\psi)=\sqrt{a_2-2a_3+4a_4}\ , \tag{3.31}$$

$$\cos(\psi)=\sqrt{a_2-4a_3+8a_4}\ , \tag{3.32}$$

$$\tan(\psi)=\sqrt{\frac{a_2-2a_3+4a_4}{a_2-4a_3+8a_4}}\ , \tag{3.33}$$

$$\cos(\Delta-\delta)=\frac{a_2-3a_3+4a_4}{\sin(\psi)\cos(\psi)}. \tag{3.34}$$

The uncertainties δψ and δΔ are here calculated for the first set only and can be done for the other sets in a similar manner. Differentiating Eqs. (3.25) and (3.26) with respect a_j (j = 1, 2, 3) while keeping the other coefficients as constants gives,

$$\frac{\partial \Delta}{\partial a_1} = -\frac{1}{Q_1 Q_2 Q_3}\left[1 - \frac{a_1 - 3a_3}{2Q_1^{\,2}} - \frac{a_1 - 3a_3}{Q_2^{\,2}}\right], \tag{3.35}$$

$$\frac{\partial \Delta}{\partial a_2} = \frac{-2(a_1 - 3a_3)}{Q_1 Q_2^{\,3} Q_3}\ , \tag{3.36}$$

$$\frac{\partial \Delta}{\partial a_3} = -\frac{1}{Q_1 Q_2 Q_3}\left[-3 - \frac{a_1 - 3a_3}{2Q_1^{\,2}} - \frac{a_1 - 3a_3}{Q_2^{\,2}}\right]. \tag{3.37}$$

$$\frac{\partial \psi}{\partial a_1} = \frac{Q_2^2 - 2Q_1^2}{2Q_1 Q_2\left(Q_1^2 + Q_2^2\right)}, \tag{3.38}$$

$$\frac{\partial \psi}{\partial a_2} = \frac{2Q_1}{Q_2\left(Q_1^2 + Q_2^2\right)}, \tag{3.39}$$

and

$$\frac{\partial \psi}{\partial a_3} = \frac{Q_2^2 - 2Q_1^2}{2Q_1 Q_2\left(Q_1^2 + Q_2^2\right)}, \tag{3.40}$$

where

$$Q_1 = \sqrt{a_1 + a_3}\ , \tag{3.41}$$

$$Q_2 = \sqrt{2a_1 - 4a_2 + 2a_3}\ , \tag{3.42}$$

$$Q_3 = \sqrt{1 - \frac{(a_1 - 3a_3)^2}{(a_1 + a_3)(2a_1 - 4a_2 + 2a_3)}}. \tag{3.43}$$

3.2.3. Rotating Polarizer And Analyzer Ellipsometer With A Speed Ratio 1:3 ($\beta_c = 0^o$)

In the third case, an ellipsometric configuration in which the polarizer and the analyzer rotate at a speed ratio 1:3 is assumed. Setting $N = 3$ into Eq. (3.2) and Eq. (3.3) to find the intensity and the Fourier coefficients of this configuration, gives

$$a_0 = 1 - \frac{1}{2}\cos(2\psi), \tag{3.44}$$

$$a_1 = \frac{5}{4} - \cos(2\psi) + \frac{1}{4}\sin(2\psi)\cos(\Delta - \delta), \tag{3.45}$$

$$a_2 = \frac{1}{2} - \cos(2\psi) + \frac{1}{2}\sin(2\psi)\cos(\Delta - \delta), \tag{3.46}$$

$$a_3 = \frac{1}{2} - \cos(2\psi), \tag{3.47}$$

$$a_4 = \frac{1}{2} - \frac{1}{2}\cos(2\psi) - \frac{1}{2}\sin(2\psi)\cos(\Delta - \delta), \tag{3.48}$$

and

$$a_5 = \frac{1}{4} - \frac{1}{4}\sin(2\psi)\cos(\Delta - \delta). \tag{3.49}$$

In analogy to the 1:2 configuration, many sets are available from which the ellipsometric parameters can be obtained. When the speed ratio is 1:3, six sets can be taken without considering the DC term. Some of these cases are listed below

Case I: obtaining ψ and Δ using the set (a_1, a_2, a_3)

$$\sin(\psi) = \sqrt{\frac{2a_1 - a_2 + 2a_3}{6}}, \tag{3.50}$$

$$\cos(\psi) = \sqrt{\frac{2a_1 - a_2 - 2a_3}{2}}, \tag{3.51}$$

$$\tan(\psi) = \sqrt{\frac{2a_1 - a_2 + 2a_3}{3(2a_1 - a_2 - 2a_3)}}, \tag{3.52}$$

and

$$\cos(\Delta - \delta) = \frac{-a_3 + a_2}{\sin(\psi)\cos(\psi)}. \tag{3.53}$$

Case II: obtaining ψ and Δ using the set (a_1, a_2, a_4)

$$\sin(\psi) = \sqrt{\frac{2a_1 + a_2 + 2a_4}{4}}, \tag{3.54}$$

$$\cos(\psi) = \sqrt{\frac{10a_1 - 11a_2 - 6a_4}{4}}, \tag{3.55}$$

$$\tan(\psi) = \sqrt{\frac{2a_1 + a_2 + 2a_4}{10a_1 - 11a_2 - 6a_4}}, \tag{3.56}$$

and

$$\cos(\Delta - \delta) = \frac{2a_1 + a_2 - 6a_4}{4\sin(\psi)\cos(\psi)}, \tag{3.57}$$

Case III: obtaining ψ and Δ using the set (a_1, a_2, a_5)

$$\sin(\psi) = \sqrt{2a_2 + 4a_5} \ , \tag{3.58}$$

$$\cos(\psi) = \sqrt{8a_1 - 10a_2 - 12a_5} \ , \tag{3.59}$$

$$\tan(\psi) = \sqrt{\frac{2a_2 + 4a_5}{8a_1 - 10a_2 - 12a_5}} \ , \tag{3.60}$$

and

$$\cos(\Delta - \delta) = \frac{4a_1 - 4a_2 - 12a_5}{\sin(\psi)\cos(\psi)} . \tag{3.61}$$

Case IV: obtaining ψ and Δ using the set (a_2, a_3, a_4)

$$\sin(\psi) = \sqrt{2a_2 - 2a_3 + 2a_4} \ , \tag{3.62}$$

$$\cos(\psi) = \sqrt{6a_2 - 10a_3 + 6a_4} \ , \tag{3.63}$$

$$\tan(\psi) = \sqrt{\frac{2a_2 - 2a_3 + 2a_4}{6a_2 - 10a_3 + 6a_4}} \ , \tag{3.64}$$

$$\cos(\Delta - \delta) = \frac{2a_2 - 2a_3}{\sin(\psi)\cos(\psi)} . \tag{3.65}$$

Differentiating Eqs. (3.52) and (3.53) with respect a_j (j = 1, 2, 3) while keeping the other coefficients as constants gives the uncertainties in δψ and δΔ as follows,

$$\frac{\partial \Delta}{\partial a_1} = \frac{A_4}{A_2^3 A_3^3 A_1}\left(\frac{2}{3}A_3^2 + 2A_2^2\right), \tag{3.66}$$

$$\frac{\partial \Delta}{\partial a_2} = \frac{-1}{A_1 A_2 A_3}\left(4 + \frac{A_4\left(A_3^2 + 3A_2^2\right)}{3A_2^2 A_3^2}\right), \tag{3.67}$$

$$\frac{\partial \Delta}{\partial a_3} = \frac{-1}{A_1 A_2 A_3}\left(-4 - \frac{2A_4\left(A_3^2 - 3A_2^2\right)}{3A_2^2 A_3^2}\right), \tag{3.68}$$

$$\frac{\partial \psi}{\partial a_1} = \left(\frac{2A_3^2 - 6A_2^2}{3A_2 A_3\left(A_3^2 + A_2^2\right)}\right), \tag{3.69}$$

$$\frac{\partial \psi}{\partial a_2} = \left(\frac{-A_3^2 + 3A_2^2}{3A_2 A_3\left(A_3^2 + A_2^2\right)}\right), \tag{3.70}$$

$$\frac{\partial \psi}{\partial a_3} = \left(\frac{2A_3^2 + 6A_2^2}{3A_2 A_3\left(A_3^2 + A_2^2\right)}\right), \tag{3.71}$$

where

$$A_1 = \sqrt{1 - \frac{A_4^2}{A_2^2 A_3^2}}\ , \tag{3.72}$$

$$A_2 = \sqrt{\frac{4a_1 - 2a_2 + 4a_3}{3}}\ , \tag{3.73}$$

$$A_3 = \sqrt{4a_1 - 2a_2 - 4a_3}\,, \tag{3.74}$$

$$A_4 = 4a_2 - 4a_3\,. \tag{3.75}$$

3.3 Rotating Polarizer And Analyzer Ellipsometer With A Speed Ratio 1 : N And A Fixed Compensator With $\beta_c = 45^o$

The orientation of the compensator is a key parameter in the results extracted from the proposed ellipsometric configurations. To introduce this point in this study, we assume another orientation for the compensator for which $\beta_c = 45^o$ is assumed**.** The product of matrices given by Eq. (3.1) is performed again with $\beta_c = 45^o$**.** Stokes-vector elements, S_0 through S_3, are then obtained as mentioned before. The detected intensity is given by S_0.

$$
\begin{aligned}
I = S_0 &= [1-\frac{1}{2}\cos(2\psi)\cos(\delta)] + [1-\cos(2\psi)\cos(\delta)]\cos(2\omega t) \\
&\quad -\frac{1}{2}\cos(2\psi)\cos(\delta)\cos(4\omega t) + [\frac{\cos(\delta)}{2} - \cos(2\psi)]\cos(2N\omega t) \\
&+ \frac{1}{2}[\cos(\delta) - \cos(2\psi) - \sin(2\psi)\cos(\Delta)]\cos 2(N+1)\omega t \\
&\quad + \frac{1}{2}[\cos(\delta) - \cos(2\psi) + \sin(2\psi)\cos(\Delta)]\cos 2(N-1)\omega t \\
&+ \frac{1}{4}[\cos(\delta) - \sin(2\psi)\cos(\Delta)]\cos 2(N+2)\omega t \\
&\quad + \frac{1}{4}[\cos(\delta) + \sin(2\psi)\cos(\Delta)]\cos 2(N-2)\omega t \\
&+ \frac{1}{2}[\sin(2\psi)\sin(\Delta)\sin(\delta)]\sin(2N\omega t) \\
&+ \frac{1}{2}[\sin(2\psi)\sin(\Delta)\sin(\delta)]\sin 2(N+1)\omega t \\
&+ \frac{1}{2}[\sin(2\psi)\sin(\Delta)\sin(\delta)]\sin 2(N-1)\omega t \\
&+ \frac{1}{4}[\sin(2\psi)\sin(\Delta)\sin(\delta)]\sin 2(N+2)\omega t \qquad . \qquad (3.76) \\
&+ \frac{1}{4}[\sin(2\psi)\sin(\Delta)\sin(\delta)]\sin 2(N-2)\omega t
\end{aligned}
$$

The Fourier transform of the detected intensity generates the DC term, (N+2) cosine AC terms, and (N+2) sine AC terms which may be written

$$
I(t) = a_0 + \sum_{n=1}^{N+2} a_n \cos(2n\omega t) + \sum_{n=1}^{N+2} b_n \sin(2n\omega t), \qquad (3.77)
$$

The following subsections show three special cases in which N = 1, 2, and 3.

3.3.1 Rotating Polarizer And Analyzer Ellipsometer With A Speed Ratio 1:1 ($\beta_c = 45^o$)

First consider the case that N = 1 in Eqs. (3.76) and (3.77). The comparison between the results gives the coefficients a_1, a_2, a_3, b_1, b_2, b_3 as

$$a_1 = 1 - \cos(2\psi)\cos(\delta) - \cos(2\psi) + \frac{6}{8}\cos(\delta) + \frac{1}{4}\sin(2\psi)\cos(\Delta), \qquad (3.78)$$

$$a_2 = -\frac{1}{2}\cos(2\psi)\cos(\delta) - \frac{1}{2}\cos(2\psi) + \frac{1}{2}\cos(\delta) - \frac{1}{2}\sin(2\psi)\cos(\Delta), \qquad (3.79)$$

$$a_3 = \frac{1}{4}\cos(\delta) - \frac{1}{4}\sin(2\psi)\cos(\Delta), \qquad (3.80)$$

$$b_1 = \frac{1}{4}\sin(2\psi)\sin(\Delta)\sin(\delta), \qquad (3.81)$$

$$b_2 = \frac{1}{2}\sin(2\psi)\sin(\Delta)\sin(\delta), \qquad (3.82)$$

and

$$b_3 = \frac{1}{4}\sin(2\psi)\sin(\Delta)\sin(\delta). \qquad (3.83)$$

As mentioned above, only three coefficients are needed to calculate the ellipsometric parameters. If a_1, a_2 and a_3 are considered and Eqs. (3.78), (3.79), and (3.80) are solved, ψ and Δ are then given by

$$\tan(\psi) = \sqrt{\frac{a_1 + a_3}{a_1 - 4a_2 + 9a_3}}, \qquad (3.84)$$

$$\cos(\Delta) = \frac{2\left(a_1 - 2a_2 + a_3 - \frac{4}{\cos(\delta)}a_3\right)\cos(\delta)}{\sqrt{2a_1 + 2a_3}\sqrt{2a_1 - 8a_2 + 18a_3}}. \tag{3.85}$$

The comparison of Eqs. (3.84) and (3.85) with Eqs. (3.10) and (3.11), illustrates the independence of ψ and the dependence of Δ on β_c. As a result, the uncertainty $\delta\psi$ is still given by Eqs. (3.12), (3.13), and (3.14) whereas $\delta\Delta$ is given by

$$\frac{\partial\Delta}{\partial a_1} = -\frac{2\,T - \frac{RT}{2a_1 + 2a_3} - \frac{RT}{2a_1 - 8a_2 + 18a_3}}{\sqrt{1 - T^2R^2}}, \tag{3.86}$$

$$\frac{\partial\Delta}{\partial a_2} = \frac{4T - \frac{4RT}{2a_1 - 8a_2 + 18a_3}}{\sqrt{1 - T^2R^2}}, \tag{3.87}$$

$$\frac{\partial\Delta}{\partial a_3} = -\frac{\left(2 - \frac{8}{\cos(\delta)}\right)T - \frac{RT}{2a_1 + 2a_3} - \frac{9RT}{2a_1 - 8a_2 + 18a_3}}{\sqrt{1 - T^2R^2}}, \tag{3.88}$$

Where *T* and *R* are given by:

$$T = \frac{\cos(\delta)}{\sqrt{2a_1 + 2a_3}\sqrt{2a_1 - 8a_2 + 18a_3}}, \tag{3.89}$$

$$R = 2a_1 - 4a_2 + 2a_3 - \frac{8\,a_3}{\cos(\delta)}. \tag{3.90}$$

3.3.2 Rotating Polarizer And Analyzer Ellipsometer With A Speed Ratio 1:2 ($\beta_c = 45^o$)

Letting N = 2 into Eq. (3.76) and comparing with Eq. (3.77), gives one DC term and eight AC terms. The AC terms are

$$a_1 = 1 - \cos(2\psi)\cos(\delta) - \frac{1}{2}\cos(2\psi) + \frac{1}{2}\cos(\delta) + \frac{1}{2}\sin(2\psi)\cos(\Delta), \tag{3.91}$$

$$a_2 = -\frac{1}{2}\cos(2\psi)\cos(\delta) - \cos(2\psi) + \frac{1}{2}\cos(\delta), \tag{3.92}$$

$$a_3 = -\frac{1}{2}\cos(2\psi) - \frac{1}{2}\cos(2\delta) - \frac{1}{2}\sin(2\psi)\cos(\Delta), \tag{3.93}$$

$$a_4 = \frac{1}{4}\cos(\delta) - \frac{1}{4}\sin(2\psi)\cos(\Delta), \tag{3.94}$$

$$b_1 = \frac{1}{2}\sin(2\psi)\sin(\Delta)\sin(\delta), \tag{3.95}$$

$$b_2 = \frac{1}{2}\sin(2\psi)\sin(\Delta)\sin(\delta), \tag{3.96}$$

$$b_3 = \frac{1}{2}\sin(2\psi)\sin(\Delta)\sin(\delta), \tag{3.97}$$

and

$$b_4 = \frac{1}{4}\sin(2\psi)\sin(\Delta)\sin(\delta). \tag{3.98}$$

A large number of three-term sets can be obtained to extract the ellipsometric parameters. The first set including (a_1, a_2, a_3) will be only considered. Solving Eqs. (3.91), (3.92), and (3.93) for ψ and Δ, gives

$$\tan(\psi) = \sqrt{\frac{a_1 + a_3}{(a_1 - 2a_2 + a_3)(1 + \cos(\delta))}}\ , \tag{3.99}$$

$$\cos(\Delta) = \frac{\frac{1}{2}\cos(\delta)a_1 + (1 - \cos(\delta))a_2 - \frac{1}{2}(4 - \cos(\delta))a_3}{\sqrt{\frac{a_1 + a_3}{(1 + \cos(\delta))}}\sqrt{a_1 - 2a_2 + a_3}}. \tag{3.100}$$

Differentiating the last two equations to find the uncertainty in the ellipsometric parameters due to the uncertainty in the Fourier coefficients, yields

$$\frac{\partial \psi}{\partial a_1} = -2B_1B_2B_3\ a_2\ , \tag{3.101}$$

$$\frac{\partial \psi}{\partial a_2} = 2B_1B_2B_3\ (a_1 + a_3)\ , \tag{3.102}$$

and

$$\frac{\partial \psi}{\partial a_3} = -2B_1B_2B_3\ a_2\ . \tag{3.103}$$

where

$$B_1 = \frac{1}{1+\tan^2(\psi)}, \tag{3.104}$$

$$B_2 = \frac{1}{2\tan(\psi)}, \tag{3.105}$$

and

$$B_3 = \frac{1}{(a_1 - 2a_2 + a_3)^2(1+\cos(\delta))}. \tag{3.106}$$

moreover,

$$\frac{\partial\Delta}{\partial a_1} = \frac{1}{4\sin(\Delta)\sin(\psi)\cos(\psi)}\left[-\cos(\delta)+\cos(\Delta)\left(\tan(\psi)+\frac{\cot(\psi)}{1+\cos(\delta)}\right)\right], \tag{3.107}$$

$$\frac{\partial\Delta}{\partial a_2} = \frac{1}{2\sin(\Delta)\sin(\psi)\cos(\psi)}\left[-1+\cos(\delta)-\cos(\Delta)\tan(\psi)\right], \tag{3.108}$$

and

$$\frac{\partial\Delta}{\partial a_3} = \frac{1}{4\sin(\Delta)\sin(\psi)\cos(\psi)}\left[4-\cos(\delta)+\cos(\Delta)\left(\tan(\psi)+\frac{\cot(\psi)}{1+\cos(\delta)}\right)\right]. \tag{3.109}$$

3.3.3 Rotating Polarizer And Analyzer Ellipsometer With A Speed Ratio 1:3 ($\beta_c = 45^o$)

The last case to be considered here is the configuration with N = 3. Following the same methodology as above, the AC Fourier coefficients are found to be

$$a_1 = 1-\cos(2\psi)\cos(\delta)+\frac{1}{4}\cos(\delta)+\frac{1}{4}\sin(2\psi)\cos(\Delta), \tag{3.110}$$

$$a_2 = -\frac{1}{2}\cos(2\psi)\cos(\delta)-\frac{1}{2}\cos(2\psi)+\frac{1}{2}\cos(\delta)+\frac{1}{2}\sin(2\psi)\cos(\Delta), \tag{3.111}$$

$$a_3 = -\cos(2\psi) + \frac{1}{2}\cos(2\delta), \tag{3.112}$$

$$a_4 = -\frac{1}{2}\cos(2\psi) + \frac{1}{2}\cos(\delta) - \frac{1}{2}\sin(2\psi)\cos(\Delta), \tag{3.113}$$

$$a_5 = \frac{1}{4}\cos(\delta) - \frac{1}{4}\sin(2\psi)\cos(\Delta), \tag{3.114}$$

$$b_1 = \frac{1}{4}\sin(2\psi)\sin(\Delta)\sin(\delta), \tag{3.115}$$

$$b_2 = \frac{1}{2}\sin(2\psi)\sin(\Delta)\sin(\delta), \tag{3.116}$$

$$b_3 = \frac{1}{2}\sin(2\psi)\sin(\Delta)\sin(\delta), \tag{3.117}$$

$$b_4 = \frac{1}{2}\sin(2\psi)\sin(\Delta)\sin(\delta), \tag{3.118}$$

and

$$b_5 = \frac{1}{4}\sin(2\psi)\sin(\Delta)\sin(\delta). \tag{3.119}$$

The first set including the coefficients (a_1, a_2, a_3) is only considered. ψ and Δ are calculated as

$$\sin(\psi) = \sqrt{\frac{\left(4 - 2\cos(\delta)\right)a_1 - \left(2 - \cos(\delta)\right)a_2 + \left(5 - 3\cos(\delta)\right)a_3}{D_o}}, \tag{3.120}$$

$$\cos(\psi) = \sqrt{\frac{\left(4+2\cos(\delta)\right)a_1 - \left(2+\cos(\delta)\right)a_2 - \left(3+3\cos(\delta)\right)a_3}{D_o}}\,, \tag{3.121}$$

$$\tan(\psi) = \sqrt{\frac{\left(4-2\cos(\delta)\right)a_1 - \left(2-\cos(\delta)\right)a_2 + \left(5-3\cos(\delta)\right)a_3}{\left(4+2\cos(\delta)\right)a_1 - \left(2+\cos(\delta)\right)a_2 - \left(3+3\cos(\delta)\right)a_3}}\,, \tag{3.122}$$

$$\cos(\Delta) = \frac{\left[\frac{2\left(a_2 - a_3\right)}{\left(1-\cos(\delta)\right)} + \sin^2(\psi) - \cos^2(\psi)\right]\left(1-\cos(\delta)\right)}{2\sin(\psi)\cos(\psi)}\,. \tag{3.123}$$

Finally, the uncertainties in the ellipsometric parameters are given by

$$\frac{\partial\psi}{\partial a_1} = \frac{1}{2\sin(\psi)\cos(\psi)}\left(\frac{4\cos(2\psi)}{D_o} - \frac{2\cos(\delta)}{D_o}\right), \tag{3.124}$$

$$\frac{\partial\psi}{\partial a_2} = \frac{1}{2\sin(\psi)\cos(\psi)}\left[\left(\frac{-2\cos(2\psi)}{D_o} + \frac{\cos(\delta)}{D_o}\right)\right], \tag{3.125}$$

$$\frac{\partial\psi}{\partial a_3} = \frac{1}{2\sin(\psi)\cos(\psi)}\left[\left(D_8\cos(2\psi) + \frac{8\cos^2(\psi)}{D_o}\right)\right], \tag{3.126}$$

$$\frac{\partial\Delta}{\partial a_1} = \frac{1}{\sin(\Delta)2\sin(\psi)\cos(\psi)}\left[D_1 + \cos(\Delta)(D_2\tan(\psi) + D_3\cot(\psi)\right], \tag{3.127}$$

$$\frac{\partial\Delta}{\partial a_2} = \frac{1}{\sin(\Delta)2\sin(\psi)\cos(\psi)}\left[D_4 + \cos(\Delta)(D_5\tan(\psi) + D_6\cot(\psi)\right], \tag{3.128}$$

and

$$\frac{\partial \Delta}{\partial a_3} = \frac{1}{\sin(\Delta) 2 \sin(\psi)\cos(\psi)} \left[D_7 + \cos(\Delta)(D_8 \tan(\psi) + D_9 \cot(\psi) \right], \qquad (3.129)$$

where

$$D_o = 8 + \cos(\delta) - 3\cos(\delta)^2, \qquad (3.130)$$

$$D_1 = \frac{4\cos(\delta) - 4\cos^2(\delta)}{D_o}, \qquad (3.131)$$

$$D_2 = \frac{4 + 2\cos(\delta)}{D_o}, \qquad (3.132)$$

$$D_3 = \frac{4 - 2\cos(\delta)}{D_o}, \qquad (1.133)$$

$$D_4 = \frac{-16 - 4\cos(\delta) + 8\cos^2(\delta)}{D_o}, \qquad (3.134)$$

$$D_5 = \frac{-2 - \cos(\delta)}{D_o}, \qquad (3.135)$$

$$D_6 = \frac{-2 + \cos(\delta)}{D_o}, \qquad (3.136)$$

$$D_7 = \frac{8 + 12\cos(\delta) - 6\cos^2(\delta)}{D_o}, \qquad (3.137)$$

$$D_8 = \frac{-3 - 3\cos(\delta)}{D_o}, \qquad (3.138)$$

and

$$D_9 = \frac{5 - 3\cos(\delta)}{D_o}. \qquad (3.139)$$

3.4. Results And Discussion

3.4.1 The Noise Effect

The applicability of the proposed structure is tested numerically in this section by considering a sample of one interface separating a semi-infinite air layer of refractive index N_0 and a bulk c-Si material of refractive index N_1. The angle of incidence is taken to be 70^o which is a common angle used in spectroscopic ellipsometry. The real and imaginary parts of the refractive index of c-Si are taken from Ref. [35]. Phase retarders made from MgF_2 are extensively used in ellipsometric measurements. A zero order MgF_2 compensator centered at 4 eV is considered.

The general approach used to obtain the ellipsometric coefficients is as follows: The Fresnel reflection coefficients are calculated to the assumed one-interface structure. All of the matrices given by Eqs. (1.88) – (1.91) are then calculated. From the product of these matrices the intensity received by the detector, which is the element S_0 of the product vector is calculated. The Fourier transform of the signal is taken in order to extract the Fourier coefficients. The ellipsometric parameters ψ and Δ are then calculated in the photon energy range 1.5–6 eV using the Fourier coefficients. These values of the ellipsometric parameters correspond to the clean signal without considering any noise. Such a case with no noise is not realistic case. In real situations, random fluctuations in the recorded signal appear due to the noise from many sources. To simulate reality, noise was generated using a MathCAD code and was superimposed on the clean signal according to the eqn. (2.34)

This noise is then added to the pure signal. Fourier transform of the noisy signal is taken to extract the new coefficients a_0 through a_n in the presence of the noise.

To calculate the complex refractive index of the sample, Eq. (2.35) can be used.

The calculated values of the real (*n*) and imaginary (*k*) parts of the refractive index of c-Si, obtained from ellipsometric configuration, are plotted in Fig. 3.2 along with the published values [35]. The points in Fig. 3.2 represent the calculated *n* and *k* of c-Si using the noisy signal. These points are calculated using any configuration of the six ellipsometric configurations mentioned above. The difference between them is not obviously seen in this figure. To differentiate between them, the percent error in the calculated values of *n* and *k* for each ellipsometric configuration is calculated.

The percent error in the calculated values of *n* for c-Si is shown in Fig. 3.3 using the set containing (a_1, a_2, a_3). The figure shows the error arising from calculating *n* using six different structures which are 1:1, 1:2 and 1:3 with β_c equal to either 0^o or 45^o. The fluctuations shown in the figure are due to the noise imposed on the clean signal as mentioned before. As can be seen from the figure, the percent error in *n* has small values (of order10^{-2}) for all ellipsometric configurations with a clear preference of structures having $\beta_c = 0^o$ over those with $\beta_c = 45^o$. The percent error in *n* at high energies is relatively high (for all ellipsometric configurations) compared to the low energy region due to the relatively small value of *n* at high energies.

Figure 3.4 shows the percent error in *k* in the photon energy range 1.5 to 3 eV. The range from 3 to 6 eV is not plotted because the error in *k* almost goes to zero in this region. The percent error in *k* is much higher than that in *n* in the low energy region. That is the imaginary part *k* is much sensitive to the noise imposed on the signal. Generally, the percent error is considerable for *k* because it has a small value (0.019) at a wavelength of 632.8 nm. The figure shows clearly a considerable preference of the ellipsometric configurations having $\beta_c = 0^o$ over those with $\beta_c = 45^o$. Moreover, for the same β_c, the structure with the speed ratio 1:1 has much less percent error compared to the structures having speed ratios 1:2 and 1:3. This result is compatible with results obtained in ref [32].

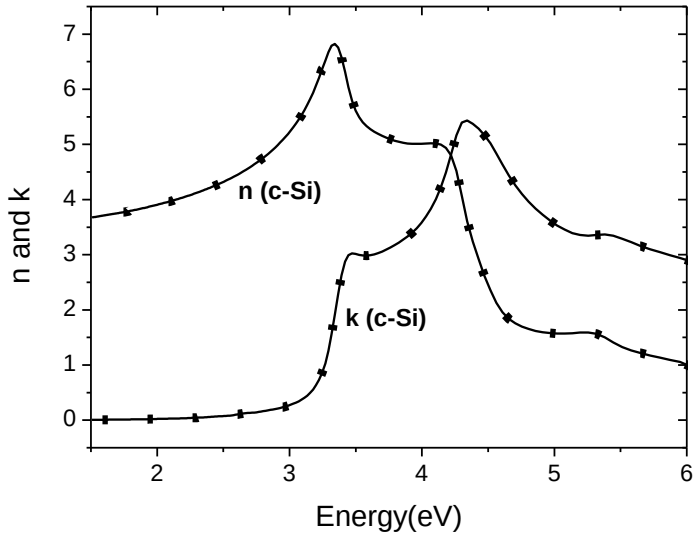

Figure 3.2. The real and the imaginary parts of the refractive index of c-Si in the photon energy range 1.5 to 6 eV. Lines: accepted values, Points: calculated values.

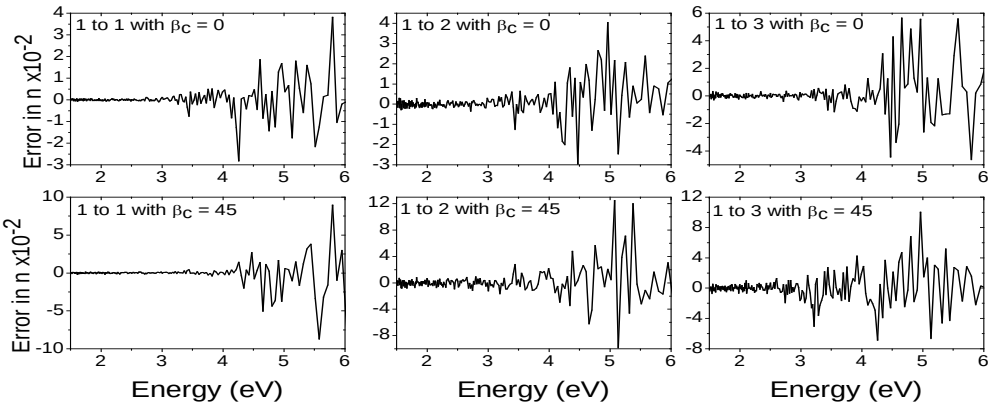

Figure 3.3. The percent error in the real part of the refractive index of c-Si in the photon energy range 1.5 to 6 eV.

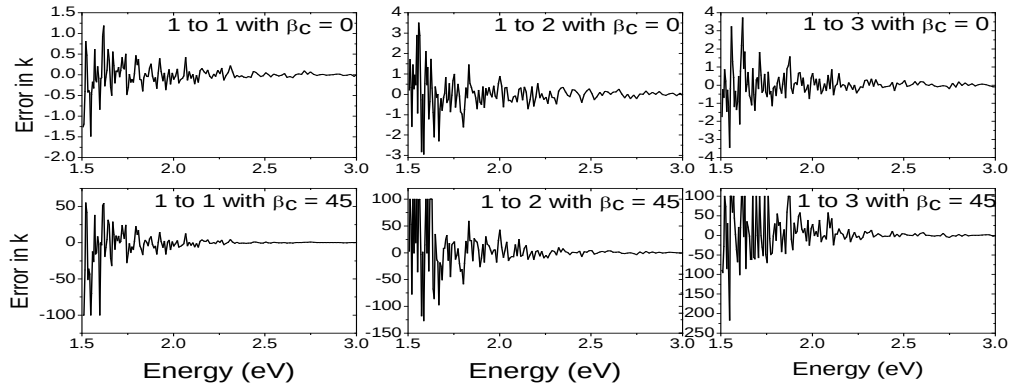

Figure 3.4. The percent error in the imaginary part of the refractive index of c-Si in the photon energy range 1.5 to 3 eV.

3.4.2 Uncertainty In ψ And Δ

The attention to the uncertainties δψ and δΔ in ψ and Δ, respectively, as functions of the uncertainties of the Fourier coefficients will be discussed. Figure 3.5 shows δψ versus the photon energy in the spectral range 1.5 to 6 eV for the six ellipsometric configurations under study. Generally, the sensitivity exhibited by ψ to the uncertainties of the Fourier coefficients is not considerable for all ellipsometric structures. Compared to the sensitivity in the high energy region, a relatively high sensitivity of ψ at low energies is observed in the figure. As can be seen from the figure, the uncertainty of ψ does not depend on the β_c . A little dependence of δψ on the speed ratio, at which the polarizer and the analyzer rotate, can be seen. The 1:3 configuration has the highest sensitivity.

The phase change Δ is much sensitive to the uncertainty in the Fourier coefficients than ψ. Figure 3.6 shows the uncertainty of Δ with respect to the uncertainty of the Fourier coefficients versus the photon energy for the six ellipsometric configurations under study. Many interesting features can be seen in the figure. First, in analogy to δψ, at low energies, where c-Si is essentially transparent, the sensitivity of Δ is high compared to the high-energy region. Second, there is a strong dependence of δΔ on β_c . The phase

change Δ is much sensitive to the uncertainty in the Fourier coefficients when $\beta_c = 45^o$ than the case when $\beta_c = 0^o$. For $\beta_c = 45^o$, the sensitivity of Δ exceeds 400 for some cases whereas it does not exceed 5 for all configurations when $\beta_c = 0^o$. This enhances the conclusion mentioned above that there is a considerable preference of the ellipsometric configurations having $\beta_c = 0^o$ over those with $\beta_c = 45^o$. Third, the sensitivity of Δ to the coefficient a_2 has the lowest values for most cases. Fourth, the maximum sensitivity can be seen in the ellipsometric configuration with speed ratio 1:3 for $\beta_c = 45^o$.

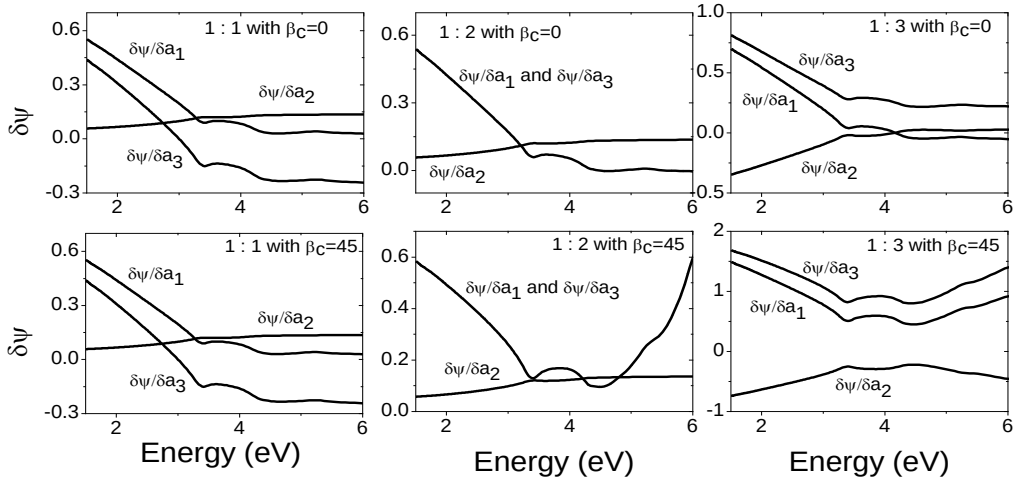

Figure 3.5. The variation in ψ for all structures versus the photon energy frm 1.5 to 6 (eV)

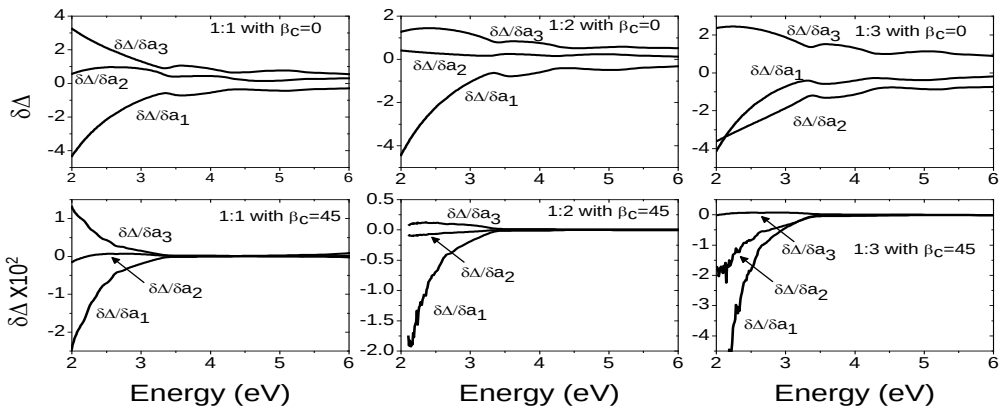

Figure 3.6. The variation in Δ for all structures versus the photon energy from 1.5 to 6 (eV).

3.4.3 Offset Error

In reality, random and systematic errors are the main error sources affecting ellipsometric measurements. Random errors are attributed to random or statistical processes but systematic errors result from the experimental setup errors. In ellipsometric measurements, random errors could be due to thermally generated noise in electronic elements. This type of error can be significantly reduced by signal averaging of multiple identical runs and by calculating the mean and the standard deviation. On the other hand, systematic errors can be reduced by careful calibration of high quality optical element setup. Some sources of systematic errors are due to the azimuthally misalignment of optical elements with respect to the plane of incidence, sample mispositioning, beam deviation, and collimation errors [24]. Other sources of systematic error could be the light wavelength and the angle of incidence. Therefore, it is very important to mention systematic errors in the proposed structures. For the verification process, we will assume misalignment of the fixed polarizer, rotating polarizer, and rotating analyzer. The effect of these misalignments on ψ, Δ, n, and k will be investigated. We will restrict the following calculations to the case $\beta_c = 0$. Figure 3.7 shows the percent error in ψ, Δ, n,

and k for the three ellipsometric configurations at $\beta_c = 0$ as a function of the error of the fixed polarizer azimuth angle θ, varied from -0.2° to 0.2° in steps of 0.01^o; while keeping the two other variables (τ and α) equal to zero. As can be seen from the figure, the impact of these errors on ψ, Δ, and n is not significant for small misalignment in θ. On the other hand, it is relatively considerable for k for the ellipsometric configuration of ratio 1:3. The figure also reveals that the ellipsometric configuration with the speed ratio 1:2 has the lowest impact on the parameters under investigation. On the other hand, the ellipsometric configuration with the speed ratio 1:3 has the highest impact on these parameters.

In analogy to Fig. 3.7, Fig. 3.8 shows the percent error in ψ, Δ, n, and k for the three ellipsometric configurations as a function of the error of the rotating analyzer initial azimuth angle α, varied from -0.2° to 0.2° in steps of 0.01°; while keeping the two other variables (τ and θ) equal to zero. The figure reveals the same observations that have been seen in Fig. 3.7. Any misalignment in the rotating analyzer azimuth angle has a neglected impact on ψ, Δ, and n and a relatively considerable impact on k. The structure with the speed ratio 1:2 corresponds to the minimum percent error in these parameters among all structures whereas the maximum error is accompanied with the structure having the speed ratio 1:3.

The percent error in ψ, Δ, n, and k for the three ellipsometric configurations as a function of the error of the rotating polarizer initial azimuth angle τ is plotted in Fig. 3.9. The same comments that have been extracted from Figs. 3.7 and 3.8 can also be seen in Fig. 3.9.

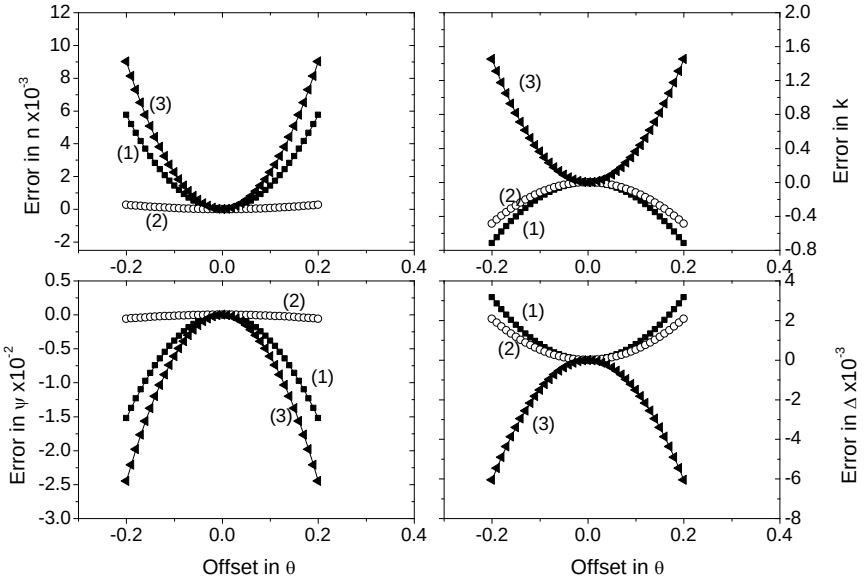

Figure 3.7. Percent error in *n*, *k*, ψ, and Δ for c-Si sample at λ=632.8 nm as a function of the error in θ while keeping the two other variables (τ and α) equal to zero. (1) 1:1, (2) 1:2, and (3) 1:3.

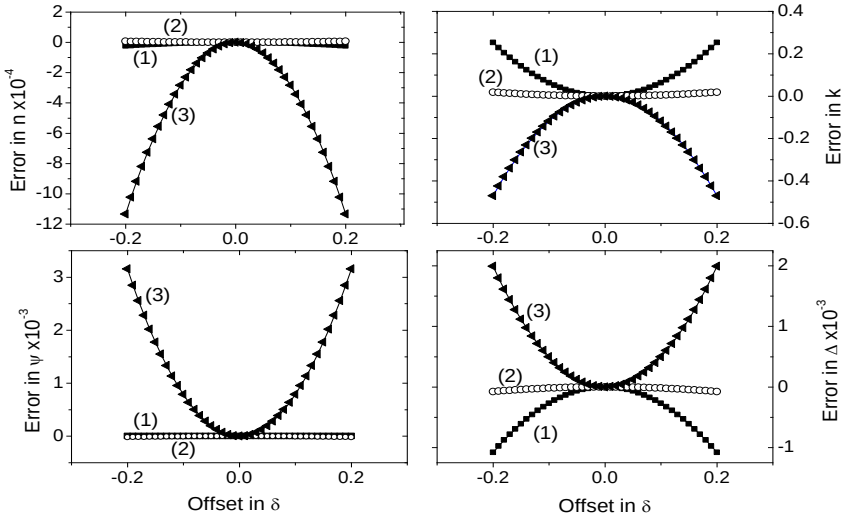

Figure 3.8. Percent error in *n*, *k*, ψ, and Δ for c-Si sample at λ=632.8 nm as a function of the error in α while keeping the two other variables (τ and θ) equal to zero. (1) 1:1, (2) 1:2, and (3) 1:3.

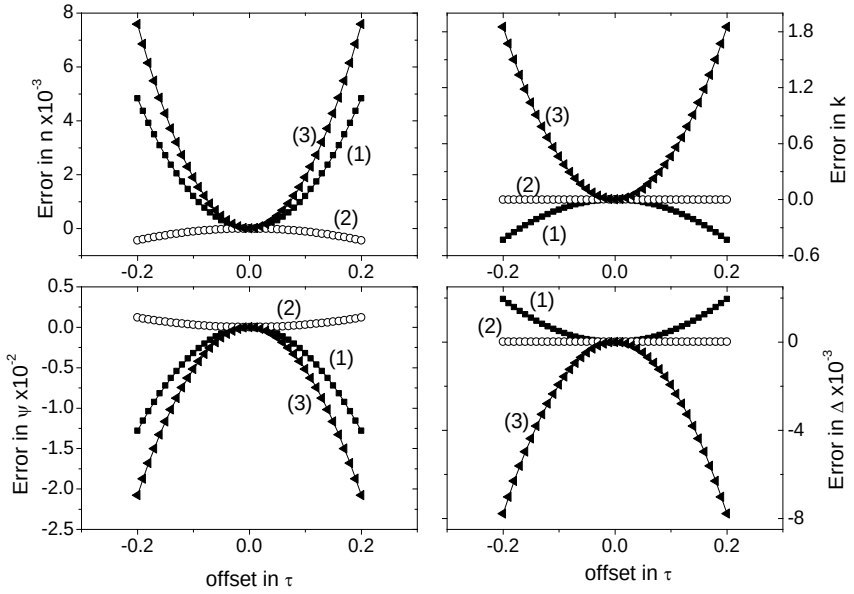

Figure 3.9. Percent error in *n*, *k*, ψ, and Δ for c-Si sample at λ=632.8 nm as a function of the error in τ while keeping the two other variables (θ and α) equal to zero. (1) 1:1, (2) 1:2, and (3) 1:3.

CHAPTER FOUR

Rotating Compensator Ellipsometric Configurations

In this chapter, a set of an ellipsometric configurations using a rotating polarizer, compensator, and analyzer at a speed ratio of $N_1\omega$:$N_2\omega$:$N_3\omega$, respectively are proposed theoretically. Different ellipsometric configurations can be obtained by giving different integers to N_1, N_2, and N_3. All configurations are applied to bulk c-Si and GaAs to calculate the real and imaginary parts of the refractive index of the samples. The accuracy of all ellipsometric configurations is investigated when a hypothetical noise is present and with small misalignments in the optical elements. Moreover, the uncertainties in the ellipsometric parameters as functions of the uncertainties of the Fourier coefficients are studied. The comparison among different configurations reveals that rotating compensator-analyzer configuration corresponds to the minimum error in the calculated optical parameters.

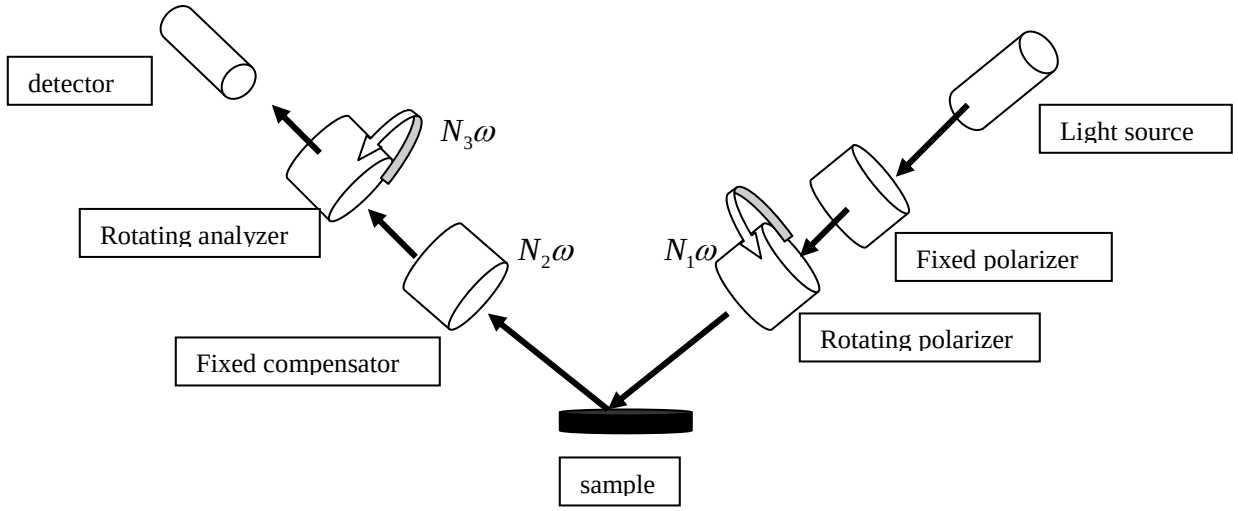

Figure 4.1 Optical configuration of ellipsometry, rotating polarizer, compensator and analyzer with speed ratio N_1 :N_2 :N_3.

4.1. Rotating Polarizer, Compensator And Analyzer Ellipsometer At Any Speed Ratio

In this section, a general ellipsometric structure in which three elements are rotating is proposed. The speed ratio at which the polarizer, compensator, and analyzer rotate is $N_1\omega$:$N_2\omega$:$N_3\omega$, respectively. The approach has the advantage that the equations of any ellipsometric configuration can be obtained just by substituting for N_1, N_2, and N_3. Six examples are obtained by assigning N_1, N_2, and N_3 some specific values thus, six different ellipsometric configurations will be studied and compared.

The proposed structure consists of a rotating polarizer, rotating compensator and rotating analyzer with angles $\beta_p = N_1 P + \gamma$, $\beta_c = N_2 P + \kappa$, and $\beta_A = N_3 P + \alpha$, where $P = \omega t$, and γ, κ, and α are the initial azimuth angles of the optical elements at $t = 0$. The Stokes vector of the detected light is given by

$$S = R(-\beta_A)\, A\, R(\beta_A)\, B R(-\beta_c)\, C R(\beta_c)\, R(-\beta_P)\, P\, R(\beta_P)\, P\, S_i, \qquad (4.1)$$

where S is a four-element column vector containing Stokes parameters S_0 through S_3, and $S_i = [1,0,0,0]^T$.

Using the matrices in Eqs. (1.88-1.91) and after performing the product of these matrices given by Eq. (4.1) and rearranging the result, the detected light intensity can be found from S_o which is the first component of the column vector S. To simplify the result, the following notation is considered

$$A = 1 - \frac{\cos(2\psi)}{4} - \frac{\cos(2\psi)\cos(\delta)}{4}, \qquad (4.2)$$

$$B = 1 - \frac{\cos(2\psi)}{2} - \frac{\cos(2\psi)\cos(\delta)}{2}, \tag{4.3}$$

$$C = -\frac{\cos(2\psi)}{4} - \frac{\cos(2\psi)\cos(\delta)}{4}, \tag{4.4}$$

$$D = -\frac{\cos(2\psi)}{2} + \frac{\cos(2\psi)\cos(\delta)}{2}, \tag{4.5}$$

$$E = \frac{1}{4} - \cos(2\psi) - + \frac{\cos(\delta)}{4}, \tag{4.6}$$

$$F = \frac{1}{4} - \frac{\cos(2\psi)}{2} + \frac{\cos(\delta)}{4}, \tag{4.7}$$

$$G = \frac{\sin(2\psi)\cos(\Delta)}{8} + \frac{\sin(2\psi)\cos(\Delta)\cos(\delta)}{8}, \tag{4.8}$$

$$H = \frac{1}{8} + \frac{\cos(\delta)}{8}, \tag{4.9}$$

$$J = \frac{1}{8} - \frac{\cos(\delta)}{8}, \tag{4.10}$$

$$K = \frac{\sin(2\psi)\cos(\Delta)}{4} - \frac{\sin(2\psi)\cos(\Delta)\cos(\delta)}{4}, \tag{4.11}$$

and

$$L = \frac{-\sin(2\psi)\sin(\Delta)\sin(\delta)}{4}. \tag{4.12}$$

In term of these coefficients, the general equation of the detected light intensity can be written as

$$
\begin{aligned}
I = {} & A + B\cos(2N_1)P + C\cos(4N_1)P + 2D\cos(4N_2)P + E\cos(2N_3)P \\
& + D\cos 2(2N_2 - N_1)P + 2D\cos 4(N_2 - N_1)P \\
& + F\left[\cos 2(N_1 - N_3)P + \cos 2(N_1 + N_3)P\right] \\
& + 2G\left[\cos 2(N_1 - N_3)P + \cos 2(N_1 + N_3)P\right] \\
& + H\left[\cos 2(2N_1 + N_3)P + \cos 2(2N_1 - N_3)P\right] \\
& + G\left[\cos 2(2N_1 + N_3)P - \cos 2(2N_1 - N_3)P\right] \\
& + J\left[\cos 2(2N_2 + N_3)P + \cos 2(2N_2 - N_3)P\right] \\
& + K\left[\cos 2(2N_2 - N_3)P - \cos 2(2N_2 + N_3)P\right] \\
& + 2J\left[\cos 2(2N_2 - N_1 + N_3)P + \cos 2(2N_2 - N_1 - N_3)P\right] \\
& + 2K\left[\cos 2(2N_2 - N_1 + N_3)P - \cos 2(2N_2 - N_1 - N_3)P\right] \\
& + J\left[\cos 2(2N_1 - 2N_2 + N_3)P + \cos 2(2N_1 - 2N_2 - N_3)P\right] \\
& + K\left[\cos 2(2N_1 - 2N_2 + N_3)P - \cos 2(2N_1 - 2N_2 - N_3)P\right] \\
& + 2L\left[\cos 2(N_1 - N_2 - N_3)P - \cos 2(N_1 - N_2 + N_3)P\right] \\
& + L\left[\cos 2(N_2 + N_3)P - \cos 2(N_2 - N_3)P\right] \\
& + L\left[+\cos 2(2N_1 - N_2 - N_3)P - \cos 2(2N_1 - N_2 + N_3)P\right] \quad . \qquad (4.13)
\end{aligned}
$$

Eq. (4.13) gives a general expression for the intensity received by the detector of the proposed structure. We will consider two cases. In the first case, both the compensator and the analyzer are rotated whereas the polarizer is fixed. In the second case, the compensator and the polarizer are rotated whereas the analyzer is fixed. In each case, three ellipsometric configurations are investigated by considering different speed ratios of the rotating elements. Section 4 covers the first case and section 5 presents the second one.

4.2. Rotating Compensator Analyzer Ellipsometer With A Fixed Polarizer

In this case, N_1 is set to be zero while N_2 and N_3 could be any integer. Also, $\gamma = 0$, $N_2 = 1$ and N_3=1, 2 or 3 is assumed. Three different ellipsometric configurations are

then obtained. For each configuration, the Fourier transform of the intensity is used to deduce the Fourier coefficients and the ellipsometric parameters.

4.2.1. Rotating Compensator Analyzer Ellipsometer With A Speed Ratio 1 : 1

In the first configuration, the following parameters and assumed $N_1 = 0$, $\gamma = 0$, $\kappa = 0$, $\alpha = 0$ and $N_2 = N_3 = 1$. Substituting these values into Eq. (4.13) and taking the Fourier transform of the result gives

$$I(t) = a_0 + \sum_{n=1}^{3} a_n \cos(2n\omega t), \tag{4.14}$$

where a_0 and a_n are the Fourier coefficients which are given by

$$a_0 = 2 - \cos(2\psi) - \cos(2\psi)\cos(\delta) + \sin(2\psi)\sin(\Delta)\sin(\delta), \tag{4.15}$$

$$a_1 = \frac{3}{2} - 2\cos(2\psi) + \frac{\cos(\delta)}{2} - \frac{\sin(2\psi)\cos(\Delta)}{2} - \frac{\sin(2\psi)\cos(\Delta)\cos(\delta)}{2}, \tag{4.16}$$

$$a_2 = -\cos(2\psi) + \cos(2\psi)\cos(\delta) - \sin(2\psi)\sin(\Delta)\sin(\delta), \tag{4.17}$$

$$a_3 = \frac{1}{2} - \frac{\cos(\delta)}{2} - \frac{\sin(2\psi)\cos(\Delta)}{2} + \frac{\sin(2\psi)\cos(\Delta)\cos(\delta)}{2}. \tag{4.18}$$

Note that the intensity contains three AC Fourier coefficients a_1, a_2 and a_3 in addition to a DC term a_0. The intensity is symmetric since $\sin(2n\omega t)$ terms are missing. That is, the intensity has cosine terms only. Solving Eqs. (4.16-4.18) for tan(ψ) and cos(Δ) gives

$$\sin(\psi) = \sqrt{\frac{a_1 + a_3}{4}}\,, \tag{4.19}$$

$$\cos(\psi) = \sqrt{\frac{4 - a_1 - a_3}{4}}\,, \tag{4.20}$$

$$\tan(\psi) = \sqrt{\frac{a_1 + a_3}{4 - a_1 - a_3}}\,, \tag{4.21}$$

and

$$\cos(\Delta) = \frac{-2a_3 + 1 - \cos(\delta)}{2(1-\cos(\delta))\sin(\psi)\cos(\psi)}\quad . \tag{4.22}$$

It is worth to investigate the uncertainties $\delta\psi$ and $\delta\cos(\Delta)$ in the ellipsometric parameters ψ and Δ due to the fluctuations in the Fourier coefficients. The uncertainties $\delta\psi$ and $\delta\cos(\Delta)$ are calculated by differentiating Eq. (4.21) and Eq. (4.22) as follows

$$\partial\psi = \frac{\partial\psi}{\partial a_1}\partial a_1 + \frac{\partial\psi}{\partial a_3}\partial a_3\,, \tag{4.23}$$

$$\partial\cos(\Delta) = \frac{\partial\cos(\Delta)}{\partial a_1}\partial a_1 + \frac{\partial\cos(\Delta)}{\partial a_3}\partial a_3\ , \tag{4.24}$$

where

$$\frac{\partial\psi}{\partial a_1} = \frac{1}{1+\tan^2(\psi)}\frac{1}{8\cos^2(\psi)}\left(\cot(\psi) + \tan(\psi)\right), \tag{4.25}$$

$$\frac{\partial \psi}{\partial a_3} = \frac{1}{1+\tan^2(\psi)} \frac{1}{8\cos^2(\psi)} \left(\cot(\psi) + \tan(\psi)\right),$$

(4.26)

$$\frac{\partial \cos(\Delta)}{\partial a_1} = \frac{\cos(\Delta)}{8} \left(\frac{\tan(\psi) - \cot(\psi)}{\sin(\psi)\cos(\psi)} \right), \tag{4.27}$$

and

$$\frac{\partial \cos(\Delta)}{\partial a_3} = \frac{\cos(\Delta)}{8} \left(\frac{\tan(\psi) - \cot(\psi)}{\sin(\psi)\cos(\psi)} \right) - \frac{1}{(1-\cos(\delta))\sin(\psi)\cos(\psi)}. \tag{4.28}$$

4.2.2 Rotating Compensator Analyzer Ellipsometer With A Speed Ratio 1 : 2

In the second configuration, the following values $\gamma = 0$, $\kappa = 0$, $\alpha = 0$, $N_1 = 0$, $N_2 = 1$ and $N_3 = 2$ are assumed. The Fourier transformation of Eq. (4.13) contains one DC and four AC coefficients. It is given by

$$I(t) = a_0 + \sum_{n=1}^{4} a_n \cos(2n\omega t), \tag{4.29}$$

where

$$a_0 = \frac{5}{2} - \frac{\cos(\delta)}{2} - \cos(2\psi) - \cos(2\psi)\cos(\delta) + \sin(2\psi)\cos(\Delta) - \sin(2\psi)\cos(\Delta)\cos(\delta),$$

(4.30)

$$a_1 = \sin(2\psi)\sin(\Delta)\sin(\delta), \tag{4.31}$$

$$a_2 = 1 - 3\cos(2\psi) + \cos(2\psi)\cos(\delta), \tag{4.32}$$

$$a_3 = -\sin(2\psi)\sin(\Delta)\sin(\delta), \tag{4.33}$$

and

$$a_4 = \frac{1}{2} - \frac{\cos(\delta)}{2} - \frac{\sin(2\psi)\cos(\Delta)}{2} + \frac{\sin(2\psi)\cos(\Delta)\cos(\delta)}{2}. \tag{4.34}$$

From these Fourier coefficients we can derive ψ and Δ can be derived as follows

$$\tan(\psi) = \sqrt{\frac{-a_2 - 2 + 2\cos(\delta)}{a_2 - 4}}, \tag{4.35}$$

$$\cos(\Delta) = \frac{-2a_4 + 1 - \cos(\delta)}{D}, \tag{4.36}$$

where

$$D = (1 - \cos(\delta))\sqrt{\frac{a_1^2}{1 - \cos^2(\delta)} + \left(\frac{2a_4 - 1 + \cos(\delta)}{1 - \cos(\delta)}\right)^2}. \tag{4.37}$$

Differentiation of Eqs. (4.35) and (4.36) to get $\delta\psi$ and $\delta\cos(\Delta)$ as follows

$$\delta\psi = \frac{\delta\psi}{\delta a_2}\delta a_2, \tag{4.38}$$

$$\delta\cos(\Delta) = \frac{\delta\cos(\Delta)}{\delta a_1}\delta a_1 + \frac{\delta\cos(\Delta)}{\delta a_4}\delta a_4, \tag{4.39}$$

where

$$\frac{\partial\psi}{\partial a_2} = \frac{1}{1 + \tan^2(\psi)}\frac{1}{\tan(\psi)}\left(\frac{3 - \cos(\delta)}{(a_2 - 4)^2}\right), \tag{4.40}$$

$$\frac{\partial \cos(\Delta)}{\partial a_1} = \frac{\cos(\Delta)}{D^2}\left(\frac{1-\cos(\delta)}{1+\cos(\delta)}\right)a_1 \ . \tag{4.41}$$

and

$$\frac{\partial \cos(\Delta)}{\partial a_4} = \frac{-2}{D} - \frac{2(2a_4 - 1 + \cos(\delta))\cos(\Delta)}{D^2}, \tag{4.42}$$

4.2.3 Rotating Compensator Analyzer Ellipsometer With A Speed Ratio 1 : 3

Another ellipsometric configuration can be obtained by letting $N_2 = 1$ and $N_3 = 3$ provided that $N_1 = \gamma = 0$, $\kappa = 0$ and $\alpha = 0$. When these values are inserted into Eq. (4.13), the Fourier transformation is found to have five AC terms in addition to one DC term. It is given by

$$I(t) = a_0 + \sum_{n=1}^{5} a_n \cos(2n\omega t), \tag{4.43}$$

where

$$a_0 = 2 - \cos(2\psi) - \cos(2\psi)\cos(\delta), \tag{4.44}$$

$$a_1 = \frac{1}{2} - \frac{\cos(\delta)}{2} + \frac{\sin(2\psi)\cos(\Delta)}{2} - \frac{\sin(2\psi)\cos(\Delta)\cos(\delta)}{2}, \tag{4.45}$$

$$a_2 = \cos(2\psi) + \cos(2\psi)\cos(\delta) + \sin(2\psi)\sin(\Delta)\sin(\delta), \tag{4.46}$$

$$a_3 = 1 + \cos(\delta) - 2\cos(2\psi), \tag{4.47}$$

$$a_4 = -\sin(2\psi)\sin(\Delta)\sin(\delta), \tag{4.48}$$

and

$$a_5 = \frac{1}{2} - \frac{\cos(\delta)}{2} - \frac{\sin(2\psi)\cos(\Delta)}{2} + \frac{\sin(2\psi)\cos(\Delta)\cos(\delta)}{2}. \quad (4.49)$$

The ellipsometric parameters ψ and Δ can be derived from these coefficients, as follows

$$\sin(\psi) = \sqrt{\frac{a_1 + a_3 + a_5}{4}}, \quad (4.50)$$

$$\cos(\psi) = \sqrt{\frac{3 + \cos(\delta)}{1 - \cos(\delta)}\left(\frac{a_1 + a_5}{4}\right) - \frac{a_3}{4}}, \quad (4.51)$$

$$\tan(\psi) = \frac{\sin(\psi)}{\cos(\psi)}, \quad (4.52)$$

$$\cos(\Delta) = \frac{a_1 - a_5}{2(1 - \cos(\delta))\sin(\psi)\cos(\psi)}. \quad (4.53)$$

Moreover, the uncertainties of ψ and Δ are given by,

$$\delta\psi = \frac{\delta\psi}{\delta a_1}\delta a_1 + \frac{\delta\psi}{\delta a_3}\delta a_3 + \frac{\delta\psi}{\delta a_5}\delta a_5, \quad (4.54)$$

$$\delta\cos(\Delta) = \frac{\delta\cos(\Delta)}{\delta a_1}\delta a_1 + \frac{\delta\cos(\Delta)}{\delta a_3}\delta a_3 + \frac{\delta\cos(\Delta)}{\delta a_5}\delta a_5, \quad (4.55)$$

where

$$\frac{\partial\psi}{\partial a_1} = \frac{1}{1 + \tan^2(\psi)}\frac{1}{8\cos^2(\psi)}\left(\cot(\psi) - \frac{3 + \cos(\delta)}{1 - \cos(\delta)}\tan(\psi)\right), \quad (4.56)$$

$$\frac{\partial \psi}{\partial a_3} = \frac{1}{1+\tan^2(\psi)} \frac{1}{8\cos^2(\psi)} \big(\cot(\psi) - \tan(\psi)\big), \tag{4.57}$$

$$\frac{\partial \psi}{\partial a_5} = \frac{1}{1+\tan^2(\psi)} \frac{1}{8\cos^2(\psi)} \left(\cot(\psi) - \frac{3+\cos(\delta)}{1-\cos(\delta)} \tan(\psi) \right), \tag{4.58}$$

$$\frac{\partial \cos(\Delta)}{\partial a_1} = \frac{1}{E} - \frac{\big[(3+\cos(\delta))\tan(\psi) + \big(1-\cos(\delta)\big)\cot(\psi)\big]\cos(\Delta)}{4E}, \tag{4.59}$$

$$\frac{\partial \cos(\Delta)}{\partial a_3} = \frac{(1-\cos(\delta))\big[-\tan(\psi) + \cot(\psi)\big]\cos(\Delta)}{4E}, \tag{4.60}$$

$$\frac{\partial \cos(\Delta)}{\partial a_5} = \frac{-1}{E} - \frac{\big[(3+\cos(\delta))\tan(\psi) + \big(1-\cos(\delta)\big)\cot(\psi)\big]\cos(\Delta)}{4E}, \tag{4.61}$$

and

$$E = 2\big(1-\cos(\delta)\big)\sin(\psi)\cos(\psi). \tag{4.62}$$

4.3. Rotating Polarizer Compensator Ellipsometer With A Fixed Analyzer

In the second case, the analyzer is fixed while both the compensator and polarizer are rotated with different ratios. To achieve this, $N_3 = 0$ and $\alpha = \frac{\pi}{4}$ are assumed while N_1 and N_2 may take any integral values to obtain different ellipsometric configurations as will be shown in the following subsections.

4.3.1 Rotating Polarizer Compensator Ellipsometer With A Speed Ratio 1 : 1

In the first configuration, $N_1 = N_2 = 1$, $\kappa = 0$ and $\gamma = 0$ are assumed. Substituting these values into Eq. (4.13) and taking the Fourier transform of the results gives the following expression for the intensity

$$I(t) = a_0 + \sum_{n=1}^{2} a_n \cos(2n\omega t) + \sum_{n=1}^{2} b_n \sin(2n\omega t), \tag{4.63}$$

where,

$$a_0 = 1 - \frac{\cos(2\psi)}{2}, \tag{4.64}$$

$$a_1 = 1 - \cos(2\psi), \tag{4.65}$$

$$a_2 = \frac{-\cos(2\psi)}{2}, \tag{4.66}$$

$$b_1 = \sin(2\psi)\cos(\Delta), \tag{4.67}$$

$$b_2 = \frac{\sin(2\psi)\cos(\Delta)}{2}. \tag{4.68}$$

For this ellipsometric configuration, ψ and Δ are given in terms of Fourier coefficients as

$$\sin(\psi) = \sqrt{\frac{a_1}{2}}, \tag{4.69}$$

$$\cos(\psi) = \sqrt{\frac{a_1 - 4a_2}{2}}, \tag{4.70}$$

$$\tan(\psi) = \sqrt{\frac{a_1}{a_1 - 4a_2}}, \tag{4.71}$$

$$\cos(\Delta) = \frac{b_1}{2\sin(\psi)\cos(\psi)}. \tag{4.72}$$

The last two equations are differentiated to get $\delta\psi$ and $\delta\cos(\Delta)$ as follows

$$\delta\psi = \frac{\delta\psi}{\delta a_1}\delta a_1 + \frac{\delta\psi}{\delta a_2}\delta a_2, \tag{4.73}$$

$$\delta\cos(\Delta) = \frac{\delta\cos(\Delta)}{\delta a_1}\delta a_1 + \frac{\delta\cos(\Delta)}{\delta a_2}\delta a_2 + \frac{\delta\cos(\Delta)}{\delta b_1}\delta b_1, \tag{4.74}$$

where

$$\frac{\partial\psi}{\partial a_1} = \frac{1}{1+\tan^2(\psi)}\frac{1}{4\cos^2(\psi)}\left(\cot(\psi) - \tan(\psi)\right), \tag{4.75}$$

$$\frac{\partial\psi}{\partial a_2} = \frac{1}{1+\tan^2(\psi)}\frac{1}{4\cos^2(\psi)}\left(\tan(\psi)\right), \tag{4.76}$$

$$\frac{\partial\cos(\Delta)}{\partial a_1} = \frac{-\cos(\Delta)}{4}\left(\frac{1}{\cos^2(\psi)\sin^2(\psi)}\right), \tag{4.77}$$

$$\frac{\partial\cos(\Delta)}{\partial a_2} = \frac{\cos(\Delta)}{4}\left(\frac{1}{\cos^2(\psi)}\right), \tag{4.78}$$

and

$$\frac{\partial\cos(\Delta)}{\partial b_1} = \frac{1}{2\sin(\psi)\cos(\psi)}. \tag{4.79}$$

4.3.2 Rotating Polarizer Compensator Ellipsometer With A Speed Ratio 1 : 2

In the second configuration, the following values are assumed $N_1 = 1$ and $N_2 = 2$, κ = 0, γ = 0 and $\alpha = \pi/4$. The Fourier transformation of Eq. (4.13) contains one DC and eight AC coefficients. It is given by

$$I(t) = a_0 + \sum_{n=1}^{4} a_n \cos(2n\omega t) + \sum_{n=1}^{4} b_n \sin(2n\omega t), \tag{4.80}$$

where

$$a_0 = 1 - \frac{\cos(2\psi)}{4} - \frac{\cos(2\psi)\cos(\delta)}{4}, \tag{4.81}$$

$$a_1 = 1 - \frac{\cos(2\psi)}{2} - \frac{\cos(2\psi)\cos(\delta)}{2}, \tag{4.82}$$

$$a_2 = \frac{-\cos(2\psi)}{2}, \tag{4.83}$$

$$a_3 = -\frac{\cos(2\psi)}{2} + \frac{\cos(2\psi)\cos(\delta)}{2}, \tag{4.84}$$

$$a_4 = -\frac{\cos(2\psi)}{4} + \frac{\cos(2\psi)\cos(\delta)}{4}, \tag{4.85}$$

$$b_1 = \frac{\sin(2\psi)\cos(\Delta)}{2} + \frac{\sin(2\psi)\cos(\Delta)\cos(\delta)}{2} + \sin(2\psi)\sin(\Delta)\sin(\delta), \tag{4.86}$$

$$b_2 = \frac{\sin(2\psi)\cos(\Delta)}{2} + \frac{\sin(2\psi)\sin(\Delta)\sin(\delta)}{2}, \tag{4.87}$$

$$b_3=\frac{\sin(2\psi)\cos(\Delta)}{2}-\frac{\sin(2\psi)\cos(\Delta)\cos(\delta)}{2}, \tag{4.88}$$

and,

$$b_3=\frac{\sin(2\psi)\cos(\Delta)}{4}-\frac{\sin(2\psi)\cos(\Delta)\cos(\delta)}{4}. \tag{4.89}$$

Using Eqs. (4.82-4.84), ψ and Δ can be found in terms of AC Fourier coefficients a_1, a_2 and a_3 such that

$$\sin(\psi)=\sqrt{\frac{a_1+a_3}{2}}, \tag{4.90}$$

$$\cos(\psi)=\sqrt{\frac{a_1+a_3-4a_2}{2}}, \tag{4.91}$$

$$\tan(\psi)=\sqrt{\frac{a_1+a_3}{a_1+a_3-4a_2}}, \tag{4.92}$$

and

$$\cos(\Delta)=\frac{b_3}{(1-\cos(\delta))\sin(\psi)\cos(\psi)}. \tag{4.93}$$

As mentioned above, $\delta\psi$ and $\delta\cos(\Delta)$ can be obtained by differentiating Eqs. (4.92) and (4.93)

$$\delta\psi=\frac{\delta\psi}{\delta a_1}\delta a_1+\frac{\delta\psi}{\delta a_2}\delta a_2+\frac{\delta\psi}{\delta a_3}\delta a_3, \tag{4.94}$$

$$\delta\cos(\Delta)=\frac{\delta\cos(\Delta)}{\delta a_1}\delta a_1+\frac{\delta\cos(\Delta)}{\delta a_2}\delta a_2+\frac{\delta\cos(\Delta)}{\delta a_3}\delta a_3+\frac{\delta\cos(\Delta)}{\delta b_3}\delta b_3, \tag{4.95}$$

where

$$\frac{\partial \psi}{\partial a_1} = \frac{1}{1+\tan^2(\psi)} \frac{1}{4\cos^2(\psi)} \left(\cot(\psi) - \tan(\psi)\right), \tag{4.96}$$

$$\frac{\partial \psi}{\partial a_2} = \frac{1}{1+\tan^2(\psi)} \frac{1}{4\cos^2(\psi)} \left(\tan(\psi)\right), \tag{4.97}$$

$$\frac{\partial \psi}{\partial a_3} = \frac{1}{1+\tan^2(\psi)} \frac{1}{4\cos^2(\psi)} \left(\cot(\psi) - \tan(\psi)\right), \tag{4.98}$$

$$\frac{\partial \cos(\Delta)}{\partial a_1} = \frac{-\cos(\Delta)}{4} \left(\frac{1}{\cos^2(\psi)\sin^2(\psi)} \right), \tag{4.99}$$

$$\frac{\partial \cos(\Delta)}{\partial a_2} = \frac{\cos(\Delta)}{4} \left(\frac{1}{\cos^2(\psi)} \right), \tag{4.100}$$

$$\frac{\partial \cos(\Delta)}{\partial a_3} = \frac{-\cos(\Delta)}{4} \left(\frac{1}{\cos^2(\psi)\sin^2(\psi)} \right), \tag{4.101}$$

and

$$\frac{\partial \cos(\Delta)}{\partial b_3} = \frac{1}{\left(1-\cos(\delta)\right)\sin(\psi)\cos(\psi)}. \tag{4.102}$$

4.4.3 Rotating Polarizer Compensator Ellipsometer With A Speed Ratio 1 : 3

Another ellipsometric configuration can be obtained letting $N_1 = 1$ and $N_2 = 3$ provided that $N_3 = 0$, κ = 0, γ = 0 and $\alpha = \pi/4$. This represents a rotating polarizer compensator ellipsometer with a speed ratio 1:3. When these values are inserted into Eq. (4.13) the Fourier transformation is found to has twelve AC terms in addition to a DC term, then

$$I(t) = a_0 + \sum_{n=1}^{6} a_n \cos(2n\omega t) + \sum_{n=1}^{6} b_n \sin(2n\omega t), \tag{4.103}$$

where

$$a_0 = 1 - \frac{\cos(2\psi)}{4} - \frac{\cos(2\psi)\cos(\delta)}{4}, \tag{4.104}$$

$$a_1 = 1 - \frac{\cos(2\psi)}{2} - \frac{\cos(2\psi)\cos(\delta)}{2}, \tag{4.105}$$

$$a_2 = -\frac{\cos(2\psi)}{4} - \frac{\cos(2\psi)\cos(\delta)}{4}, \tag{4.106}$$

$$a_3 = 0, \tag{4.107}$$

$$a_4 = -\frac{\cos(2\psi)}{4} + \frac{\cos(2\psi)\cos(\delta)}{4}, \tag{4.108}$$

$$a_5 = -\frac{\cos(2\psi)}{2} + \frac{\cos(2\psi)\cos(\delta)}{2}, \tag{4.109}$$

$$a_6 = -\frac{\cos(2\psi)}{4} + \frac{\cos(2\psi)\cos(\delta)}{4}, \tag{4.110}$$

$$b_1 = \frac{\sin(2\psi)\cos(\Delta)}{2} + \frac{\sin(2\psi)\cos(\Delta)\cos(\delta)}{2} + \frac{\sin(2\psi)\sin(\Delta)\sin(\delta)}{2}, \tag{4.111}$$

$$b_2 = \frac{\sin(2\psi)\cos(\Delta)}{2} + \frac{\sin(2\psi)\cos(\Delta)\cos(\delta)}{2} - \sin(2\psi)\sin(\Delta)\sin(\delta), \tag{4.412}$$

$$b_3=\frac{\sin(2\psi)\sin(\Delta)\sin(\delta)}{2}, \tag{4.113}$$

$$b_4=\frac{\sin(2\psi)\cos(\Delta)}{4}-\frac{\sin(2\psi)\cos(\Delta)\cos(\delta)}{4}, \tag{4.114}$$

$$b_5=\frac{\sin(2\psi)\cos(\Delta)}{2}-\frac{\sin(2\psi)\cos(\Delta)\cos(\delta)}{2}, \tag{4.115}$$

and

$$b_6=\frac{\sin(2\psi)\cos(\Delta)}{4}-\frac{\sin(2\psi)\cos(\Delta)\cos(\delta)}{4}. \tag{4.116}$$

Solving Eqs. (4.105), (4.109) and (4.115) for ψ and Δ in terms of a_1, a_5, and b_5, yields

$$\sin(\psi)=\sqrt{\frac{a_1+a_5}{4}}, \tag{4.117}$$

$$\cos(\psi)=\sqrt{\frac{4-a_1-a_5}{4}}, \tag{4.118}$$

$$\tan(\psi)=\sqrt{\frac{a_1+a_5}{4-a_1-a_5}}, \tag{4.119}$$

$$\cos(\Delta)=\frac{b_5}{(1-\cos(\delta))\sin(\psi)\cos(\psi)}. \tag{4.120}$$

$\delta\psi$ and $\delta\cos(\Delta)$ are now given as follows

$$\delta\psi = \frac{\delta\psi}{\delta a_1}\delta a_1 + \frac{\delta\psi}{\delta a_5}\delta a_5, \tag{4.121}$$

$$\delta\cos(\Delta) = \frac{\delta\cos(\Delta)}{\delta a_1}\delta a_1 + \frac{\delta\cos(\Delta)}{\delta a_5}\delta a_5 + \frac{\delta\cos(\Delta)}{\delta b_5}\delta b_5, \tag{4.122}$$

where

$$\frac{\partial\psi}{\partial a_1} = \frac{1}{1+\tan^2(\psi)}\frac{1}{8\cos^2(\psi)}\left(\cot(\psi)+\tan(\psi)\right), \tag{4.123}$$

$$\frac{\partial\psi}{\partial a_5} = \frac{1}{1+\tan^2(\psi)}\frac{1}{8\cos^2(\psi)}\left(\cot(\psi)+\tan(\psi)\right), \tag{4.124}$$

$$\frac{\partial\cos(\Delta)}{\partial a_1} = \frac{\left[(-\tan(\psi)+\cot(\psi)\right]\cos(\Delta)}{8\sin(\psi)\cos(\psi)}, \tag{4.125}$$

$$\frac{\partial\cos(\Delta)}{\partial a_5} = \frac{\left[(-\tan(\psi)+\cot(\psi)\right]\cos(\Delta)}{8\sin(\psi)\cos(\psi)}, \tag{4.126}$$

and

$$\frac{\partial\cos(\Delta)}{\partial b_5} = \frac{1}{\left(1-\cos(\delta)\right)\sin(\psi)\cos(\psi)}. \tag{4.127}$$

4.5. Results And Discussion

Two cases have been discussed: rotating compensator analyzer with fixed polarizer ellipsometer (RCAE) and rotating polarizer and compensator with fixed analyzer ellipsometer (RPCE). For each case three different speed ratios for the rotating optical elements are assumed. In this section, the results obtained when applying these configurations to c-Si and GaAs samples will be presented. A sample consisting of one interface separating a semi-infinite air layer of refractive index N_0 as an ambient and a

bulk c-Si material of refractive index N_1 will be assumed. The incidence angle is taken to be $\theta_0 = 70^o$. The most common compensators are usually made from $CaCO_3$ crystal (calcite), MgF_2, and mica. $CaCO_3$ compensators are rarely used because the value of $|n_e - n_o|$ is relatively large. In spectroscopic ellipsometry MgF_2 and mica are commonly used. A MgF_2 compensator with retardance of $\pi/2$ at 4 eV will be assumed. The extraordinary and ordinary refractive indices of the compensator are taken from Ref. [35]. Based on Eq. (4.13), simulated light signals are generated. Fourier transform of the generated signal is taken to extract the Fourier coefficients using the equations derived above for each ellipsometric configuration. The ellipsometric parameters ψ and Δ in the photon energy range 1.5–6 eV are then derived using Eqs. (4.21) and (4.22) for RCAE with speed ratio 1:1, Eqs. (4.35) and (4.36) for RCAE with speed ratio 1:2, Eqs. (4.52) and (4.53) for RCAE with speed ratio 1:3, Eqs. (4.71) and (4.72) for RPCE with speed ratio 1:1, Eqs. (4.92) and (4.93) for RPCE with speed ratio 1:2, and Eqs. (4.119) and (4.120) for RPCE with speed ratio 1:3. These values of the ellipsometric parameters correspond to the clean signal without considering any noise. In practical situations, random fluctuations in the recorded signal appear due to the noise from many sources. to simulate reality, a random noise generated using a MathCAD code was superimposed on the clean signal according to the eqn. (2.34)

This noise is added to the pure signal. Fourier transform of the noisy signal is taken to extract the new Fourier coefficients in the presence of the noise. The same equations are then used to calculate the ellipsometric parameters ψ and Δ for the noisy signal in the same photon energy range. To calculate the complex refractive index of the sample, we use Eq. (2.35).

4.5.1 *n* And *k* Of c-Si And GaAs

The calculated values of *n* and *k* for c-Si and GaAs are plotted in Fig. 4.2 and Fig. 4.3, respectively along with the published values [35]. The points in Fig. 4.2 and Fig. 4.3 represent the calculated real and imaginary parts of the refractive index of c-Si and GaAs for the noisy signal using RCAE with speed ratio 1:1. If another ellipsometric

configuration is used the difference among them can not be obviously observed in this figure. To differentiate among them, the percent error in the calculated values of *n* and *k* for each ellipsometric configuration is calculated.

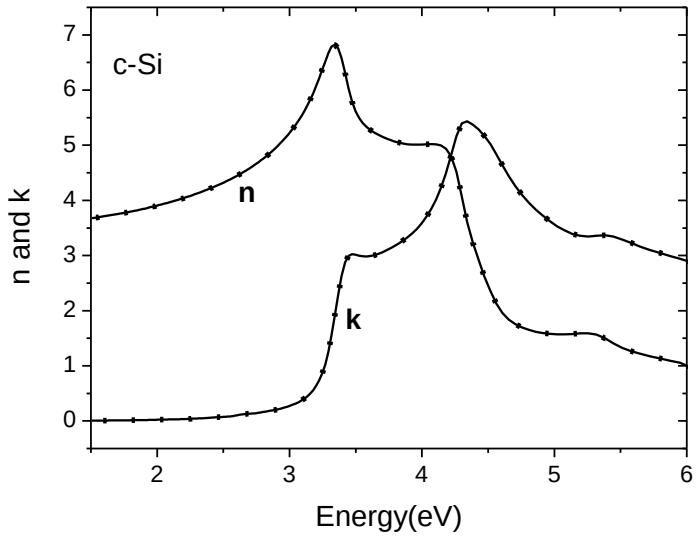

Figure 4.2. The real and the imaginary parts of the refractive index of c-Si in the photon energy range 1.5 to 6 eV. Lines: accepted values, Points: calculated values.

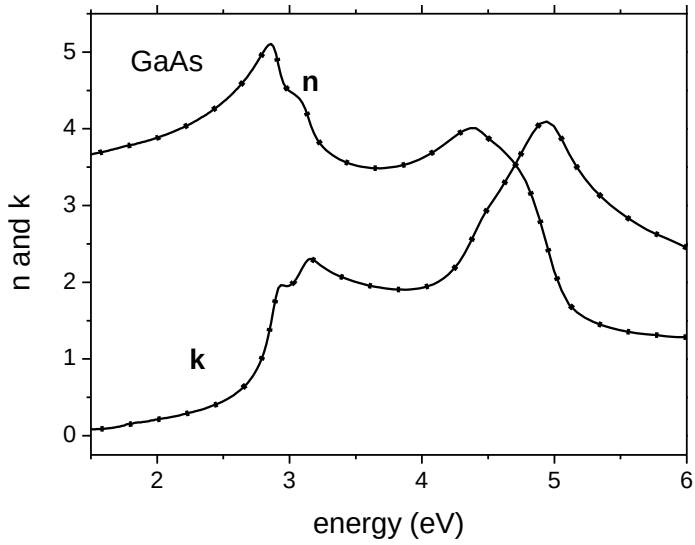

Figure 4.3. The real and the imaginary parts of the refractive index of GaAs in the photon energy range 1.5 to 6 eV. Lines: accepted values, Points: calculated values.

4.5.2 Percent Error In *n* And *k* Of c-Si And GaAs

The percent error in the calculated values of *n* has been calculated for the two samples (c-Si, GaAs) as shown in Figs. 4.4 and 4.5 for all ellipsometric configurations which are rotating polarizer and compensator with fixed analyzer (RPCE) using different speed ratios as well as rotating compensator and analyzer with fixed polarizer (RCAE) using different speed ratios. It should be emphasized that the fluctuations shown in the two figures are due to the noise imposed on the clean signal as mentioned before. Generally, the percent error in *n* for the two samples is low (of order 10^{-2}) for all ellipsometric configurations. As a result the comparison between them concerning the percent error in *n* is not of high significance.

Figures 4.6 and 4.7 show the percent error in *k* for the two samples. As can be seen from the figures, the percent error in *k* is much higher than that in *n*. Moreover, this percent error in *k* is crucially dependent on the ellipsometric configuration used. The two figures show that the RCAE with speed ratio 1:2 correspond to the minimum percent error in *k*.

For c-Si sample, the percent error ranges from -0.1% to 0.08% as shown in Fig. 4.6 whereas it ranges between ± 0.02% for GaAs sample as shown in Fig. 4.7. We can conclude that the RCAE with speed ratio 1:2 has a preference among other configurations. It is worth to mention that these values of *n* and *k* where calculated using a set of AC Fourier coefficients without depending on the DC coefficient. If the DC term is considered in the calculations, the percent error in *n* and *k* would be much higher [24, 25].

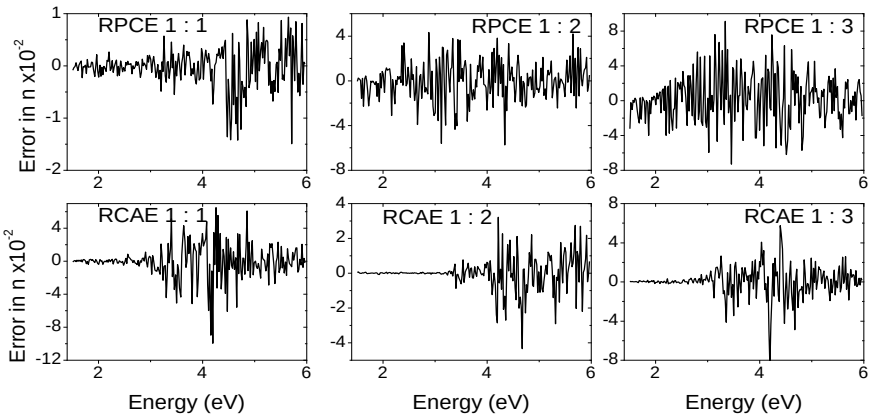

Figure 4.4. Percent error in the real part of the refractive index of c-Si for all the ellipsometric configurations.

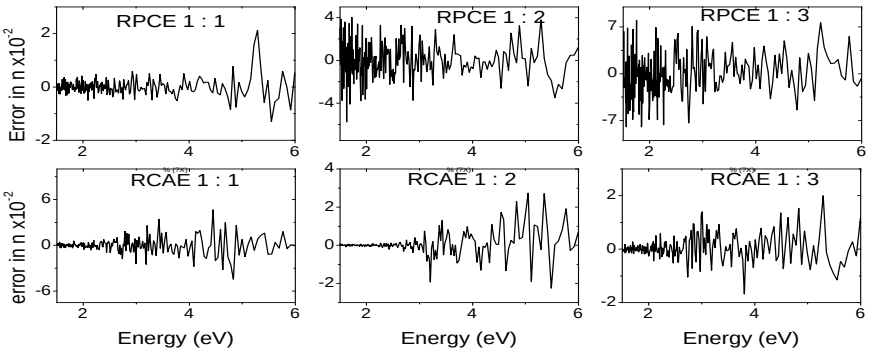

Figure 4.5. Percent error in the real part of the refractive index of GaAs for all the ellipsometric configurations.

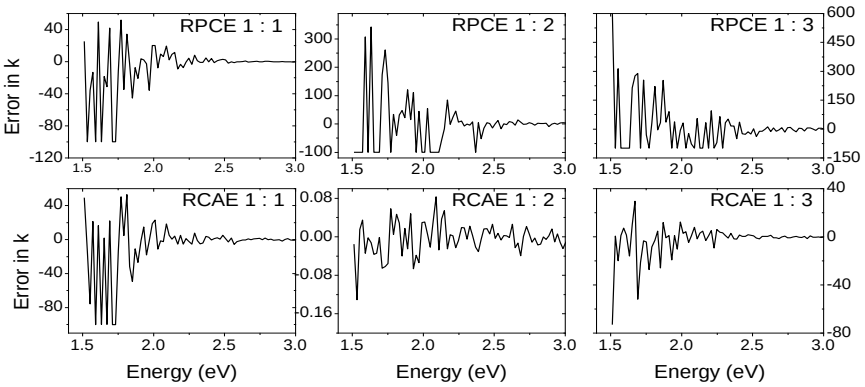

Figure 4.6. Percent error in the imaginary part of the refractive index of C-Si for all the ellipsometric configurations in the range 1.5eV to 3eV.

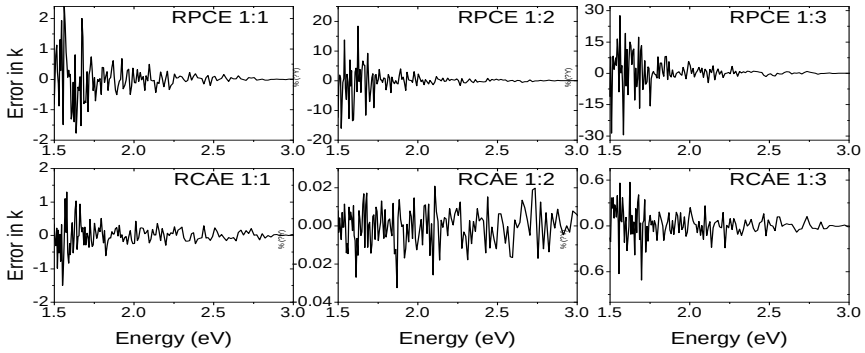

Figure 4.7. Percent error in the imaginary part of the refractive index of GaAs in the photon range 1.5 to 3 eV for all the ellipsometric configurations.

4.5.3 Uncertainties ψ And Δ

In this subsection, the uncertainties $\delta\cos(\Delta)$ and $\delta\psi$ in ψ and $\cos(\Delta)$ as functions of the uncertainties of the Fourier coefficients are invistigated. $\delta\cos(\Delta)$ and $\delta\psi$ represent the fluctuations of $\cos(\Delta)$ and ψ about their ideal values. The uncertainties $\delta\cos(\Delta)$ and $\delta\psi$ for c-Si sample for the six configurations are plotted in Figs. 4.8, 4.9, 4.10 and 4.11. Figure 4.8 shows $\delta\cos(\Delta)$ for the RCAE with speed ratios 1:1, 1:2 and 1:3. The first three panels in the figure show $\delta\cos(\Delta)$ due to the uncertainty of the Fourier coefficients for each ellipsometric configuration. For example the first panel (upper left) shows $\delta\cos(\Delta)$ due to the uncertainty of a_1 and a_3 using the RCAE with a speed ratio 1:1. The fourth panel shows the total variation in $\cos(\Delta)$ due to simultaneous uncertainty in all Fourier coefficients. From the figure, it is clear that structure has lowest uncertainty is 1:2 and this is in agreement with conclusion mentioned in the previous subsection. In similar manner, Fig. 4.9 shows the uncertainty in $\cos(\Delta)$ of the RPCE with speed ratios 1:1, 1:2 and 1:3. Comparing the two figures (4.8 and 4.9), the RCAE with the speed ration 1:2 is still the best structure due to the minimum percent error obtained with this configuration.

The uncertainty in ψ for the RPCE with different speed ratios is shown in Fig. 4.10 whereas it is shown in Fig. 4.11 for RCAE. As can be seen from the two figures, the ellipsometric parameter ψ is less sensitive to the uncertainty in the Fourier coefficients than Δ. Moreover, the sensitivity of ψ to the uncertainty in the Fourier coefficients is high in the low energy region compared to the low energy region for all ellipsometric configurations. Figure 4.11 reveals that RCAE with the speed ration 1:2 is still the best structure due to the low sensitivity of this configuration compared to other configurations.

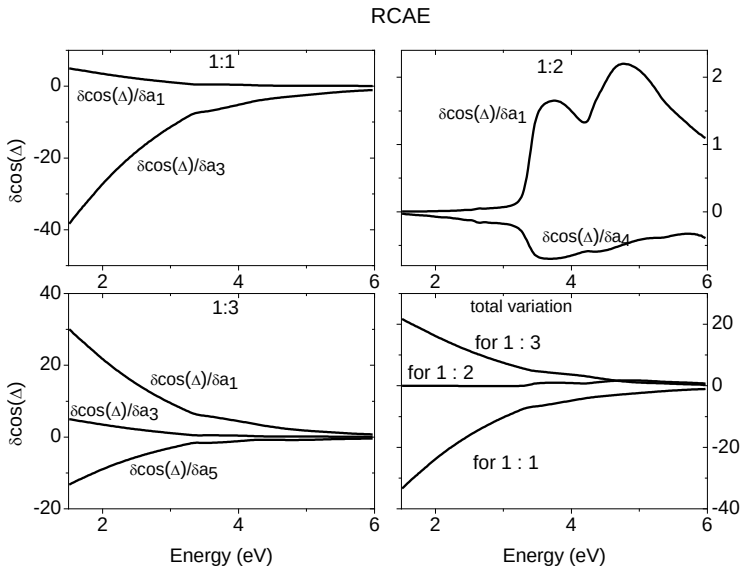

Figure 4.8. $\delta\cos(\Delta)$ with respect to Fourier coefficients in different RCAE structures.

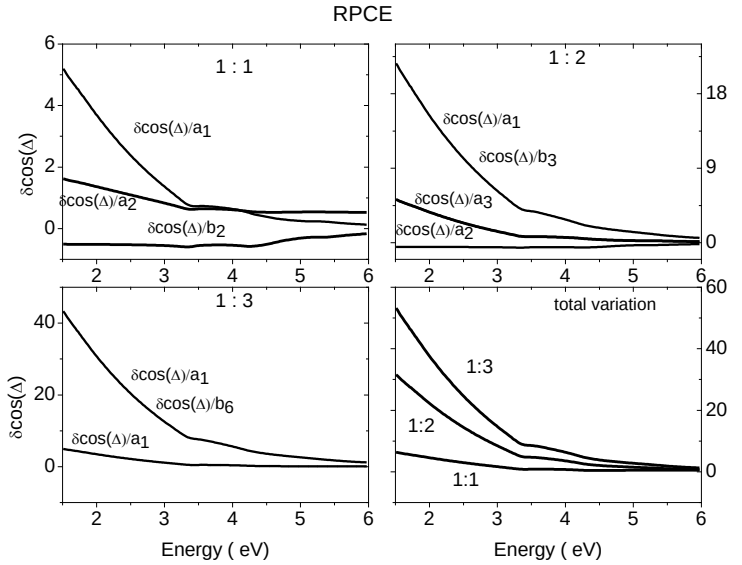

Figure 4.9. $\delta\cos(\Delta)$ with respect to Fourier coefficients in different RPCE structures.

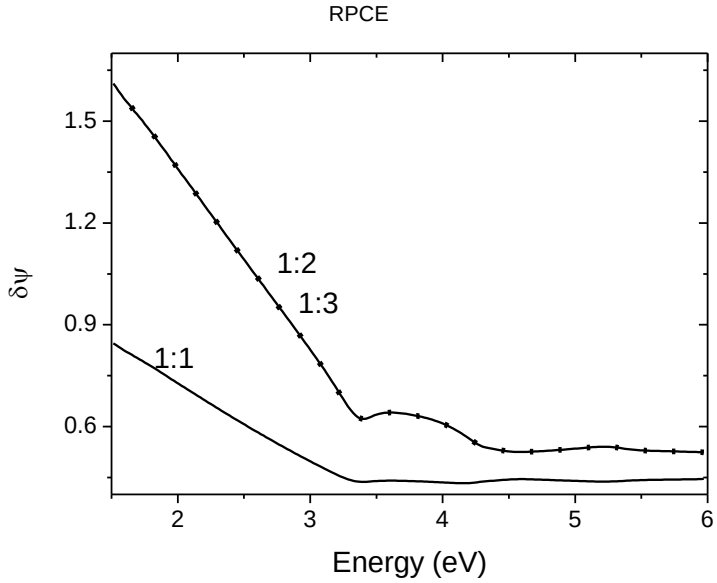

Figure 4.10. $\delta\psi$ with respect to Fourier coefficients in RPCE structure with speed ratios 1:1, 1:2 and 1:3.

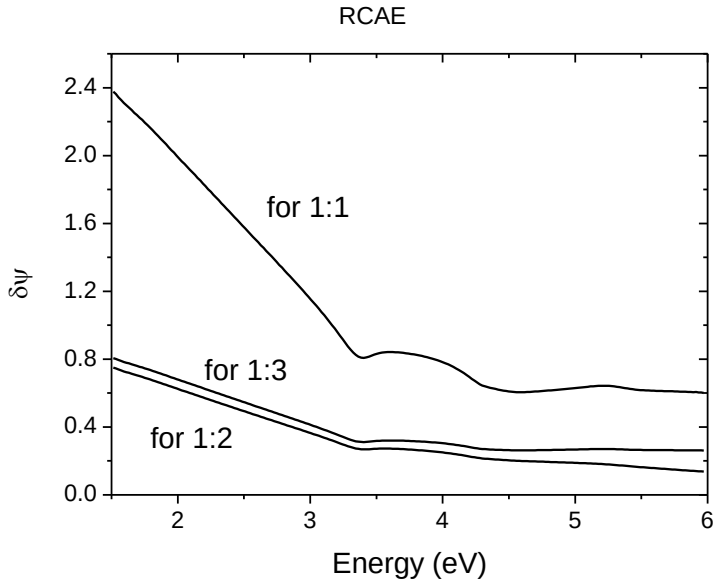

Figure 4.11. $\delta\psi$ with respect to Fourier coefficients in RCAE structure with speed ratios 1:1, 1:2 and 1:3.

4.5.4 Misalignment Of The Optical Elements

In practical situations, alignment of the optical elements with respect to the plane of incidence is not easy. Azimuthal misalignment of optical elements is considered one of the most affecting sources of systematic errors. It is very important to mention systematic error sources in such a structure. Sample mispositioning, beam deviation, collimation errors, and azimuthal misalignment of optical elements are the usual sources of systematic errors. Thus, it is important for the verification process to have some quantities for determination of the accuracy of the simulated data as a result of misalignment of the polarizer, and rotating compensator. The parameters to be checked are the ellipsometric parameters ψ and Δ as well as the real and imaginary parts of refractive index n and k.

Figures 4.12 and 4.13 show the percent error in ψ, Δ, n, and k for RCAE and RPCE respectively as a function of the error in the polarizer azimuth angle γ varied from -0.1° to 0.1° in steps of 0.01° while keeping the other variables equal to zero. Each figure shows the three ellipsometric configurations with the speed ratios 1:1, 1:2, and 1:3. As can be seen from the figures, the impact of misalignment of the rotating polarizer on ψ, Δ and n is not significant for small misalignment. On the other hand, it is considerable for k especially for RPCE with the speed ratio 1:3.

Similarly, Figs. 4.14 and 4.15 show the error in the same parameters for RPCE and RCAE for three speed ratios as a function of the error in the rotating compensator azimuth angle κ varied from -0.1° to 0.1° in steps of 0.01° while keeping the other variables equal to zero. Almost the same conclusions drawn from Figs. 4.12 and 4.13 can describe Figs. 4.14 and 4.15. The impact of misalignment of the rotating compensator on ψ, Δ and n is not considerable whereas it is relatively high for k especially for RPCE with the speed ratio 1:3.

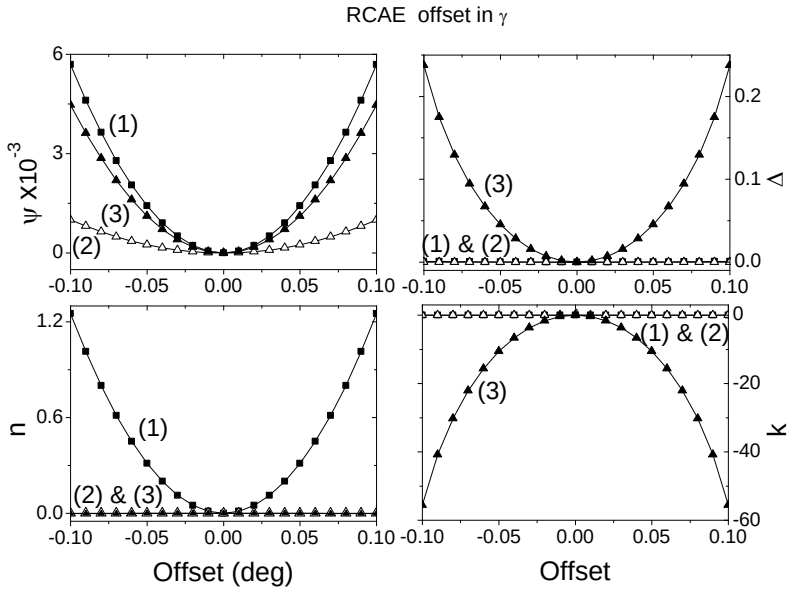

Figure 4.12. Percent error in *n*, *k*, ψ, and Δ for c-Si sample at λ=632.8 nm as a function of the error in *γ* while keeping the two other variables (κ and α) equal to zero. The figure represents RCAE with speed ratio (1) 1:1, (2) 1:2, and (3) 1:3.

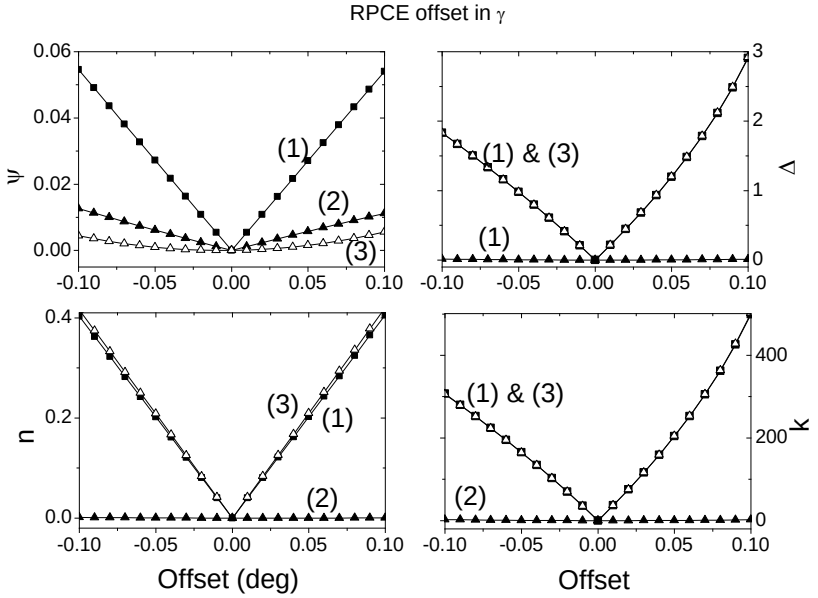

Figure 4.13. Percent error in *n*, *k*, ψ, and Δ for c-Si sample at λ=632.8 nm as a function of the error in *γ* while keeping the two other variables (κ and α) equal to zero. The figure represents RPCE with speed ratio (1) 1:1, (2) 1:2, and (3) 1:3.

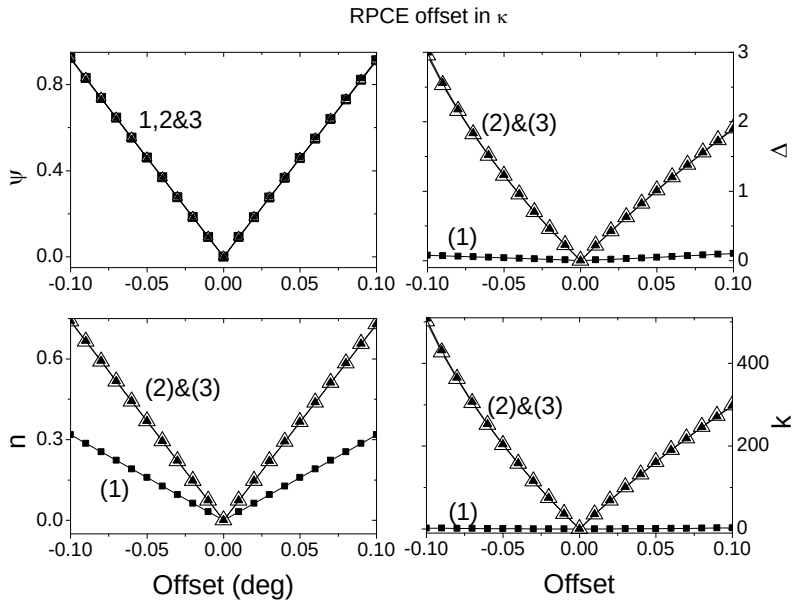

Figure 4.14. Percent error in *n*, *k*, ψ, and Δ for c-Si sample at λ=632.8 nm as a function of the error in κ while keeping the two other variables (*γ* and α) equal to zero. The figure represents RPCE with speed ratio (1) 1:1, (2) 1:2, and (3) 1:3.

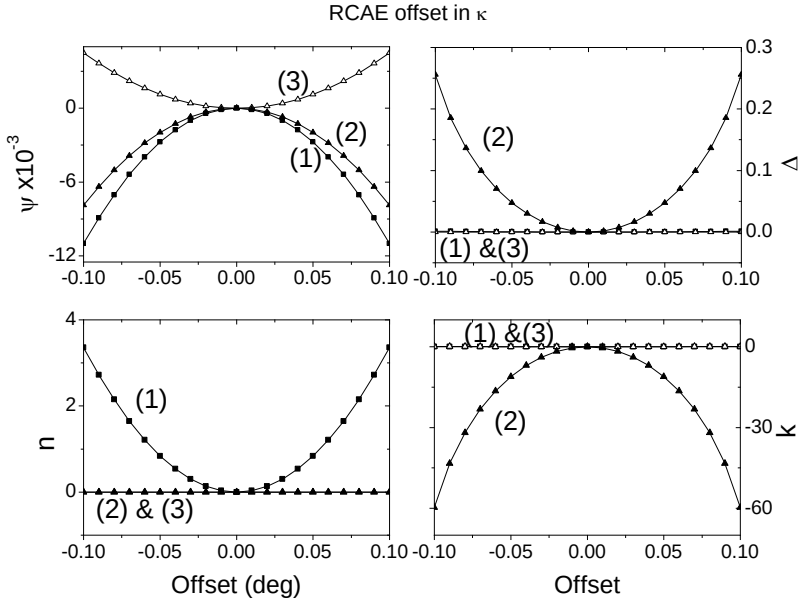

Figure 4.15. Percent error in *n*, *k*, ψ, and Δ for c-Si sample at λ=632.8 nm as a function of the error in κ while keeping the two other variables (*γ* and α) equal to zero. The figure represents RCAE with speed ratio (1) 1:1, (2) 1:2, and (3) 1:3.

Finally, it is worth to compare the best configuration in this study which is RCAE at a speed ratio 1:2 with the well known rotating compensator ellipsometer RCE [21]. The ellipsometric parameters of the RCE configuration can be obtained by setting N_1=45, N_2=1 and N_3 = 0 in Eq. (4.13), then ψ and Δ can be written as

$$\tan(\psi) = \frac{a_2}{\sqrt{a_2^{\,2} + 4b_2^{\,2}}} \qquad (4.129)$$

and

$$\cos(\Delta) = \frac{b_2}{2\sqrt{b_1^{\,2} + 4b_2^{\,2}}} \qquad (4.130)$$

Fig. (4.16) shows the variation of ψ with respect to Fourier coefficients for RCE and RCAE at a speed ratio 1:2. the figure shows that the sensitivity of ψ in the case of RCAE is much less than that in case of RCE especially for photon energies above 3.3eV.

Moreover, figure 4.17 shows the variation of $\cos(\Delta)$ due to the uncertainty in all Fourier coefficients for RCE and RCAE at a speed ratio 1 : 2. The sensitivity of $\cos(\Delta)$ in the case of RCAE is significantly less than that in the case of RCE especially for photon energies below 4eV. Therefore the preference of RCAE at a speed ratio 1 : 2 over the RCE is clear in the two figures.

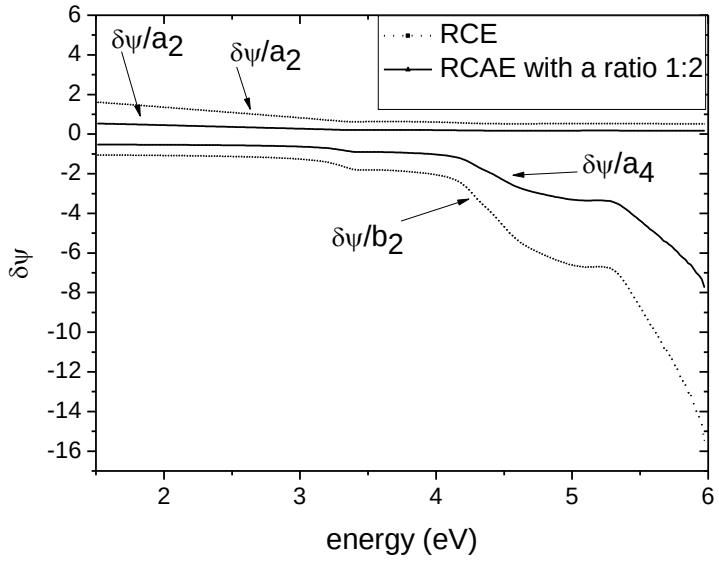

Figure 4.16. $\delta\psi$ with respect to the Fourier coefficients for RCE and RCAE at a speed ratio 1:2 for c-Si sample at 70^{o} angle of incidence.

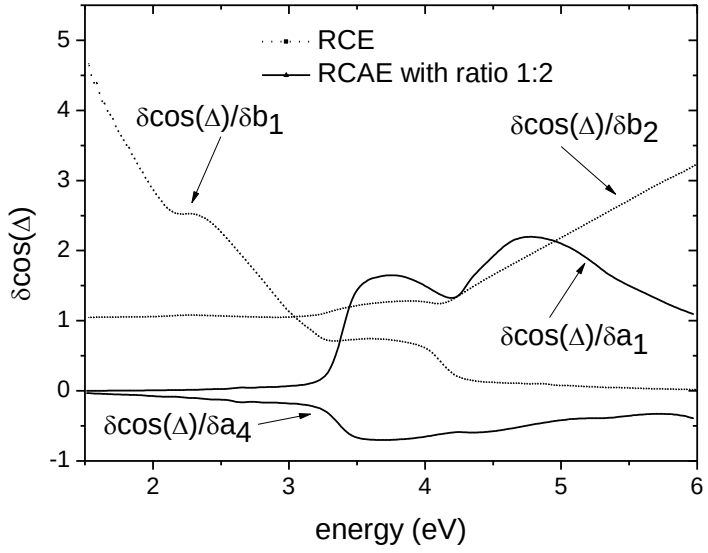

Figure 4.17. $\delta\cos(\Delta)$ with respect to the Fourier coefficients for RCE and RCAE at a speed ratio 1:2 for c-Si sample at 70^{o} angle of incidence.

CHAPTER FIVE

Characterization Of SiO_2 And Poly (9-Vinylcarbazole) Thin Films

In this chapter, a homemade rotating polarizer and analyzer spectroscopic is used to characterize some samples. In this system, the polarizer and the analyzer rotate in same directions with the same angular speed. The transmission axes of the two elements are rotated using microstepping motors. Commercial software for thin film analysis (TFCompanion-optical metrology software) obtained from Semiconsoft,Inc is used to analyze the experimental results. The results reveal a high accuracy device for thin film characterization.

5.1 Mathematical Treatment

A well-collimated beam of monochromatic unpolarized light is assumed to emerge through a fixed polarizer, a rotating polarizer, then is reflected from a sample, and finally is collected by a detector through the projection of a rotating analyzer. The analytical treatment of the proposed rotating polarizer and analyzer ellipsometer is similar to that presented in chapters 2, 3 and 4. For the sake of clarity, we here point out a part of this treatment. The intensity received by the detector can be written as [36]

$$I(t) = I_0[1 + a_1 \cos 2\omega t + a_2 \cos 4\omega t + a_3 \cos 6\omega t], \tag{5.1}$$

where I_0 is the average irradiance and ω is the mechanical angular speed of the rotating elements. The coefficients a_1, a_2, a_3, are the Fourier coefficients. The ellipsometric parameters ψ and Δ can be determined using the Fourier coefficients as follows

$$\tan\psi = \frac{\sqrt{a_1 + a_3}}{\sqrt{a_1 - 4a_2 + 9a_3}}, \tag{5.2}$$

$$\cos\Delta = \frac{-3a_3 + a_1 - 2a_2}{\sqrt{(a_1 + a_3)(a_1 - 4a_2 + 9a_3)}}. \tag{5.3}$$

5.2 Poly (9-Vinylcarbazole) , PVK

Carbazole is an aromatic tricyclic compound which was discovered in 1872 by Graebe and Glaser from the coal tar [37]. A high number of carbazole monomers linked together will form poly(vinylcarbazole) compound. The chemical structure of carbazole is illustrated in Fig. 5.1(a). Pure carbazole is a white crystalline organic material which has melting point of 246 ^{0}C, and 167.2 g/mole molecular weight. Carbazole has high boiling point compared with many of organic materials [37]. It is an electroluminescent material. Carbazole emits strong fluorescence and long phosphorescence by exciting with enough energy (ultraviolet) [38].

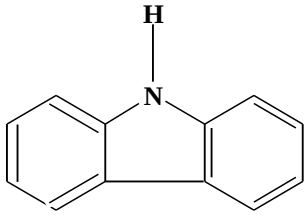

(a)

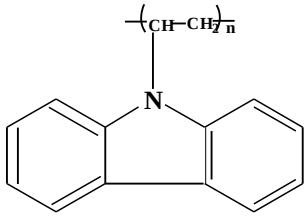

(b)

Figure 5.1. The structure of, (a) Carbazole (b) and Poly(9-vinylcarbazole).

Poly(9-vinylcarbazole) (PVK) is tricyclic organic polymeric material which is transparent plastic material. The softening point of PVK is nearly a 175 ^{0}C and glass transition temperature (Tg) is at 211^{0}C. The chemical structure of PVK is illustrated in Fig. 5.4(c). the solubility of PVK is very strong in alcohol, ether and THF. Usually PVK films are deposited by spin coating. It has good optical properties, PVK has a strong photoconductive and electroluminescence properties. It has a high refractive index ~1.69 in the visible region. Electrically, PVK is an insulator in dark but under the ultraviolet

radiation, it exhibits electro-conductivity. Commercially PVK is used as a paper capacitor, in OLEDs, data storage, sensors and transistors. In OLEDs, PVK is used as a hole transport material[37].

5.3. Experimental And Results

PVK with an average molecular weight of 11×10^5 was weighted by using a sensitive electrical balance (model N3. ESJ182-4) with a resolution of 10^{-4} gm. The PVK was dissolved in a proper amount of mixed solvents such as toluene and tetrahydrofuran (THF). A homogenous solution was then obtained. To construct a single layer of PVK thin film, 10 gm PVK + 5 ml THF +1 ml Toul. of the solution were placed on the cleaned Si substrate. Inclined coating method was used to form the film. The film thickness was increased by increasing the concentration amount of the PVK on a constant volume of mixed solvents and vice versa.

A homemade ellipsometer [36] was used to characterize samples. Measurements were taken at 70° angle of incidence. Three samples have been studied. The first one is a step-wafer (Si-SiO_2-step-wafer) 500 mm diameter. The following is the detailed data given in the calibration datasheet for this sample at the wavelength of 633 nm. For SiO_2 sample (S1), $\psi = 24.5^o$, $\Delta = 91.3^o$, thickness = 506.93 nm, and n = 1.459. The second and third samples where two thin PVK films deposited on Si substrate. Figures 5.2, 5.3 and 5.4 show the ellipsometry spectra obtained with the ellipsometer for S1 whereas Figs. 5.5,5.6 and 5.7 show the same parameters for S2 and Figs. 5.8,5.9 and 5.10 show the same parameters for S3. Discrete Fourier analysis was performed to deduce the normalized Fourier coefficients for each photon energy and then the ellipsometric parameters (ψ and Δ) were obtained using Eqs. (5.2) and (5.3). TFCompanion software is then used to analyze the results and to extract the thickness and the refractive index of the samples. TFCompanion is a powerful software for thin film analysis and metrology applications. The optical measurements are indirect in that they are measuring optical response of the physical properties not the properties themselves. One needs to solve an “inverse problem” in order to find the value of actual physical properties. The “inverse problem”

is solved numerically by finding the best fit between measured and calculated data. Physical properties are inferred from the model that gives the best fit. General solution is achieved by numerical methods of minimizing the difference between measured (target) data and simulated data, using selected optical model of the filmstack. Selected parameters of the filmstack are adjusted until the minimum error is achieved. TFCompanion uses modified Marquardt-Levenberg minimization that gives fast and robust convergence.

Our model of the samples consists of ambient-SiO_2-Si and ambient-PVK-Si. Since SiO_2 and PVK are dielectric materials with smooth dispersion, Cauchy approximation has been used to represent this dispersion.

Solid lines in Figs. 5.2-5.10 represent the calculated ellipsometric parameters using Eqs. (5.2) and (5.3) whereas circles represent the experimental data in the range 300 nm to 830 nm. The measured thickness obtained from TFCompanion software was 506.93±0.43 nm for S1, 94.48±0.745 nm for S2 and 35.33±0.00068 nm for S3. Moreover, the spectroscopic measurements of the refractive index of the SiO_2 and PVK films in the spectral range 300 nm to 830 nm are shown in Figs. 5.2,5.5 and 5.8 for S1, S2 and S3, respectively. As can be seen from the figures, at λ = 633 nm, the measured index was 1.459 with percent error of 0.05% for S1, 1.683 with a percent error of 1.5% for S2 and 1.71 with percent error 0.0013% for S3.

The following table shows the values of N_o, N_2 and N_4 in Cauchy relation described in section 1.7 for SiO_2 film on Si wafer and two samples with different thickness of PVK film on Si substrate.

Table 5.1. Cauchy coefficients of the samples

sample	N_o	N_2	N_4
SiO_2 film on Si wafer (500 nm) S1	1.451	0.0033	5×10^{-5}
The first sample of PVK film on Si wafer (94.48 nm) S2	1.681	-0.0081	0.003 67
The second sample of PVK film on Si wafer (35.33) S3	1.979	-0.1625	0.021 96

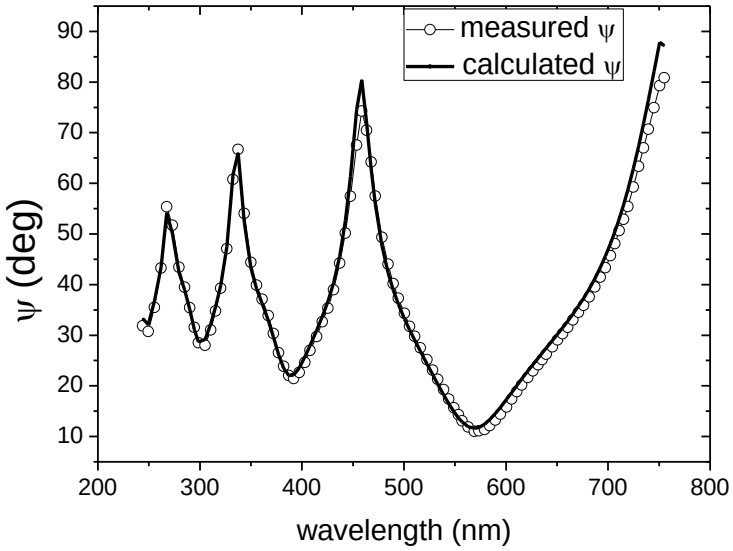

Figure 5.2. ψ of SiO_2 thin film on silicon wafer (S1) as a function of wavelength.

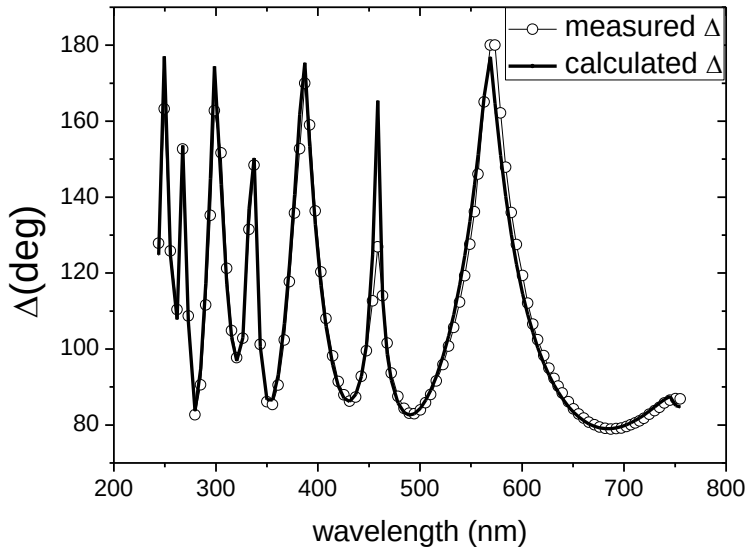

Figure 5.3. Δ of SiO_2 thin film on silicon wafer (S1) as a function of wavelength.

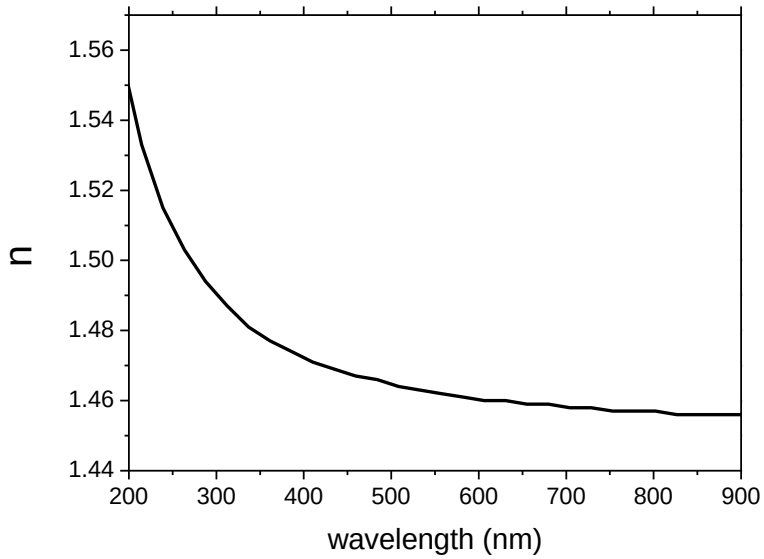

Figure 5.4. Refractive index of SiO_2 thin film on silicon wafer (S1) as a function of wavelength.

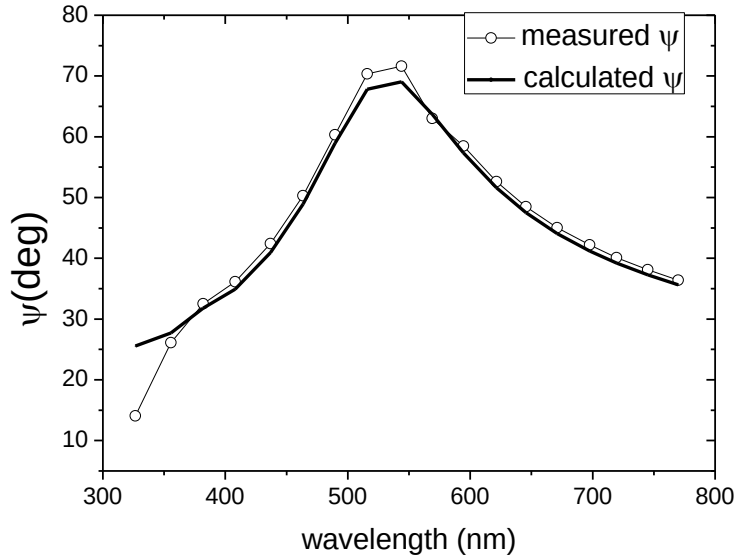

Figure 5.5. ψ of PVK thin film on silicon wafer (S2) as a function of wavelength.

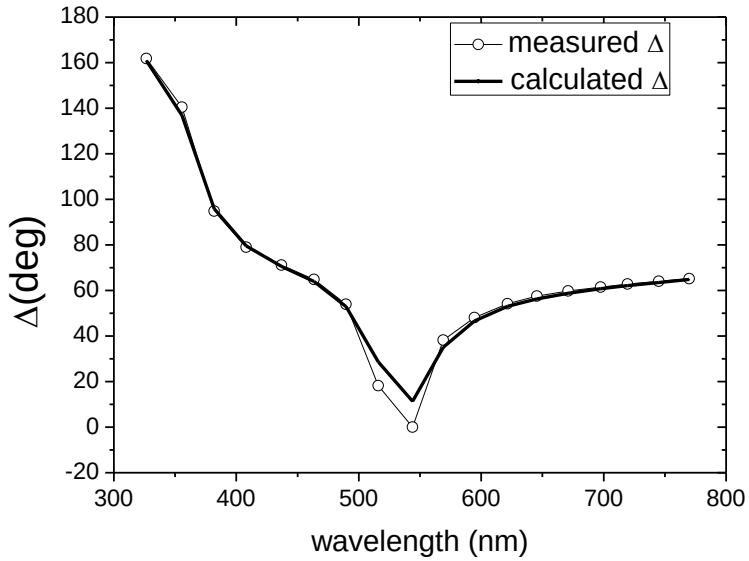

Figure 5.6. Δ of PVK thin film on silicon wafer (S2) as a function of wavelength.

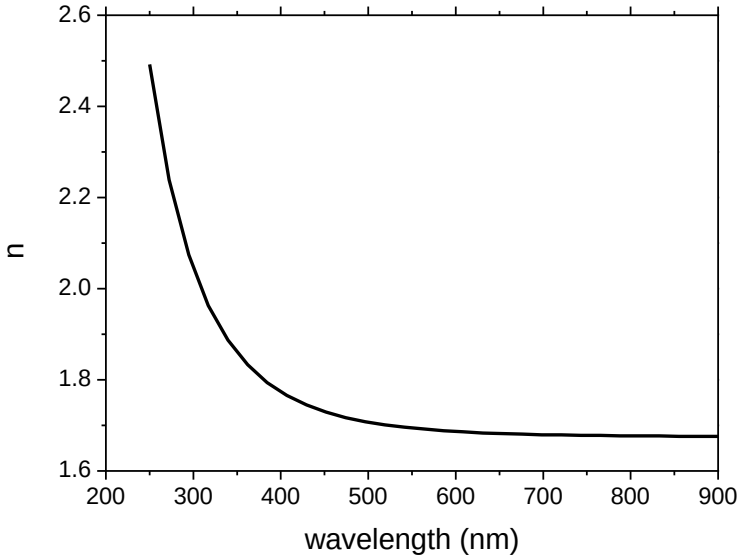

Figure 5.7. Refractive index of PVK thin film on silicon wafer (S2) as a function of wavelength .

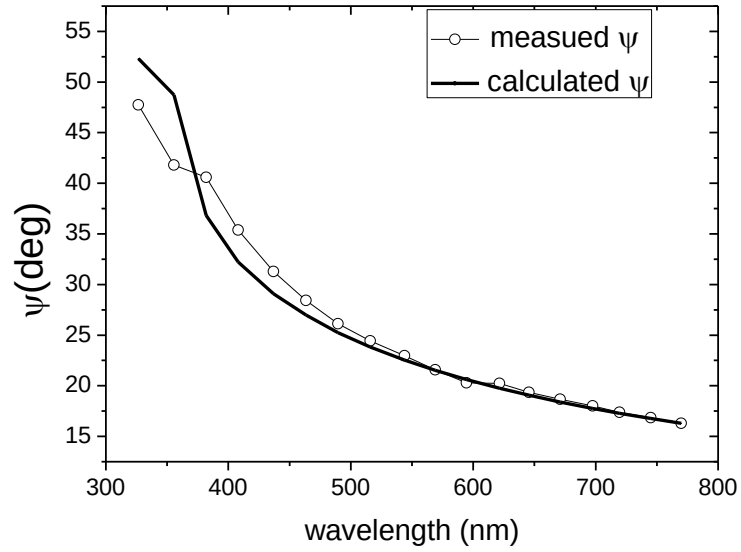

Figure 5.8. ψ of PVK thin film on silicon wafer (S3) as a function of wavelength.

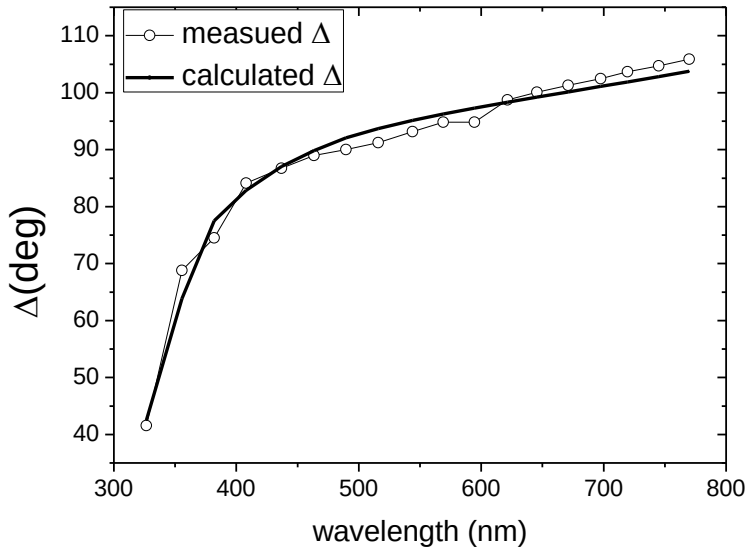

Figure 5.9. Δ of PVK thin film on silicon wafer (S3) as a function of wavelength.

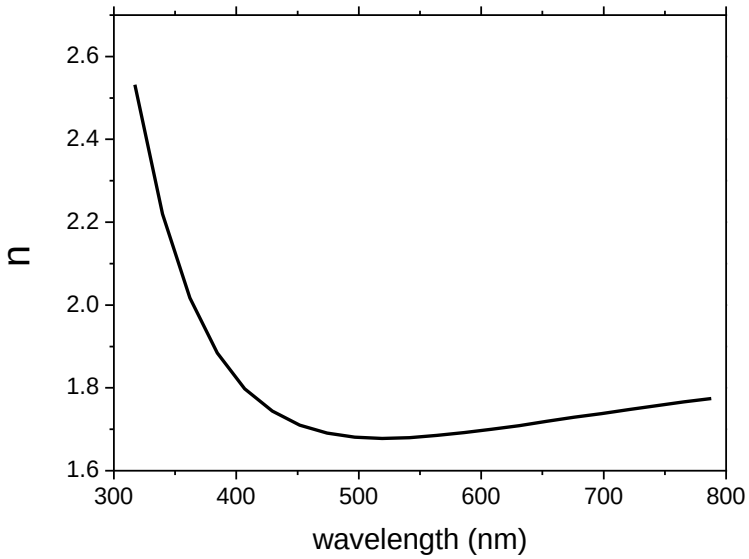

Figure 5.10. Refractive index of PVK thin film on silicon wafer (S3) as a function of wavelength.

CONCLUSIONS

Principles to electromagnetic theory and ellipsometry are presented in chapter one.

A rotating polarizer and analyzer spectroscopic ellipsometer using a fixed compensator has been proposed in chapter two. The feasibility of the proposed ellipsometric structure has been demonstrated theoretically for three samples; c-Si, SiO_2, and GaAs. Moreover, it is also has been tested for thin film characterization. Two compensator alignments have been assumed and discussed; when its fast axis makes angles 0^o and 45^o with the p-polarization.

A rotating polarizer-analyzer ellipsometer using a compensator is proposed in chapter three. Based on the speed ratio at which the polarizer and the analyzer rotate, different ellipsometric configurations are presented and compared. Moreover, two different alignments for the compensator are considered for each ellipsometric configuration. All configurations are applied to a bulk c-Si to extract the optical parameters.

In chapter four, two ellipsometeric structures which are rotating polarizer compensator (RPCE) and rotating compensator analyzer (RCAE) are presented. For each structure, we assumed three different configurations were assumed by considering different speed ratios.

In chapter five, a homemade rotating polarizer and analyzer spectroscopic ellipsometer was used to measure three different samples. The three ellipsometry samples were prepared, and then investigated at 632.8 nm as well as in the spectral range 300 nm to 830 nm.

The following conclusion have been found,

1) In all chapters, the uncertainties in the ellipsometric parameters due to the uncertainties of the Fourier coefficients have been derived and plotted. Moreover, The percent errors for noise effects and misalignment of the optical elements were investigated.
2) In chapter 2, 3 and 4, a comparison between different configurations is held regarding the effect of a hypothetical noise on the results.

3) In chapter 2, it is found that the worst offset angle of the compensator at 45^{o} and the best at 0^{o}.
4) In chapter 3, The results revealed that the ellipsometric configuration with a speed ratio 1:1 has a preference over other configurations.
5) In chapter 4, a general equation of the intensity for a rotating polarizer, compensator and analyzer ellipsometer with any speed ratio $N_1\omega$:$N_2\omega$:$N_3\omega$, is found.
6) A RCAE with a speed ratio 1 : 2 corresponds the minimum error in the calculated optical parameters in chapter 4 and all chapters.
7) A comparison between the well known rotating compensator ellipsometry (RCE) and RCAE at a speed ratio 1 : 2 reveals that RCAE has a preference over RCE.
8) In chapter 5, the results reveal high accuracy and the percent errors in all measured parameters are in the accepted range.

REFERENCES

[1] Sofyan Taya, and Taher El-Agez, "Ellipsometry of anisotropic materials: a new efficient polynomial approach", International J. for Light and Electron Optics, Optik, Vol. 122, 666–670 (2011).

[2] A. C. Boccara, C. Pickering, and J. Rivory, eds., "Proceedings of the First International Conference on Spectroscopic Ellipsometry", Elsevier, Amsterdam, 1993; published as Vols. 233-234 of Thin Solid Films, 1993.

[3] Sofyan Taya, and Taher El-Agez, "Comparing optical sensing using slab waveguides and total internal reflection ellipsometry", Turkish J. of Physics, Vol. 35, 31-36, 2011

[4] R. M. A. Azzam, "Measurement of the Stokes parameters of light: A unified analysis of Fourier photopolarimetry," Optik, Vol. 52, pp. 253-256, 1979.

[5] Taher El-Agez, Ahmed A. Tayyan, Sofyan Taya, and Hussam S. Musleh, "Characteristics of poly(9-vinylcarbazole) and 8-hydroxyquinoline aluminum using a homemade rotating analyzer ellipsometer", The Islamic University Journal (Series of Natural Studies and Engineering), Vol. 19, No. 2, 163-174, 2011.

[6] P. S. Hauge and F. H. Dill, "Design and operation of ETA, an automated ellipsometer," IBM J. Res. Develop., Vol. 17, pp. 472-489, 1973.

[7] Taher M. El-Agez, David M. Wieliczka, Chris Moffitt, and Sofyan A. Taya, "Spectroscopic ellipsometry time study of low temperature plasma-polymerized plain trimethylsilane thin films deposited on silicon", Physica Scripta, Vol. 84, (2011) 045302 (5pp). doi:10.1088/0031-8949/84/04/045302.

[8] K. Brudzewski, "Static Stokes ellipsometer: general analysis and optimization," J. Mod. Opt., Vol. 38, pp.889-896, 1991.

[9] Taher M. El-Agez, David M. Wieliczka, Chris Moffitt, and Sofyan A. Taya, "Aging of oxygen treated trimethylsilane plasma polymerized films using spectroscopic ellipsometry", Journal of Atomic, Molecular, and Optical Physics, Vol. 2011, Article ID 295304, 6 pages, 2011. doi:10.1155/2011/295304.

[10] R. H. Muller, R. M. A. Azzam, and D. E. Aspnes, eds., "Proceedings of the Fourth International Conference on Ellipsometry", Surface Science Vol. 96, North-Holland, Amsterdam, 1980.

[11] E. Passaglia, R. R. Stromberg, and J. Kruger, eds., "Ellipsometry in the Measurement of Surfaces and Thin Films", NBS Misc. Publ. 256, USGPO,Washington, D. C., 1964.

[12] H. G. Tompkins and W. A. McGahan, "Spectroscopic Ellipsometry and Reflectometry", A User's Guide,Wiley, New York, 1999.

[13] H. Fujiwara, Spectroscopic ellipsometry principles and applications, John Wiley & Sons, West Sussex, 2007.

[14] D. E. Aspnes and A. A. Studna, "High precision scanning ellipsometer", Appl. Opt., 14 (1975) 220–228.

[15] R. H. Muller and J. C. Farmer, Fast, self-compensating spectral-scanning ellipsometer, Rev. Sci. Instrum., 55 (1984) 371–374.

[16] D. E. Aspnes, "Fourier transform detection system for rotating analyzer ellipsometers", Opt. Commun., vol. 8, pp. 222-225, 1973.

[17] R.M. Azzam, "A sample Fourier photopolarimeter with rotating polarizer and analyzer for measuring Jones and Mueller matrices", Opt. commun. 25, 137- (1978).

[18] L. Y. Chen, and D. W. Lynch, "Scanning ellipsometer by rotating polarizer and analyzer", Appl. Opt., Vol. 26, No. 24, 5221-5228 (1987).

[19] L. Y. Chen, Xing Wei Feng, Yi Su, Hong Zhou Ma and You-Hua Qian, Improved rotating analyzer-polarizer of scanning ellipsometer, Thin Solid film, 234 (1993) pp. 385-389.

[20] L. Y. Chen, Xing Wei Feng, Yi Su, Hong Zhou Ma and You-Hua Qian, "Design of a scanning ellipsometer by synchronous rotation of the polarizer and analyzer". Appl. Opt. vol. 33, No. 7 (1994) pp. 1299-1305.

[21] D. E. Aspnes, "Optimizing precision of rotating-analyzer and rotating-compensator ellipsometers", J. Opt. Soc. Am. A, vol. 21, no. 3, pp. 403-410, 2004.

[22] R. Kleim, L. Kuntzler, and A. El Ghemmaz, "Systematic errors in rotating-compensator ellipsometry", J. Opt. Soc. Am. A/Vol. 11, No. 9/September 1994

[23] T.Mori , D.E.Aspnes, "Comparison of the capabilities of rotating-analyzer and rotatingcompensator ellipsometers by measurements on a single system", Thin Solid Films 455 –456 (2004) 33–38.

[24] Taher M. El-Agez, Ahmed A. El Tayyan, and Sofyan A. Taya, "Rotating polarizer-analyzer scanning ellipsometer", Thin solid films, vol. 518, No. 19, 5610-5614, 2010

[25] Taher M. El-Agez and Sofyan A. Taya "A Fourier ellipsometer using rotating polarizer and analyzer at a speed ratio 1:1", Journal of Sensors, vol. 2010, Article ID 706829, 7 pages, doi:10.1155/2010/706829, (2010).

[26] Taher M. El-Agez and Sofyan A. Taya "An extensive theoretical analysis of the 1 : 2 ratio rotating polarizer–analyzer Fourier ellipsometer", Physica Scripta, Vol. 83, No. 2, 7 pages, 025701, (2011). doi:10.1088/0031-8949/83/02/025701.

[27] Taher El-Agez, and Sofyan A. Taya "Development and construction of rotating polarizer analyzer ellipsometer", Optics and lasers in engineering, Vol. 49, 507–513 (2011).

[28] Taher El-Agez, Sofyan A. Taya, and Ahmed El Tayayn, "An improvement of scanning ellipsometer by rotating a polarizer and an analyzer at a speed ratio of 1:3", International Journal of Optomechatronics, Vol. 5, 51-67, 2011.

[29] Sofyan A. Taya and Taher M. El-Agez, "Noise effect on thin film characterization using rotating polarizer analyzer ellipsometer", Acta Physica Polonica A, (in press).

[30] Taher El-Agez, and Sofyan A. Taya "Characterization of SiO2 thin film using rotating polarizer analyzer ellipsometer ", International Journal of Microwave and Optical Technology (IJMOT), Vol. 6, No. 6, 363-371, 2011.

[31] Sofyan A. Taya, Taher M. El-Agez, and Anas A. AlKanoo, "Thin film characterization using rotating polarizer analyzer ellipsometer with a speed ratio 1:3", Journal of Electromagnetic Analysis and Applications, Vol. 3, No. 9, 351-358, 2011. doi: 10.4236/jemaa.2011.39056.

[32] Sofyan A. Taya and Taher M. El-Agez, "Effect of noise on the optical parameters extracted from different ellipsometric configurations", Physica Scripta, Phys. Scr. 85 (2012) 045706 (6pp), doi:10.1088/0031-8949/85/04/045706.

[33] A.R.M. Zaghloul and R.M. Azzam, "Single-element rotating polarizer ellipsometer: psi meter", Surf Sci., 96, 168-173 (1980).

[34] L. Vina, C. Umbatch, M. Cardona, and L. Vodopyanov, "Ellipsometric studies of electric interband transitions in CdxHg1-xTe" Phys. Rev. B 29, 6752-6760 (1984).

[35] E.D. Palik, Handbook of optical constants of solids (Academic Press, San Diego, CA 1985).

[36] Sofyan A. Taya and Taher M. El-Agez, "Design of a spectroscopic ellipsometer by synchronous rotation of the polarizer and analyzer in opposite directions", Sensors and Actuators A: Phys., (in submission).

[37] M. A. Baldo, M. E. Thompson and S. R. Forrest1," Phosphorescent Materials for Application to Organic Light Emitting Devices". Pure Appl. Chem., 71,11-18 (1999).

[38] F.W.Billmryer, Textbook of Polymer Science, 2^{ed} edition, Wiley, New York (1984).

[39] W. Rasmussen, Novel Carbazole Based Methacrylates, Acrylates, and Dimethacrylates to Produce High Refractive Index Polymers, Ph.D., Virginia Polytechnic Institute and State University,Virginia (2002).